

Reconciling dark matter, $R_{K^{(*)}}$ anomalies and $(g - 2)_\mu$ in an $L_\mu - L_\tau$ scenario

Anirban Biswas^{1,*} and Avirup Shaw^{2,†}

¹*School of Physical Sciences, Indian Association for the Cultivation of Science,
2A & 2B Raja S.C. Mullick Road, Kolkata 700032, India*

²*Theoretical Physics, Physical Research Laboratory, Ahmedabad 380009, India*

Abstract

We propose an anomaly free unified scenario by invocation of an extra local $U(1)_{L_\mu - L_\tau}$ gauge symmetry. This scenario simultaneously resolves the $R_{K^{(*)}}$ anomalies, the dark matter puzzle and the long-standing discrepancy in muon's anomalous magnetic moment. A complex scalar (η) having nonzero $L_\mu - L_\tau$ charge has been introduced to break this new $U(1)$ symmetry spontaneously. Moreover, for the purpose of studying dark matter phenomenology and $R_{K^{(*)}}$ anomalies in a correlated manner, we introduce an inert $SU(2)_L$ scalar doublet (Φ), a \mathbb{Z}_2 -odd real singlet scalar (S) and a \mathbb{Z}_2 -odd coloured fermion (χ) which transforms vectorially under the $U(1)_{L_\mu - L_\tau}$ symmetry. This extra gauge symmetry provides a new gauge boson $Z_{\mu\tau}$ which not only gives additional contribution to both $b \rightarrow s\ell\ell$ transition and $(g - 2)_\mu$ but also provides a crucial annihilation channel for dark matter candidate ρ_1 of the present scenario. This ρ_1 is an admixture of CP-even neutral component of Φ and S . Our analysis shows that the low mass dark matter regime ($M_{\rho_1} \lesssim 60$ GeV) is still allowed by the experiments like XENON1T, LHC (via Higgs invisible branching) and Fermi-LAT, making the dark matter phenomenology drastically different from the standard Inert Doublet and the Scalar Singlet models. Furthermore, the present model is also fairly consistent with the observed branching ratio of $B \rightarrow X_s \gamma$ in 3σ range and is quite capable of explaining neutrino masses and mixings via Type-I seesaw mechanism if we add three right handed neutrinos in the particle spectrum. Finally, we use the latest ATLAS data of non-observation of a resonant $\ell^+\ell^-$ signal at the 13 TeV LHC to constrain the mass-coupling plane of $Z_{\mu\tau}$.

*Electronic address: anirban.biswas.sinp@gmail.com

†Electronic address: avirup.cu@gmail.com

I. INTRODUCTION

With the discovery of the missing piece, the Higgs boson at the Large Hadron Collider (LHC) [1, 2] at CERN the Standard Model (SM) of particle physics has been turned into a complete theory. From the last several decades it has been a well known fact that most of the theoretical predictions of this theory are in good agreement with various experimental results. However, at the same time, different experimental results in various directions compelling us to formulate physics beyond the SM (BSM). For example, dark matter relic density has been measured with a great precision from the temperature and polarization anisotropies of the cosmic microwave background (CMB) radiation by experiments like WMAP [3] and Planck [4]. On top of that various indirect evidence such as rotation curve [5], gravitational lensing of distant objects [6], collision between galaxy clusters (such as Bullet cluster [7] etc.) etc. have strongly support for the existence of dark matter. However, in the SM there is no such candidate for dark matter. On the other hand neutrino oscillation experiments [8–11] firmly established massive nature of at least two neutrinos and have accurately measured three intergenerational mixing angles, both of which are missing in the SM due to non-existence of the right handed counterparts of left handed neutrinos. Besides, the CP-violation in the quark sector is not at all sufficient to explain the observed baryon asymmetry of the Universe [12]. Furthermore, there is an enduring $\sim 3.5\sigma$ discrepancy [12] between experimentally measured value of the anomalous magnetic moment of muon $[(g-2)_\mu]$ and its SM predictions, which strongly indicates the presence of a new physics (NP) beyond the SM.

Apart from the above mentioned facts, over the last few years different flavour physics experiments like LHCb, Belle and Babar have been consistently shown that experimental data for different observables are in significant disagreement with respect to the corresponding SM predictions. Indeed this situation demands the invocation of NP effects. Recently the LHCb collaboration has reported additional hints for violation of Lepton Flavour Universality (LFU) between $b \rightarrow s\mu^+\mu^-$ and $b \rightarrow se^+e^-$ processes. The LFU violation¹ (LFUV) can be measured with the help of following observables R_K and R_{K^*}

$$R_{K^{(*)}} = \frac{\text{Br}(B \rightarrow K^{(*)}\mu^+\mu^-)}{\text{Br}(B \rightarrow K^{(*)}e^+e^-)} . \quad (1)$$

Summary of the corresponding experimental results with their SM predictions for different di-lepton invariant mass squared (q^2) ranges are given in Table I.

¹ Evidences of LFUV via charge current semileptonic $b \rightarrow c\ell\nu$ transition processes have also been observed. For example experimental results show significant deviations for observables $R_{D^{(*)}}$ [13] and $R_{J/\psi}$ [14] from the corresponding SM predictions.

Observable	SM prediction	Measurement	Deviations
$R_K : q^2 = [1.1, 6] \text{ GeV}^2$	1.00 ± 0.01 [15, 16]	$0.846^{+0.060+0.016}_{-0.054-0.014}$ [17]	2.5σ
$R_{K^*}^{\text{low}} : q^2 = [0.045, 1.1] \text{ GeV}^2$	0.92 ± 0.02 [18]	$0.660^{+0.110}_{-0.070} \pm 0.024$ [19]	$2.1\sigma - 2.3\sigma$
$R_{K^*}^{\text{central}} : q^2 = [1.1, 6] \text{ GeV}^2$	1.00 ± 0.01 [15, 16]	$0.685^{+0.113}_{-0.069} \pm 0.047$ [19]	$2.4\sigma - 2.5\sigma$

Table I: The experimental values of the observables along with their SM predictions for different ranges of q^2 .

Deviations from the SM predictions shown in the Table I² can be resolved by invoking additional NP contributions to some of the Wilson Coefficients (WCs) which are involved in the effective Hamiltonian for $b \rightarrow s\ell\ell$ ($\ell \equiv$ charged lepton, i.e., electron (e) and muon (μ)) transition. Furthermore, if these anomalies are associated with other observables for the rare processes $b \rightarrow s\mu\mu$ transitions, then it has been observed that a NP scenario with *additional* contribution to the WC C_9^μ (but not in C_9^e) is more acceptable. The operator corresponding to the WC C_9^ℓ is $\mathcal{O}_9 \equiv \frac{e^2}{16\pi^2}(\bar{s}\gamma_\alpha P_L b)(\bar{\ell}\gamma^\alpha \ell)$. From the Table I, it is readily evident that NP interfere destructively with the SM, which ensures the sign of $C_9^{\text{NP},\mu}$ is negative. The best-fit value of $C_9^{\text{NP},\mu}$ is ≈ -1 [15, 18, 21–27]. Moreover, NP scenario with $C_9^{\text{NP},\mu} = -C_{10}^{\text{NP},\mu}$ (where the WC C_{10}^ℓ is associated with the operator $\mathcal{O}_{10} \equiv \frac{e^2}{16\pi^2}(\bar{s}\gamma_\alpha P_L b)(\bar{\ell}\gamma^\alpha \gamma_5 \ell)$) is also a very appealing from the model building point of view [15, 18, 23–27]. Inspired by these results, several BSM scenarios using extra non-standard Z -boson [28–53] and leptoquark [22, 44, 54–76] have been demonstrated the viable interpretation of the anomalies.

In this article, we ameliorate some of these problems in a correlated manner within a single framework by introducing an extra local $U(1)_{L_\mu-L_\tau}$ symmetry to the SM gauge symmetry, where L_μ and L_τ indicate lepton numbers for the second and third generations of charged leptons and their corresponding neutrinos. Apart from being an anomaly free gauged $U(1)$ extension, the $L_\mu - L_\tau$ symmetry naturally violets the LFU between e and μ because the $L_\mu - L_\tau$ charge of leptons are such that the corresponding new non-standard gauge boson couples only to $\mu(\tau)$ but not to e . This scenario was originally formulated by Volkas et. al. [77, 78]. Thereafter, several variants of $U(1)_{L_\mu-L_\tau}$ model have been studied in the context of different phenomenological purposes: e.g., contribution of the $U(1)_{L_\mu-L_\tau}$ gauge boson to explain the $(g-2)_\mu$ anomaly [79–86], dark matter phenomenology [84, 85, 87–91], generation of neutrino masses and mixing parameters [79, 84, 86, 92–95] etc.

For the purpose of explaining $b \rightarrow s\mu^+\mu^-$ anomaly, this type of $U(1)_{L_\mu-L_\tau}$ model has also been modified from its minimal version, *albeit* in a different approach [31, 43, 50, 51, 96–101]. In the present article, we introduce a \mathbb{Z}_2 -odd bottom quark like non-standard fermion field χ which is vectorial in nature under the $U(1)_{L_\mu-L_\tau}$ symmetry. It couples to all generations of the down-

² For R_{K^*} , new preliminary measurements have been given by Belle [20] for two q^2 ranges. For $q^2 \in [0.1, 8] \text{ GeV}^2$ the value of R_{K^*} is $0.90^{+0.27}_{-0.21} \pm 0.10$ while for $q^2 \in [15, 19] \text{ GeV}^2$ the corresponding value is $1.18^{+0.52}_{-0.32} \pm 0.10$.

type SM quarks via Yukawa like interaction involving a \mathbb{Z}_2 -odd scalar doublet Φ . Moreover, we introduce a \mathbb{Z}_2 -odd singlet scalar S which helps us to explain the flavour anomaly, dark matter and $(g-2)_\mu$ anomaly simultaneously. A \mathbb{Z}_2 -even complex scalar singlet field η with a nonzero $L_\mu - L_\tau$ charge has been introduced for the purpose of breaking of $U(1)_{L_\mu - L_\tau}$ symmetry spontaneously. Apart from these fields we have the usual Higgs doublet field H which breaks the $SU(2)_L \times U(1)_Y$ symmetry. Therefore, in the broken phase of both electroweak ($SU(2)_L \times U(1)_Y$) and $U(1)_{L_\mu - L_\tau}$ symmetries, we have three physical \mathbb{Z}_2 -odd neutral scalars emerge from the mixing between Φ and S . The lightest field among the three physical \mathbb{Z}_2 -odd neutral scalars can be considered as a potentially viable dark matter candidate. This is an admixture of both doublet and singlet scalar representations and have distinct phenomenology compared to the standard Inert Doublet [102–104] and the Scalar Singlet models [105–108], where the low mass dark matter regime is almost ruled by the latest bound on spin independent scattering cross section from XENON1T [109] as well as by the upper limit on Higgs invisible branching fraction from LHC [110]. This is mainly due to the fact that in these models in the low mass regime ($M_{\text{DM}} \leq 62.5$ GeV), dark matter candidate predominantly annihilates into $b\bar{b}$ final state.

On the contrary, in the present scenario, the dark matter candidate in the low mass regime can annihilate into a pair of $L_\mu - L_\tau$ gauge boson $Z_{\mu\tau}$ and the branching fraction of this annihilation channel is controlled by dark sector mixing angle θ_D . This actually makes the dark matter freeze-out process extremely correlated with the flavour physics anomalies and $(g-2)_\mu$ anomaly, where an $\mathcal{O}(\text{MeV})$ light $Z_{\mu\tau}$ plays a pivotal role. Since, $Z_{\mu\tau}$ does not have direct couplings to the first generation leptons and quarks, constraints from the LEP and more recently from the LHC on the $g_{Z_{\mu\tau}} - M_{Z_{\mu\tau}}$ plane are relatively relaxed. Particularly, light gauge boson with $M_{Z_{\mu\tau}} \lesssim 100$ MeV and also with moderate gauge coupling $g_{Z_{\mu\tau}} \lesssim 10^{-3}$ is still allowed from the experiments measuring neutrino trident processes namely CCFR [111] CHARM-II [112]. Moreover, apart from $(g-2)_\mu$ anomaly and flavour physics related issues, such a light gauge boson has excellent cosmological implication. The reason is that it can relax the $\sim 3\sigma$ tension between the measurements of Hubble constant (H_0) from two different epochs³ by providing extra contribution to the radiation energy density ($\Delta N_{\text{eff}} \sim 0.2-0.5$) through the alteration of neutrino decoupling temperature [114]. In the present scenario the non-standard neutral gauge boson $Z_{\mu\tau}$ emerge from all three neutral gauge bosons associated with $SU(2)_L$, $U(1)_Y$ and $U(1)_{L_\mu - L_\tau}$ gauge groups by diagonalising a 3×3 mixing matrix. The additional contribution to the anomalous magnetic moment of muon comes from an effective $\mu^+ \mu^- \gamma$ vertex which has been generated from one loop penguin diagram involving $Z_{\mu\tau}$. Moreover, we also have one loop contribution from a diagram involving other BSM scalar (an orthogonal state of the SM-like Higgs boson arises from the mixing between H and η in the broken phase of the theory). However, its effect on $(g-2)_\mu$ is negligibly small.

To this end, we would like to mention another novel signature of the present scenario. The

³ At two different redshifts (z), one is from the CMB experiment Planck [4] at high z while another one is from the local measurement using Hubble Space Telescope [113] at low z .

correlation between dark sector and flavour physics sector is not only due to $L_\mu - L_\tau$ gauge boson but also due to all the \mathbb{Z}_2 -odd neutral particles (including dark matter candidate of the present scenario) along with the coloured \mathbb{Z}_2 -odd fermion χ generate non-standard one loop contributions to produce $b \rightarrow s\mu^+\mu^-$ transition. In the present scenario, one can produce non-standard contributions to both the WCs C_9^μ and C_{10}^μ respectively, however, the contribution of the latter is insignificant and hence our analysis will be furnished with $C_9^{\text{NP},\mu}$ only. The NP contribution to C_9^μ is obtained from non-standard penguin and self-energy diagrams and there is no further NP contribution from box-diagram at one loop level. Moreover, we consider the constraint from the branching ratio of another flavour changing neutral current (FCNC) process $B \rightarrow X_s\gamma$. Hence, we have computed the branching ratio of this decay in the present scenario. Further, neutrino masses and mixings can easily be addressed in these class of $L_\mu - L_\tau$ models via Type-I seesaw mechanism by adding three right handed neutrinos, which are singlet under the SM gauge groups and two of them have equal and opposite $L_\mu - L_\tau$ charges for anomaly cancellation. Since a detailed analysis on neutrino masses and mixings in the present scenario is beyond the scope of this article, hence for the sake of completeness, we just have added three right handed neutrinos in the Lagrangian and find the Majorana mass matrix for the light neutrinos. A more comprehensive analysis on diagonalisation of the light neutrino mass matrix and thereby finding the mass eigenvalues and mixing angles in the $L_\mu - L_\tau$ scenario has already been done in [84].

Finally, in order to impose the constraints on the parameter space of the present scenario from the LHC experiment, we use the latest ATLAS data [115] of non-observation of a resonant $\ell^+\ell^-$ signal at the LHC running at 13 TeV for the high mass range of $Z_{\mu\tau}$. Hence, we will estimate the cross section for the process $pp \rightarrow Z_{\mu\tau} \rightarrow \ell^+\ell^-$ at the 13 TeV LHC in the present scenario. Consequently, it will be an interesting part of this exercise that, how the LHC data can constrain the values of non-standard gauge coupling constant as well as the $Z - Z_{\mu\tau}$ mixing angle.

The article is organised as follows. In Sec. II we introduce the model with possible field content and interactions as well as we set our notations. Then in Sec. III, we show the calculational details of flavour physics observables and after that we will discuss $(g-2)_\mu$ anomaly in Sec. IV. In Sec. V, we show the viability of our dark matter candidate of the present scenario considering all possible bounds from ongoing experiments and explain how can we correlate the dark matter with the flavour physics anomalies. We briefly discuss neutrino mass generation via Type-I seesaw mechanism in Sec. VI. Sec. VII deals with constraint that are obtained from non-observation of a resonant $\ell^+\ell^-$ signal at the LHC running at 13 TeV. Finally, we summarize our results and conclude in Sec. VIII.

II. THE $U(1)_{L_\mu-L_\tau}$ MODEL

In order to facilitate our motivations (discussed in Section I), we propose an anomaly free $U(1)_{L_\mu-L_\tau}$ gauge extension of the SM. This scenario is free from mixed gauge-gravitational and axial vector gauge anomalies because these anomalies cancel between second and third generations of charged leptons and their corresponding neutrinos due to their equal and opposite $L_\mu - L_\tau$ charges. The Lagrangian which remains invariant under the $SU(3)_C \times SU(2)_L \times U(1)_Y \times U(1)_{L_\mu-L_\tau} \times \mathbb{Z}_2$ symmetry is given by,

$$\begin{aligned} \mathcal{L} = & \mathcal{L}_{\text{SM}} + \mathcal{L}_N + \mathcal{L}_\chi + (D_\alpha \eta)^\dagger (D^\alpha \eta) + (D_\alpha \Phi)^\dagger (D^\alpha \Phi) + \frac{1}{2} \partial_\alpha S \partial^\alpha S \\ & - \frac{1}{4} \hat{B}_{\alpha\beta} \hat{B}^{\alpha\beta} - \frac{1}{4} \hat{X}_{\alpha\beta} \hat{X}^{\alpha\beta} + \frac{\epsilon}{2} \hat{X}_{\alpha\beta} \hat{B}^{\alpha\beta} - V(H, \eta, \Phi, S) , \end{aligned} \quad (2)$$

where

$$\hat{B}_{\alpha\beta} = \partial_\alpha \hat{B}_\beta - \partial_\beta \hat{B}_\alpha \quad \text{and} \quad \hat{X}_{\alpha\beta} = \partial_\alpha \hat{X}_\beta - \partial_\beta \hat{X}_\alpha , \quad (3)$$

are field strength tensors for the two $U(1)$ gauge fields⁴ \hat{B}_α and \hat{X}_α respectively while the Lorentz indices $\alpha, \beta \equiv 0, 1 \dots 3$. The term contains both field strength tensors is the kinetic mixing term between \hat{B}_α and \hat{X}_α , which is not forbidden by any of the symmetries of the present model. Full list of particle contents and their quantum numbers under various symmetry groups are given in Table II.

Gauge groups	Fermion fields												Scalar fields				
	Quark fields			Lepton fields									χ	H	η	Φ	S
Q_{Li}	u_{Ri}	d_{Ri}	L_{Le}	$L_{L\mu}$	$L_{L\tau}$	e_R	μ_R	τ_R	N_{eR}	$N_{\mu R}$	$N_{\tau R}$						
$SU(3)_C$	3	3	3	1	1	1	1	1	1	1	1	1	3	1	1	1	1
$SU(2)_L$	2	1	1	2	2	2	1	1	1	1	1	1	1	2	1	2	1
$U(1)_Y$	$\frac{1}{6}$	$\frac{2}{3}$	$-\frac{1}{3}$	$\frac{1}{2}$	$\frac{1}{2}$	$\frac{1}{2}$	-1	-1	-1	0	0	0	$-\frac{1}{3}$	$\frac{1}{2}$	0	$\frac{1}{2}$	0
$U(1)_{L_\mu-L_\tau}$	0	0	0	0	1	-1	0	1	-1	0	1	-1	-1	0	-1	1	0
\mathbb{Z}_2 symmetry	+	+	+	+	+	+	+	+	+	+	+	+	-	+	+	-	-

Table II: Gauge quantum numbers and \mathbb{Z}_2 parity of different SM and BSM particles.

As has been discussed in earlier that the $L_\mu - L_\tau$ extension of the SM is anomaly free, however, for the purpose of neutrino mass generation via Type-I seesaw mechanism we invoke three SM gauge singlet right handed neutrinos (N_{Ri}) having nonzero $L_\mu - L_\tau$ charge in such a manner so that their inclusion does not introduce any further anomaly. The Lagrangian of right handed

⁴ We are denoting the basis of gauge fields having off-diagonal kinetic term by using a hat notation.

neutrinos is denoted by \mathcal{L}_N which contains kinetic energy terms, mass terms and Yukawa terms associated with the SM lepton doublets (L_{Li}) allowed by the symmetries of the present model.

$$\begin{aligned}\mathcal{L}_N = & \sum_{j=e,\mu,\tau} \frac{i}{2} \overline{N_R^j} \gamma^\alpha D_\alpha N_R^j - \frac{1}{2} M_{ee} \overline{(N_R^e)^c} N_R^e - \frac{M_{\mu\tau}}{2} (\overline{(N_R^\mu)^c} N_R^\tau + \overline{(N_R^\tau)^c} N_R^\mu) \\ & - \frac{y_{e\mu}}{2} (\overline{(N_R^e)^c} N_R^\mu + \overline{(N_R^\mu)^c} N_R^e) \eta - \frac{y_{e\tau}}{2} (\overline{(N_R^e)^c} N_R^\tau + \overline{(N_R^\tau)^c} N_R^e) \eta^* \\ & - \sum_{i=e,\mu,\tau} y_i \overline{L}_L^i \tilde{H} N_R^i + \text{h.c.} ,\end{aligned}\tag{4}$$

where $\tilde{H} = i\sigma_2 H^*$. M_{ee} , $M_{\mu\tau}$ are the bare mass parameters while $y_{e\mu}$, $y_{e\tau}$ and y_i are the dimensionless Yukawa couplings. In order to generate $b \rightarrow s$ transition at one loop level involving \mathbb{Z}_2 -odd scalars a non-standard $\text{SU}(2)_L$ singlet fermionic field χ with a colour charge has been introduced in this scenario. This fermion is also \mathbb{Z}_2 -odd and has an electric charge identical to SM down-type quarks. Furthermore, both left and right chiral parts of χ field have same $L_\mu - L_\tau$ charge making it a vector like fermion under $\text{U}(1)_{L_\mu - L_\tau}$ symmetry. The Lagrangian of this field is given by

$$\mathcal{L}_\chi = i \bar{\chi} \gamma^\alpha D_\alpha \chi - M_\chi \bar{\chi} \chi - \left(\sum_{j=1}^3 f_j \overline{Q_{Lj}} \Phi \chi_R + \text{h.c.} \right) ,\tag{5}$$

where M_χ is the bare mass parameter for the χ field and f_j s are couplings of the Yukawa type interactions among the SM quark doublets (Q_{Lj}), \mathbb{Z}_2 -odd scalar doublet Φ and the right chiral part of χ . The above Yukawa type interactions terms involving s and b quarks have significant roles in $b \rightarrow s$ transition and hence in the explanation of $R_{K^{(*)}}$ anomalies. The covariant derivative D_α for the field χ is defined as

$$D_\alpha \chi \equiv \left(\partial_\alpha - ig_1 \frac{1}{3} \hat{B}_\alpha + ig_{Z_{\mu\tau}} n_\chi \hat{X}_\alpha + ig_3 \frac{\Lambda^a}{2} G_\alpha^a \right) \chi ,\tag{6}$$

where g_1 , $g_{Z_{\mu\tau}}$ and g_3 are the $\text{U}(1)_Y$, $\text{U}(1)_{L_\mu - L_\tau}$ and $\text{SU}(3)_C$ gauge coupling constants respectively. n_χ is the $L_\mu - L_\tau$ charge of χ . Further, Λ^a s ($a = 1, 2, \dots, 8$) are the eight Gell-Mann matrices representing the generators for $\text{SU}(3)_C$ while the corresponding gauge fields are denoted by G_α^a . The 4th, 5th and 6th terms of the Eq. (2) represent the kinetic terms for all the non-standard scalar representations (η , Φ and S) introduced in the present model for specific purposes. Particularly, the complex singlet (under the SM gauge group) scalar η is necessary to break the $\text{U}(1)_{L_\mu - L_\tau}$ symmetry spontaneously as it is the only scalar field which has not only a $\text{U}(1)_{L_\mu - L_\tau}$ charge but also has a nonzero vacuum expectation value (VEV) v_2 . Consequently, after $L_\mu - L_\tau$ symmetry breaking one obtains a massive non-standard neutral gauge boson. It has played crucial roles in different aspects: e.g., $(g - 2)_\mu$ anomaly explanation, amelioration of the anomalies that are related to $b \rightarrow s\mu\mu$ transition and most importantly it provides new annihilation channels for the dark matter candidate, which alters its dynamics from the standard case. Moreover, a \mathbb{Z}_2 -odd $\text{SU}(2)_L$ scalar doublet Φ having both $\text{U}(1)_Y$ and $\text{U}(1)_{L_\mu - L_\tau}$ charges which are required to get the NP contribution to $b \rightarrow s$ transition via the Yukawa

like interaction given in Eq. (5). Although, one of the neutral components of Φ (lightest one) is stable, but for the simultaneous explanation of the dark matter enigma, $(g-2)_\mu$ anomaly and $R_{K^{(*)}}$ anomalies we include another real singlet scalar field S which is also odd under \mathbb{Z}_2 symmetry. Covariant derivatives for the scalar fields η and Φ are given as follows

$$D_\alpha \eta \equiv \left(\partial_\alpha + ig_{Z_{\mu\tau}} n_\eta \hat{X}_\alpha \right) \eta, \quad (7)$$

$$D_\alpha \Phi \equiv \left(\partial_\alpha + ig_1 \frac{1}{2} \hat{B}_\alpha + ig_{Z_{\mu\tau}} n_\Phi \hat{X}_\alpha + ig_2 \frac{\sigma^a}{2} W_\alpha^a \right) \Phi, \quad (8)$$

where σ^a are the three Pauli's spin matrices with a runs from 1 to 3. n_X denotes the $L_\mu - L_\tau$ charge of the corresponding scalar fields $X = \Phi, \eta$. Further, g_2 is the $SU(2)_L$ gauge coupling constant and W_α^a s are the corresponding gauge bosons.

Finally, the scalar potential $V(H, \eta, \Phi, S)$ in Eq. (2) contains those interactions terms among the scalar fields which remain invariant under all the symmetries of the present model, has the following form,

$$\begin{aligned} V(H, \eta, \Phi, S) = & -m_H^2(H^\dagger H) - m_\eta^2(\eta^\dagger \eta) + m_\Phi^2(\Phi^\dagger \Phi) + \frac{m_S^2}{2} S^2 \\ & + \lambda_H(H^\dagger H)^2 + \lambda_\eta(\eta^\dagger \eta)^2 + \lambda_\Phi(\Phi^\dagger \Phi)^2 + \frac{\lambda_S}{4} S^4 \\ & + \lambda_1(H^\dagger H)(\eta^\dagger \eta) + \lambda_2(H^\dagger H)(\Phi^\dagger \Phi) + \lambda_3(H^\dagger \Phi)(\Phi^\dagger H) \\ & + \lambda_4(\Phi^\dagger \Phi)(\eta^\dagger \eta) + \lambda_5(\Phi^\dagger \Phi)S^2 + \lambda_6(\eta^\dagger \eta)S^2 + \lambda_7(H^\dagger H)S^2 \\ & + [\lambda_8(H^\dagger \Phi)S\eta + \text{h.c.}] , \end{aligned} \quad (9)$$

where m_H, m_η, m_Φ and m_S are real parameters having dimension of mass and λ_i s ($i = H, \eta, S, 1, 2 \dots 7$) are dimension less, real quartic coupling constants because the corresponding operators are self-conjugate in nature. However, the quartic coupling λ_8 can in general be a complex parameter and thus can act as an extra source of CP-violation. Since in this work we are not studying any CP-violating effects, we have taken λ_8 as a real parameter and this assumption will not alter our conclusions. Although, the term proportional to λ_8 has important significance in this model as it generates mixing between Φ and S . Later we will discuss more elaborately on this issue. The component wise structure of the scalar fields are given in the following

$$H = \begin{pmatrix} h^+ \\ \frac{h_1 + v_1 + iz_1}{\sqrt{2}} \end{pmatrix}, \quad \eta = \begin{pmatrix} \frac{h_2 + v_2 + iz_2}{\sqrt{2}} \end{pmatrix}, \quad \Phi = \begin{pmatrix} \frac{\phi^+}{\sqrt{2}} \\ \frac{\phi^0 + a^0}{\sqrt{2}} \end{pmatrix}, \quad (10)$$

where v_1 and v_2 are the VEVs of the scalar fields⁵ H and η respectively. After breaking of both electroweak and $L_\mu - L_\tau$ symmetries by the respective VEVs v_1 and v_2 , one can have mixing

⁵ H and η are even under \mathbb{Z}_2 symmetry and hence \mathbb{Z}_2 remains unbroken.

between the real components h_1 and h_2 due to the presence of an interaction term proportional to λ_1 in $V(H, \eta, \Phi, S)$. The mixing matrix in the basis $\frac{1}{\sqrt{2}}(h_1 \ h_2)^T$ has the following form,

$$\mathcal{M}_{\text{scalar}}^2 = \begin{pmatrix} 2\lambda_H v_1^2 & \lambda_1 v_1 v_2 \\ \lambda_1 v_1 v_2 & 2\lambda_\eta v_2^2 \end{pmatrix}. \quad (11)$$

Diagonalising the mass squared matrix by an orthogonal transformation, we obtain two physical CP-even neutral scalars H_1 which has been considered as SM like Higgs of mass 125.5 GeV and H_2 . These fields are also even under \mathbb{Z}_2 symmetry similarly as h_1 and h_2 . The physical states H_1 and H_2 are related with previous states h_1 and h_2 by the following relation,

$$\begin{pmatrix} H_1 \\ H_2 \end{pmatrix} = \begin{pmatrix} \cos \theta_s & -\sin \theta_s \\ \sin \theta_s & \cos \theta_s \end{pmatrix} \begin{pmatrix} h_1 \\ h_2 \end{pmatrix}, \quad (12)$$

where θ_s is the mixing angle which can be expressed as,

$$\theta_s = \frac{1}{2} \tan^{-1} \left(\frac{\frac{\lambda_1 v_1}{\lambda_\eta v_2}}{1 - \frac{\lambda_H v_1^2}{\lambda_\eta v_2^2}} \right). \quad (13)$$

Mass eigenvalues corresponding to the physical scalars H_1 and H_2 are given by,

$$M_{H_1} = \sqrt{\lambda_H v_1^2 + \lambda_\eta v_2^2 + \sqrt{(\lambda_H v_1^2 - \lambda_\eta v_2^2)^2 + (\lambda_1 v_1 v_2)^2}}, \quad (14)$$

$$M_{H_2} = \sqrt{\lambda_H v_1^2 + \lambda_\eta v_2^2 - \sqrt{(\lambda_H v_1^2 - \lambda_\eta v_2^2)^2 + (\lambda_1 v_1 v_2)^2}}. \quad (15)$$

Furthermore, similar to the \mathbb{Z}_2 -even sector, the \mathbb{Z}_2 -odd sector also exhibits mass mixing between ϕ^0 and S . This also happens when both H and η get nonzero VEVs and in this case the term proportional to λ_8 in $V(H, \eta, \Phi, S)$ is solely responsible for such mixing. Therefore, the \mathbb{Z}_2 -odd real singlet scalar S mixes with CP-even component ϕ^0 of the \mathbb{Z}_2 -odd doublet Φ . However, as there is no spontaneous CP-violation, the CP-odd component a^0 remains decoupled from the CP-even fields and with respect to the basis $\frac{1}{\sqrt{2}}(S \ \phi^0 \ a^0)^T$, the 3×3 odd-sector mixing matrix has a block diagonal form,

$$\mathcal{M}_{\text{DM}}^2 = \begin{pmatrix} (m_S^2 + v_1^2 \lambda_7 + v_2^2 \lambda_6) & \frac{v_1 v_2 \lambda_8}{\sqrt{2}} & 0 \\ \frac{v_1 v_2 \lambda_8}{\sqrt{2}} & \frac{1}{2} \{2m_\Phi^2 + v_1^2(\lambda_2 + \lambda_3) + v_2^2 \lambda_4\} & 0 \\ 0 & 0 & \frac{1}{2} \{2m_\Phi^2 + v_1^2(\lambda_2 + \lambda_3) + v_2^2 \lambda_4\} \end{pmatrix}. \quad (16)$$

One can easily diagonalise this matrix using an orthogonal transformation by an angle θ_D between S and ϕ^0 . Therefore, after diagonalisation we have three physical states ρ_1 , ρ_1 and ρ_3 , where ρ_1 and ρ_2 are orthogonal linear combinations of S and ϕ^0 while the remaining physical

scalar ρ_3 exactly coincides with a^0 . In matrix notation, the basis transformation can be shown as

$$\begin{pmatrix} \rho_1 \\ \rho_2 \\ \rho_3 \end{pmatrix} = \begin{pmatrix} \cos \theta_D & -\sin \theta_D & 0 \\ \sin \theta_D & \cos \theta_D & 0 \\ 0 & 0 & 1 \end{pmatrix} \begin{pmatrix} S \\ \phi^0 \\ a^0 \end{pmatrix}, \quad (17)$$

where the mixing angle θ_D can be expressed in terms of parameters of the Lagrangian as,

$$\theta_D = \frac{1}{2} \tan^{-1} \left(\frac{2\sqrt{2}v_1v_2\lambda_8}{2m_\Phi^2 - 2m_S^2 + v_1^2(\lambda_2 + \lambda_3 - 2\lambda_7) + v_2^2(\lambda_4 - 2\lambda_6)} \right). \quad (18)$$

Among the three states (ρ_1 , ρ_2 and ρ_3), we choose ρ_1 as the lightest odd particle (LOP) which is regarded as the stable dark matter candidate in this scenario. Thus, the dark matter candidate in this scenario is an admixture of singlet and doublet states. The expressions for the masses of these \mathbb{Z}_2 -odd scalar fields are given below

$$M_{\rho_1} = \sqrt{(m_S^2 + v_1^2\lambda_7 + v_2^2\lambda_6) \cos^2 \theta_D - \sqrt{2}v_1v_2\lambda_8 \cos \theta_D \sin \theta_D + M_{\rho_3}^2 \sin^2 \theta_D}, \quad (19)$$

$$M_{\rho_2} = \sqrt{(m_S^2 + v_1^2\lambda_7 + v_2^2\lambda_6) \sin^2 \theta_D + \sqrt{2}v_1v_2\lambda_8 \cos \theta_D \sin \theta_D + M_{\rho_3}^2 \cos^2 \theta_D}, \quad (20)$$

where

$$M_{\rho_3} = \sqrt{m_\Phi^2 + \frac{1}{2}[v_1^2(\lambda_2 + \lambda_3) + v_2^2\lambda_4]}. \quad (21)$$

Further using Eqs. (19-21), one can establish a relation between M_{ρ_1} , M_{ρ_2} , M_{ρ_3} and θ_D , which has the following form

$$M_{\rho_3}^2 = M_{\rho_1}^2 \sin^2 \theta_D + M_{\rho_2}^2 \cos^2 \theta_D. \quad (22)$$

Therefore, the mass of the CP-odd scalar ρ_3 is not an independent quantity in the present scenario and it becomes fixed though the above relation once we know other parameters like M_{ρ_1} , M_{ρ_2} and θ_D . This is a consequence of that, the 2×2 and 3×3 elements of the dark sector mixing matrix $\mathcal{M}_{\text{DM}}^2$ are identical. From the symmetry argument this can be understood as follows. The splitting between the coefficients of ϕ^{02} ($\propto 2 \times 2$ element of $\mathcal{M}_{\text{DM}}^2$) and a^{02} ($\propto 3 \times 3$ element of $\mathcal{M}_{\text{DM}}^2$) of a \mathbb{Z}_2 -odd doublet Φ is obtained from a term like $(H^\dagger \Phi)^2$ (usual λ_5 term in the Inert Doublet Model [102]), which is forbidden here by the $U(1)_{L_\mu - L_\tau}$ symmetry invariance. Additionally, in the dark sector we also have a charged scalar ϕ^\pm and its mass term is given by

$$M_{\phi^\pm} = \sqrt{M_{\rho_3}^2 - \frac{1}{2}v_1^2\lambda_3}. \quad (23)$$

Let us now find out the effects of the extra $U(1)_{L_\mu - L_\tau}$ local gauge symmetry on the gauge sector and generate the physical states of the gauge bosons with their proper mass terms. In the Eq. (3), \hat{B}_α and \hat{X}_α are denoted as gauge fields corresponding to gauge groups $U(1)_Y$ and

$U(1)_{L_\mu-L_\tau}$ respectively. As mentioned earlier, the kinetic terms for the two $U(1)$ gauge fields with hat notation are not diagonal and it is clearly evident from the presence of a mixing term between two $U(1)$ gauge fields proportional ϵ . The kinetic mixing parameters is severely constrained from the electroweak precision data (sensitive mainly in the low mass regime of the extra gauge boson) [116, 117] and also from di-lepton searches at the LHC (for relatively high mass regime i.e., few hundred GeV to few TeV range). Now, one can perform a basis transformation from “hat” states to “un-hat” states, due to which the off-diagonal kinetic term vanishes. This can be achieved by applying a following transformation⁶,

$$\begin{pmatrix} B_\alpha \\ X_\alpha \end{pmatrix} = \begin{pmatrix} 1 & -\epsilon \\ 0 & \sqrt{1-\epsilon^2} \end{pmatrix} \begin{pmatrix} \hat{B}_\alpha \\ \hat{X}_\alpha \end{pmatrix}, \quad (24)$$

and since experiment dictates $\epsilon \ll 1$, therefore using the approximation $\mathcal{O}(\epsilon^2) \approx 0$ we have

$$\hat{B}_\alpha \simeq B_\alpha + \epsilon X_\alpha \quad \text{and} \quad \hat{X}_\alpha \simeq X_\alpha. \quad (25)$$

After the occurrence of both electroweak symmetry breaking (EWSB)⁷ and $L_\mu - L_\tau$ breaking by the VEVs of the neutral components of H and η , we obtain a 3×3 mass square matrix in the basis of three neutral gauge bosons namely W_3^α , B^α , X^α using Eqs. (7-8, 25),

$$\mathcal{M}_{\text{gauge}}^2 = \begin{pmatrix} \frac{1}{4}g_2^2v_1^2 & -\frac{1}{4}g_2g_1v_1^2 & -\frac{1}{4}g_2g_1v_1^2\epsilon \\ -\frac{1}{4}g_2g_1v_1^2 & \frac{1}{4}g_1^2v_1^2 & \frac{1}{4}g_1^2v_1^2\epsilon \\ -\frac{1}{4}g_2g_1v_1^2\epsilon & \frac{1}{4}g_1^2v_1^2\epsilon & g_{Z_{\mu\tau}}^2v_2^2 \end{pmatrix}. \quad (26)$$

The above matrix has a special symmetry. If we rotate W_3^α and B^α by the Weinberg angle $\tan \theta_W = \frac{g_1}{g_2}$, the matrix $\mathcal{M}_{\text{gauge}}^2$ reduces to a 2×2 block diagonal structure with respect to an intermediate state $\mathcal{Z}^\alpha \equiv \cos \theta_W W_3^\alpha - \sin \theta_W B^\alpha$ and X^α while the other orthogonal state i.e. $A^\alpha = \sin \theta_W W_3^\alpha + \cos \theta_W B^\alpha$ having zero mass eigenvalue becomes completely decoupled. This is possible due to the special choice of the transformation matrix we have considered in Eq. (24). Now, once we reduce a 3×3 matrix to a 2×2 block diagonal form, we already have made our life very simple and next task is to perform another orthogonal transformation between the states \mathcal{Z}^α and X^α to finally get the physical Z and $Z_{\mu\tau}$ bosons. This is mathematically demonstrated below for both mass matrix as well as eigenstates,

⁶ This transformation matrix is not a unique one. For a general 2×2 real matrix, we have four independent elements. However, using $c_1 = c_2 = 1$ and $c_3 = 0$, we have only three independent equations to solve for four variables. Here, c_1 , c_2 and c_3 are coefficients of $\frac{1}{4}B_{\mu\nu}B^{\mu\nu}$, $\frac{1}{4}X_{\mu\nu}X^{\mu\nu}$ and $\frac{\epsilon}{2}B_{\mu\nu}X^{\mu\nu}$ respectively. Thus, one can express three elements in terms of the fourth one and for each real value of that element, we will have a different transformation matrix which eventually cancels the kinetic mixing term. For the particular matrix that we have used here is obtained by setting 2×1 element of the transformation matrix equal to zero. Such a special choice easily reproduces all the phenomena of electromagnetism.

⁷ In the present scenario, after EWSB one can readily determine the mass of the W^\pm gauge boson which is exactly equal to that of the SM, i.e., $M_W = \frac{1}{2}g_2v_1$.

$$\mathcal{M}_{\text{gauge}}^2 \xrightarrow{\mathcal{O}(\theta_W)} \begin{pmatrix} \frac{1}{4}(g_1^2 + g_2^2)v_1^2 & 0 & -\frac{\epsilon}{4}g_1\sqrt{g_1^2 + g_2^2}v_1^2 \\ 0 & 0 & 0 \\ -\frac{\epsilon}{4}g_1\sqrt{g_1^2 + g_2^2}v_1^2 & 0 & g_{Z_{\mu\tau}}^2 v_2^2 \end{pmatrix} \xrightarrow{\mathcal{O}(\theta_{\mu\tau})} \begin{pmatrix} M_Z & 0 & 0 \\ 0 & 0 & 0 \\ 0 & 0 & M_{Z_{\mu\tau}} \end{pmatrix} \quad (27)$$

and

$$\begin{pmatrix} W_3^\alpha \\ B^\alpha \\ X^\alpha \end{pmatrix} \xrightarrow{\mathcal{O}(\theta_W)^T} \begin{pmatrix} \mathcal{Z}_3^\alpha \\ A^\alpha \\ X^\alpha \end{pmatrix} \xrightarrow{\mathcal{O}(\theta_{\mu\tau})^T} \begin{pmatrix} Z^\alpha \\ A^\alpha \\ Z_{\mu\tau}^\alpha \end{pmatrix}, \quad (28)$$

where, the masses of two massive neutral gauge bosons (Z and $Z_{\mu\tau}$) are respectively given as

$$M_Z = \sqrt{\frac{g_2^2(v_1^2 + v_2^2)}{4} \cos^2 \theta_{\mu\tau} + g_{Z_{\mu\tau}}^2 v_2^2 \sin^2 \theta_{\mu\tau} + \frac{g_1 \sqrt{(g_1^2 + g_2^2)} v_1^2 \epsilon}{4} \sin 2\theta_{\mu\tau}}, \quad (29)$$

$$M_{Z_{\mu\tau}} = \sqrt{\frac{g_2^2(v_1^2 + v_2^2)}{4} \sin^2 \theta_{\mu\tau} + g_{Z_{\mu\tau}}^2 v_2^2 \cos^2 \theta_{\mu\tau} - \frac{g_1 \sqrt{(g_1^2 + g_2^2)} v_1^2 \epsilon}{4} \sin 2\theta_{\mu\tau}}, \quad (30)$$

and the two orthogonal transformation matrices are given by,

$$\mathcal{O}(\theta_W) = \begin{pmatrix} \cos \theta_W & \sin \theta_W & 0 \\ -\sin \theta_W & \cos \theta_W & 0 \\ 0 & 0 & 1 \end{pmatrix}, \quad \mathcal{O}(\theta_{\mu\tau}) = \begin{pmatrix} \cos \theta_{\mu\tau} & 0 & \sin \theta_{\mu\tau} \\ 0 & 1 & 0 \\ -\sin \theta_{\mu\tau} & 0 & \cos \theta_{\mu\tau} \end{pmatrix}. \quad (31)$$

Finally, the gauge basis and the mass basis of the neutral gauge bosons are related the following orthogonal transformation

$$\begin{pmatrix} Z^\alpha \\ A^\alpha \\ Z_{\mu\tau}^\alpha \end{pmatrix} = \mathcal{O}(\theta_W, \theta_{\mu\tau})^T \begin{pmatrix} W_3^\alpha \\ B^\alpha \\ X^\alpha \end{pmatrix}, \quad (32)$$

with

$$\begin{aligned} \mathcal{O}(\theta_W, \theta_{\mu\tau})^T &= \mathcal{O}(\theta_{\mu\tau})^T \mathcal{O}(\theta_W)^T \\ &= \begin{pmatrix} \cos \theta_{\mu\tau} \cos \theta_W & -\cos \theta_{\mu\tau} \sin \theta_W & -\sin \theta_{\mu\tau} \\ \sin \theta_W & \cos \theta_W & 0 \\ \sin \theta_{\mu\tau} \cos \theta_W & -\sin \theta_{\mu\tau} \sin \theta_W & \cos \theta_{\mu\tau} \end{pmatrix}, \end{aligned} \quad (33)$$

where θ_W , as mentioned above, is the familiar Weinberg angle and $\theta_{\mu\tau}$ is the mixing angle between two neutral gauge bosons Z and $Z_{\mu\tau}$. These mixing angles can be expressed in terms gauge coupling constants, VEVs and the kinetic mixing parameters as follows,

$$\theta_W = \tan^{-1} \left(\frac{g_1}{g_2} \right), \quad \theta_{\mu\tau} = \frac{1}{2} \tan^{-1} \left(\frac{\frac{2\epsilon g_1}{\sqrt{g_1^2 + g_2^2}}}{1 - \frac{4g_{Z_{\mu\tau}}^2 v_2^2}{g_1^2 + g_2^2 v_1^2}} \right). \quad (34)$$

Before we proceed any further, it is worthwhile to mention about the independent parameters. In this model, in addition to the SM parameters, we have fourteen new parameters in the scalar sector (excluding SM-Like Higgs boson mass and VEV v_1), three additional Yukawa like coupling constants and one mass term in the extended quark sector⁸ and two more couplings in the gauge sector in the form of new gauge coupling $g_{Z\mu\tau}$ and kinetic mixing parameter ϵ . These twenty independent parameters are: M_{H_2} , M_{ϕ^\pm} , M_{ρ_1} , M_{ρ_2} , $M_{Z\mu\tau}$, θ_D , θ_s , λ_Φ , λ_S , λ_2 , λ_4 , λ_5 , λ_6 , λ_7 , f_1 , f_2 , f_3 , M_χ , $g_{Z\mu\tau}$ and $\theta_{\mu\tau}$. In terms of these independent parameters the other parameters appearing in the Lagrangian (Eq. (2)) can be obtained using Eqs. (13-15), Eqs. (18, 19), Eqs. (21, 23) and Eqs. (30, 34)⁹.

III. $b \rightarrow s$ FLAVOUR OBSERVABLES

A. $R_{K^{(*)}}$ anomalies

In the present scenario the NP part of the effective Hamiltonian $\mathcal{H}_{\text{eff}} (\equiv \mathcal{H}_{\text{eff}}^{\text{SM}} + \mathcal{H}_{\text{eff}}^{\text{NP}})$ that describes the $b \rightarrow s \ell \ell$ transitions is given by

$$\mathcal{H}_{\text{eff}}^{\text{NP}} = -\frac{4G_F}{\sqrt{2}} V_{tb} V_{ts}^* \frac{e^2}{16\pi^2} \sum_{\ell=e,\mu} C_{9\ell}^{\text{NP}} (\bar{s}\gamma_\alpha P_L b) (\bar{\ell}\gamma^\alpha \ell) + C_{10\ell}^{\text{NP}} (\bar{s}\gamma_\alpha P_L b) (\bar{\ell}\gamma^\alpha \gamma_5 \ell) + \text{h.c.}, \quad (35)$$

where G_F is the Fermi constant, V_{ij} are the Cabibbo-Kobayashi-Maskawa (CKM) matrix elements. Here we neglect other dimension-six operators for example, C_7 can not give significant contributions to the processes, because it corresponds to the dipole operator that is strictly constrained by branching ratio of $B \rightarrow X_s \gamma$ [118]. Also four-quark operators [119] cannot play any significant role for the violation of LFU, hence they are irrelevant in this work. Moreover, four-fermion contact interactions with scalar currents could be a natural source of LFU violation, although they are highly constrained by existing measurements of the $B_s \rightarrow \mu^+ \mu^-$ and $B_s \rightarrow e^+ e^-$ branching ratios [120, 121]. The NP contribution to the WC $C_9^{\text{NP},\ell} = C_{9Z}^\ell + C_{9Z\mu\tau}^\ell$

⁸ Here, we are not considering Yukawa like coupling constants and bare mass terms in the extended neutrino sector.

⁹ Additionally, one needs to use minimization conditions of the scalar potential $V(H, \eta, \Phi, S)$.

can be obtained from

$$\begin{aligned}
C_{9Z(Z_{\mu\tau})}^\ell = & -\frac{\sqrt{2}}{16\pi\alpha_{\text{em}}G_FV_{tb}V_{ts}^*}\frac{\mathcal{L}_{Z(Z_{\mu\tau})}^9}{M_{Z(Z_{\mu\tau})}^2}\left(-\frac{\mathcal{G}_{Z(Z_{\mu\tau})}f_2f_3}{4}\left[-2\ln(m_\chi^2)-1\right.\right. \\
& \left.+h_q(x_1)(1-2x_1)\sin^2\theta_D+h_q(x_2)(1-2x_2)\cos^2\theta_D+h_q(x_3)(1-2x_3)\right] \\
& +\frac{\mathcal{C}_{Z(Z_{\mu\tau})}f_2f_3}{4}\left[\{-\ln(M_{\rho_1}^2)+h_w(x_1,r_1)\}\sin^2\theta_D+\{-\ln(M_{\rho_2}^2)+h_w(x_2,r_2)\}\cos^2\theta_D\right] \\
& -\frac{\mathcal{S}_{Z(Z_{\mu\tau})}f_2f_3}{4}\left[\{-\ln(M_{\rho_1}^2)+h_s(x_1)\}\sin^2\theta_D+\{-\ln(M_{\rho_2}^2)+h_s(x_2)\}\cos^2\theta_D\right. \\
& \left.\left.+\{-\ln(M_{\rho_3}^2)+h_s(x_3)\}\right]\right), \tag{36}
\end{aligned}$$

while the NP contribution to the WC $C_{10}^{\text{NP},\ell} = C_{10Z}^\ell + C_{10Z_{\mu\tau}}^\ell$ is given by

$$\begin{aligned}
C_{10Z(Z_{\mu\tau})}^\ell = & -\frac{\sqrt{2}}{16\pi\alpha_{\text{em}}G_FV_{tb}V_{ts}^*}\frac{\mathcal{L}_{Z(Z_{\mu\tau})}^{10}}{M_{Z(Z_{\mu\tau})}^2}\left(-\frac{\mathcal{G}_{Z(Z_{\mu\tau})}f_2f_3}{4}\left[-2\ln(m_\chi^2)-1\right.\right. \\
& \left.+h_q(x_1)(1-2x_1)\sin^2\theta_D+h_q(x_2)(1-2x_2)\cos^2\theta_D+h_q(x_3)(1-2x_3)\right] \\
& +\frac{\mathcal{C}_{Z(Z_{\mu\tau})}f_2f_3}{4}\left[\{-\ln(M_{\rho_1}^2)+h_w(x_1,r_1)\}\sin^2\theta_D+\{-\ln(M_{\rho_2}^2)+h_w(x_2,r_2)\}\cos^2\theta_D\right] \\
& -\frac{\mathcal{S}_{Z(Z_{\mu\tau})}f_2f_3}{4}\left[\{-\ln(M_{\rho_1}^2)+h_s(x_1)\}\sin^2\theta_D+\{-\ln(M_{\rho_2}^2)+h_s(x_2)\}\cos^2\theta_D\right. \\
& \left.\left.+\{-\ln(M_{\rho_3}^2)+h_s(x_3)\}\right]\right), \tag{37}
\end{aligned}$$

although we have found that the contribution of $C_{10}^{\text{NP},\ell}$ ($\ell \equiv \mu$) is insignificant¹⁰ and we will focus only on $C_{9Z(Z_{\mu\tau})}^\ell$ ($\ell \equiv \mu$) in rest of the analysis¹¹. α_{em} is the fine structure constant. Here $x_{1,2,3} = \frac{M_\chi^2}{M_{\rho_{1,2,3}}^2}$ and $r_{1,2} = \frac{M_{\rho_3}^2 - M_{\rho_{1,2}}^2}{M_{\rho_{1,2}}^2}$. The expressions of the factors $\mathcal{G}_{Z(Z_{\mu\tau})}$, $\mathcal{C}_{Z(Z_{\mu\tau})}$, $\mathcal{S}_{Z(Z_{\mu\tau})}$, $\mathcal{L}_{Z(Z_{\mu\tau})}^9$, $\mathcal{L}_{Z(Z_{\mu\tau})}^{10}$ and the functions $h_q(x)$, $h_w(x,r)$, $h_s(x)$ are given in the Appendix A. In Fig. 1 we have shown relevant Feynman diagrams responsible for the additional contribution to the $b \rightarrow s\mu\mu$ transition. It is clearly evident from these Feynman diagrams that the NP contribution to the WC $C_9^{\text{NP},\ell}$ is provided by the non-standard bottom like fermion field χ and the dark matter candidate ρ_1 with its partners ρ_2 and ρ_3 . Later we provide the dark matter phenomenology of a weakly interacting massive particle (WIMP) type dark matter candidate ρ_1 and related issues by considering the constraints of flavour physics observables that we

¹⁰ Due to this reason there is no significant NP contribution to the decay $B_s \rightarrow \mu^+\mu^-$. Therefore, there is no stringent constraint from the branching ratio of this process to our analysis.

¹¹ Therefore, the present scenario can be considered as a typical scenario which can provide the NP contribution to C_9^ℓ ($\ell \equiv \mu$) only. Although, there is a NP contribution to C_9^e but practically it has no significance due to very small mixing between Z and $Z_{\mu\tau}$. Hence, the coupling between $Z_{\mu\tau}$ and e^+e^- pair is effectively vanishing in nature.

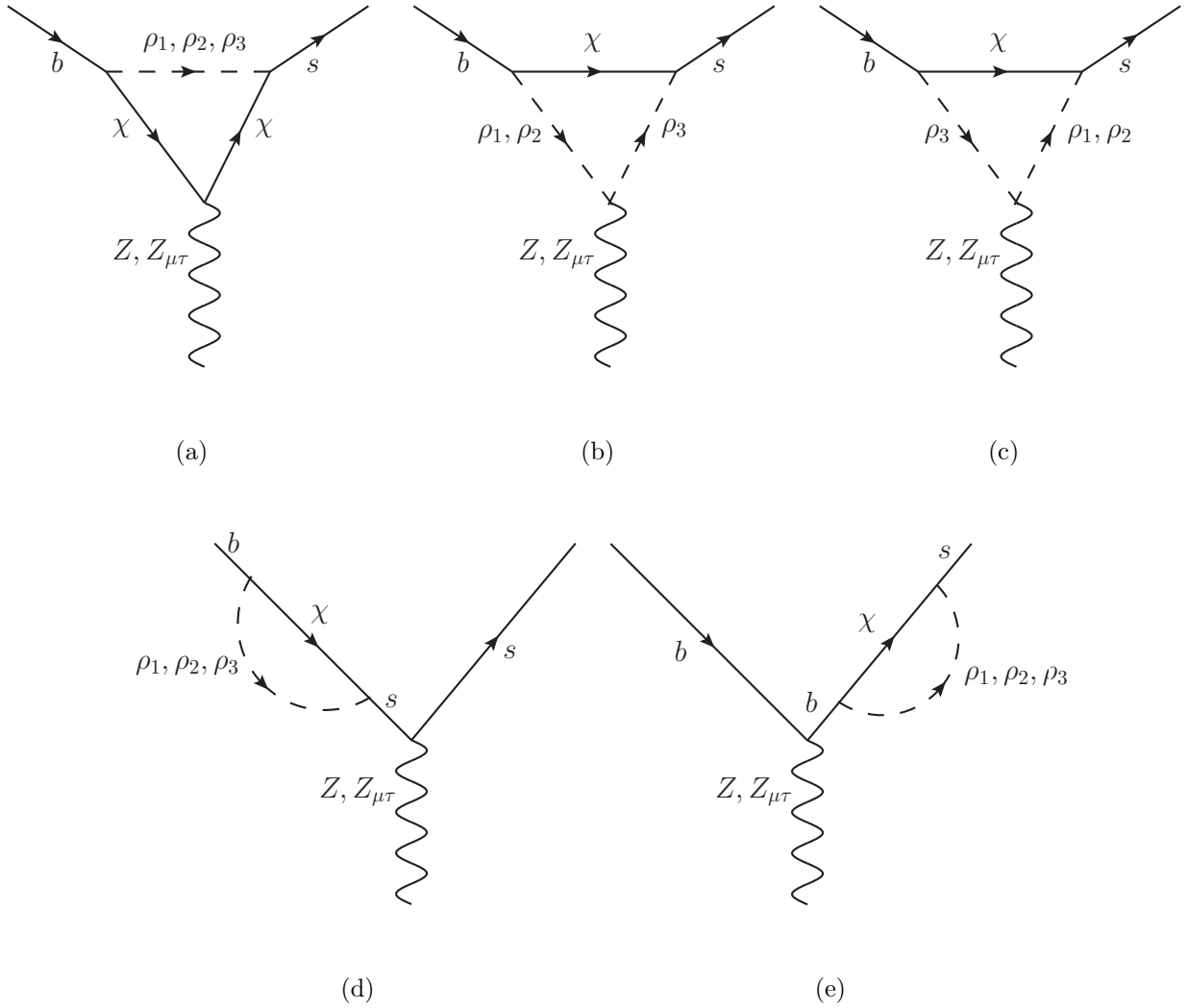
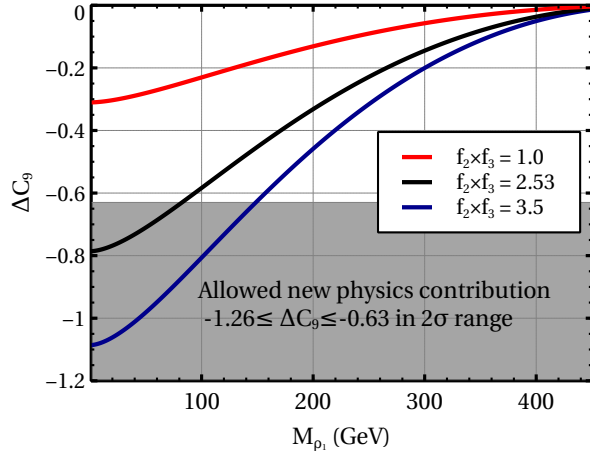


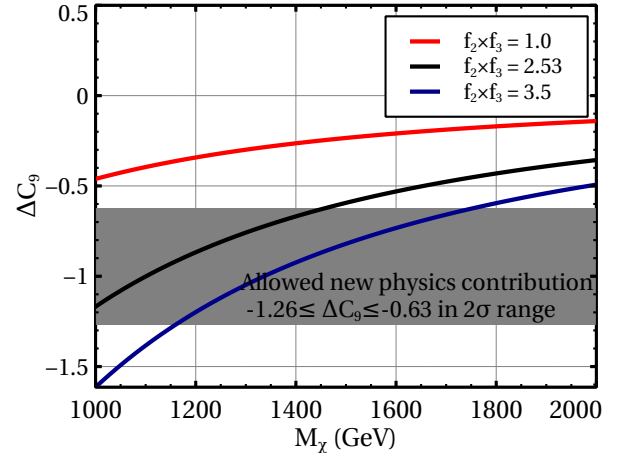
Figure 1: Z and $Z_{\mu\tau}$ -penguin and self-energy diagrams that contribute to the decay of $b \rightarrow s\mu\mu$ in addition to SM contribution.

have considered in this article. To ameliorate the tension between the SM prediction and experimental data for $R_{K^{(*)}}$ we use $C_9^{\text{NP},\mu} \in [-1.26, -0.63]$ [27] in 2σ interval. For the purpose of notational simplicity, from now and onwards, we use ΔC_9 for the total NP contributions to the WC C_9 for $\ell = \mu$, i.e., $C_9^{\text{NP},\mu} = C_9^\mu + C_9^{\mu\tau} = \Delta C_9$.

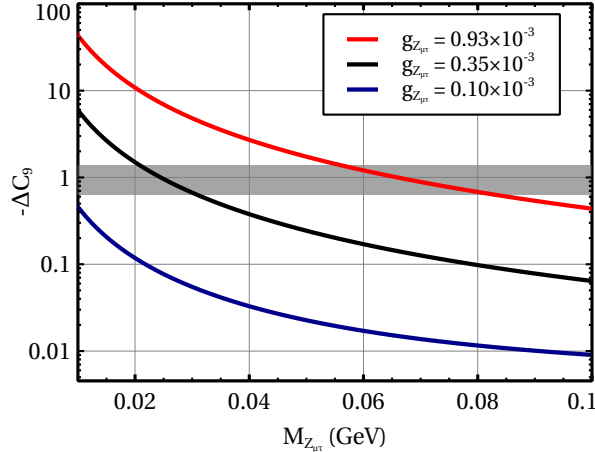
In order to understand the dependence of ΔC_9 on the model parameters we have shown the variation of ΔC_9 in Fig. 2. In this figure there are four panels which represent the variation of ΔC_9 with respect to four important parameters namely M_{ρ_1} , M_χ , $M_{Z_{\mu\tau}}$ and θ_D . In Fig. 2a, we have shown the variation of ΔC_9 with mass of ρ_1 for three different values of the product of Yukawa couplings f_2 and f_3 . Here, one can see that the magnitude of ΔC_9 increases with decreasing values of mass of ρ_1 which enters into loop diagrams (see Feynman diagrams shown in Fig. 1). Consequently, the loop functions are enhanced which in turn increase the magnitude of ΔC_9 . Moreover, as the NP contributions to the WC C_9 (Eq. (36)) is proportional to Yukawa



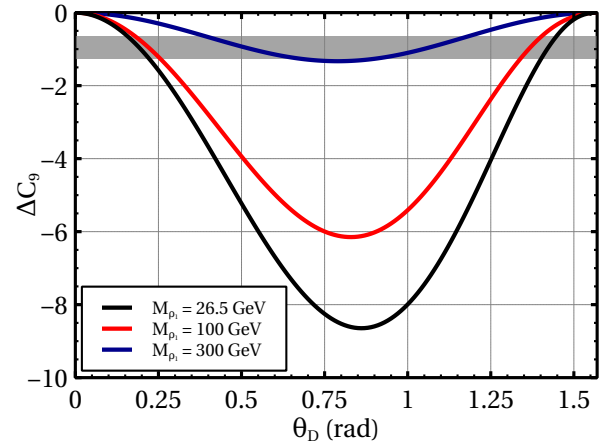
(a) Variation of ΔC_9 with M_{ρ_1} for $M_{\rho_2} = 506$ GeV, $M_\chi = 1300$ GeV, $g_{Z\mu\tau} = 0.93 \times 10^{-3}$, $M_{Z\mu\tau} = 0.076$ GeV and $\theta_D = 0.095$ rad.



(b) Variation of ΔC_9 with M_χ for $M_{\rho_2} = 506$ GeV, $M_{\rho_1} = 26.5$ GeV, $g_{Z\mu\tau} = 0.93 \times 10^{-3}$, $M_{Z\mu\tau} = 0.076$ GeV and $\theta_D = 0.095$ rad.



(c) Variation of ΔC_9 with $M_{Z\mu\tau}$ for $M_{\rho_1} = 26.5$ GeV, $M_{\rho_2} = 506$ GeV, $M_\chi = 1300$ GeV, $f_2 \times f_3 = 2.53$ and $\theta_D = 0.095$ rad.



(d) Variation of ΔC_9 with θ_D for $M_{\rho_2} = 506$ GeV, $M_\chi = 1300$ GeV, $M_{Z\mu\tau} = 0.076$ GeV, $g_{Z\mu\tau} = 0.93 \times 10^{-3}$ and $f_2 \times f_3 = 0.8$.

Figure 2: Variation of ΔC_9 with respect to different parameters.

couplings f_2 and f_3 , the magnitude of ΔC_9 enhances with $f_2 \times f_3$. This feature is also clearly demonstrated in Fig. 2a. Similar to this plot, in Fig. 2b, we have illustrated the effect of M_χ on ΔC_9 for the same three different values of $f_2 \times f_3$. Here also we have found similar behaviour of ΔC_9 with respect to M_χ as we have observed for M_{ρ_1} . Further, we have also displayed the effect of non-standard gauge boson mass $M_{Z\mu\tau}$ on ΔC_9 in Fig. 2c for three different values of gauge coupling $g_{Z\mu\tau} = 0.93 \times 10^{-3}$, 0.35×10^{-3} and 0.1×10^{-3} respectively. In this case, the magnitude of ΔC_9 decreases caused by the propagator suppression for larger values of $M_{Z\mu\tau}$. It is clearly seen from Eq. (36), where ΔC_9 is inversely proportional to $M_{Z\mu\tau}^2$. On the other hand, in this plot ΔC_9 increases significantly with the gauge coupling $g_{Z\mu\tau}$ for the considered

mass range of $M_{Z_{\mu\tau}}$ ($0.01 \leq M_{Z_{\mu\tau}} \text{ (GeV)} \leq 0.1$). Finally, in Fig. 2d we have demonstrated the variation of ΔC_9 with respect to the dark sector mixing angle θ_D for three different choices of M_{ρ_1} . In this plot, we have varied θ_D in range 0 to $\pi/2$. The oscillatory behaviour of ΔC_9 with respect to θ_D is due the combined effects of two factors. One is the direct involvement of sine and cosine functions within the expressions of ΔC_9 . Another one is the indirect effect due to the change of M_{ρ_3} with θ_D , where the former undergoes a full oscillation between M_{ρ_2} to M_{ρ_1} via Eq. (22) when θ_D changes from 0 to π . The morphology of ΔC_9 with respect to θ_D fits pretty well with a function like $-A \sin^2(2\theta_D)$, where the exact value of the normalisation constant A depends on the values of other parameters namely, M_{ρ_1} , M_{ρ_2} , $g_{Z_{\mu\tau}}$, $M_{Z_{\mu\tau}}$ and M_χ . Moreover, the oscillatory behaviour of ΔC_9 vanishes if we set $M_{\rho_1} = M_{\rho_2}$. Under this condition, the dependence of θ_D disappears from the expression of M_{ρ_3} and consequently ΔC_9 becomes independent of θ_D . Furthermore, in all the four plots of Fig. 2, the grey coloured band represents 2σ range allowed range of fit value of ΔC_9 for explaining $R_{K^{(*)}}$ anomalies [27].

B. $B \rightarrow X_s \gamma$

The measurement of inclusive radiative B decay process like $B \rightarrow X_s \gamma$ has also been shown deviation from the corresponding SM prediction. The world average experimental value of the branching ratio of this process is [122]

$$\text{Br}^{\text{Exp}}(B \rightarrow X_s \gamma) = (3.32 \pm 0.16) \times 10^{-4}, \quad (38)$$

for photon energy $E_\gamma > 1.6 \text{ GeV}$ in the B -meson rest frame. Under the same conditions the corresponding SM prediction with higher order corrections is [123]

$$\text{Br}^{\text{SM}}(B \rightarrow X_s \gamma) = (3.36 \pm 0.23) \times 10^{-4}. \quad (39)$$

It is quite evident that the theoretical prediction is in good agreement with the experimental value. Hence this small difference can tightly constrain any NP which contributes to this process. Keeping this in mind we have evaluated the NP contributions to this decay process in the present scenario. Consequently, we use the branching ratio of this process as one of the constraints in our analysis.

At quark level $B \rightarrow X_s \gamma$ decay is indicated by $b \rightarrow s \gamma$ transition. The effective Hamiltonian for this transition at the bottom quark mass ($\mu_b = m_b$) scale is given by (see ref. [124, 125])

$$\mathcal{H}_{\text{eff}}(b \rightarrow s \gamma) = -\frac{G_F}{\sqrt{2}} V_{ts}^* V_{tb} \left[\sum_{i=1}^6 C_i(\mu_b) \mathcal{O}_i + C_{7\gamma}(\mu_b) \mathcal{O}_{7\gamma} + C_{8G}(\mu_b) \mathcal{O}_{8G} \right]. \quad (40)$$

At first the WCs (C_i) have been calculated at electroweak scale (μ_W) and using renormalisation group (RG) equations [124–126] they are evolved down to $\mu_b = m_b$ scale. The local operators $\mathcal{O}_1, \dots, \mathcal{O}_6$ represent four quark interactions and the explicit form of these operators can be found in [127]. The remaining operators $\mathcal{O}_{7\gamma}$ (electromagnetic dipole) and \mathcal{O}_{8G} (chromomagnetic

dipole) which are the most important for this decay and the expressions for these operators at the leading order are given by

$$\mathcal{O}_{7\gamma} = \frac{e}{8\pi^2} m_b \bar{s}_{\alpha'} \sigma^{\alpha\beta} (1 + \gamma_5) b^{\alpha'} F_{\alpha\beta}, \quad \mathcal{O}_{8G} = \frac{g_s}{8\pi^2} m_b \bar{s}_{\alpha'} \sigma^{\alpha\beta} (1 + \gamma_5) \Lambda_{\alpha'\beta'}^a b^{\beta'} G_{\alpha\beta}^a, \quad (41)$$

with $\sigma^{\alpha\beta} = \frac{i}{2}[\gamma^\alpha, \gamma^\beta]$. The expressions of the WCs at μ_b scale is given by

$$C_{7\gamma}^{(0)eff}(\mu_b) = \eta_{23}^{16} C_{7\gamma}^{(0)}(\mu_W) + \frac{8}{3} \left(\eta_{23}^{14} - \eta_{23}^{16} \right) C_{8G}^{(0)}(\mu_W) + C_2^{(0)}(\mu_W) \sum_{i=1}^8 h_i \eta^{a_i}, \quad (42)$$

$$C_{8G}^{(0)eff}(\mu_b) = \eta_{23}^{14} C_{8G}^{(0)}(\mu_W) + C_2^{(0)}(\mu_W) \sum_{i=1}^8 \bar{h}_i \eta^{a_i}, \quad (43)$$

with

$$\eta = \frac{\alpha_s(\mu_W)}{\alpha_s(\mu_b)}, \quad \alpha_s(\mu_b) = \frac{\alpha_s(M_Z)}{1 - \beta_0 \frac{\alpha_s(M_Z)}{2\pi} \ln(M_Z/\mu_b)}, \quad \beta_0 = \frac{23}{3}, \quad (44)$$

and

$$C_2^{(0)}(\mu_W) = 1, \quad (45)$$

$$C_{7\gamma}^{(0)}(\mu_W) = -\frac{1}{2} D'(x_t, x_1, x_2, x_3) = -\frac{1}{2} \{ (D'_0(x_t) + D'(x_1, x_2, x_3)) \}, \quad (46)$$

$$C_{8G}^{(0)}(\mu_W) = -\frac{1}{2} E'(x_t, x_1, x_2, x_3) = -\frac{1}{2} \{ (E'_0(x_t) + E'(x_1, x_2, x_3)) \}. \quad (47)$$

Apart from these other WCs vanish at the electroweak scale μ_W . The superscript “0” indicates the leading logarithmic (LO) approximation. The values of a_i , h_i and \bar{h}_i can be obtained from [126]. The total (SM+NP) contribution at the LO is represented by the functions $D'(x_t, x_1, x_2, x_3)$ and $E'(x_t, x_1, x_2, x_3)$ while the functions $D'_0(x_t)$ and $E'_0(x_t)$ are designated as the corresponding SM contributions at the electroweak scale [128]

$$D'_0(x_t) = -\frac{(8x_t^3 + 5x_t^2 - 7x_t)}{12(1-x_t)^3} + \frac{x_t^2(2-3x_t)}{2(1-x_t)^4} \ln x_t, \quad (48)$$

$$E'_0(x_t) = -\frac{(x_t^3 - 5x_t^2 - 2x_t)}{4(1-x_t)^3} + \frac{3}{2} \frac{x_t^2}{(1-x_t)^4} \ln x_t, \quad (49)$$

with $x_t \equiv \frac{m_t^2}{M_W^2}$. The functions corresponding to electromagnetic and chromomagnetic dipole operators due to the NP particles (generated from Fig. 3) are given in the following respectively

$$D'(x_1, x_2, x_3) = -\frac{\sqrt{2}}{G_F V_{tb}^* V_{ts}} \frac{f_2 f_3}{8} \frac{1}{3} \left(\frac{\sin^2 \theta_D}{M_{\rho_1}^2} h_b(x_1) + \frac{\cos^2 \theta_D}{M_{\rho_2}^2} h_b(x_2) + \frac{1}{M_{\rho_3}^2} h_b(x_3) \right), \quad (50)$$

$$E'(x_1, x_2, x_3) = \frac{\sqrt{2}}{G_F V_{tb}^* V_{ts}} \frac{f_2 f_3}{8} \left(\frac{\sin^2 \theta_D}{M_{\rho_1}^2} h_b(x_1) + \frac{\cos^2 \theta_D}{M_{\rho_2}^2} h_b(x_2) + \frac{1}{M_{\rho_3}^2} h_b(x_3) \right), \quad (51)$$

$$(52)$$

while the function $h_b(x)$ is given in the Appendix A.

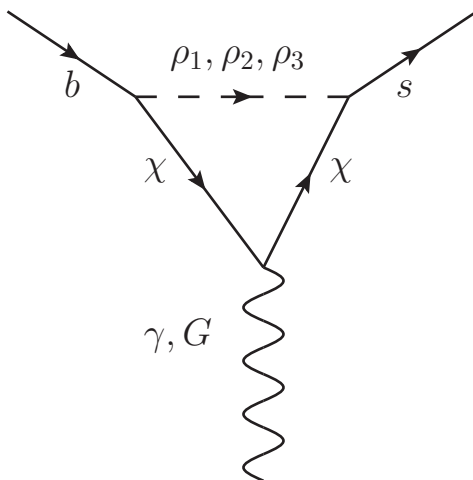


Figure 3: The possible electromagnetic and chromomagnetic penguin diagrams that are contributed to the decay $B \rightarrow X_s \gamma$ in addition to the SM.

In SM the branching ratio of $B \rightarrow X_s \gamma$ has been estimated at a very high level of accuracy including higher order QED and QCD corrections. For example in refs. [129, 130] one can find the full next-to leading order (NLO) QCD and QED corrections for this process in two different ways. The present precision level of experimental data requires that one should also include next-to-next-to leading order (NNLO) QCD corrections in this analysis. In this regard the first effort to measure NNLO QCD corrections for this process in SM was described in ref. [131]. Finally in a recent article [123] one can find an updated and more complete NNLO QCD corrections to this process. Using the [123] one can calculate the branching ratio of $B \rightarrow X_s \gamma$ incorporating NNLO QCD corrections in NP scenario. Therefore, in the current article we also follow the same approach¹² (as given in [123]) to measure NP contribution for this process with NNLO QCD corrections

$$\text{Br}^{\text{NNLO}}(B \rightarrow X_s \gamma) \times 10^4 = (3.36 \pm 0.23) - 8.22\Delta C_7 - 1.99\Delta C_8. \quad (53)$$

Here ΔC_7 and ΔC_8 represent for the NP contributions to WCs for electromagnetic and chromomagnetic dipole operators. In our convention, $\Delta C_7 = -\frac{1}{2}D'(x_1, x_2, x_3)$ and $\Delta C_8 = -\frac{1}{2}E'(x_1, x_2, x_3)$.

¹² This approach has also been used in the context of other BSM scenarios to measure the NP effects for this process: for example for nonminimal universal extra dimensional model [132] and for two higgs doublet model [133].

IV. $(g - 2)_\mu$ ANOMALY

Using Dirac equation one can define the magnetic moment \vec{M} of muon in terms of its spin \vec{S} and gyromagnetic ratio (g_μ) in the following way

$$\vec{M} = g_\mu \frac{e}{2m_\mu} \vec{S}, \quad (54)$$

which is one of the most accurately measured physical quantities. Ideally the value of g_μ is equal to “2”. In SM one can easily calculate the one loop correction to this quantity and that gives marginal shift from “2”. Hence, to measure the deviation of g_μ from its tree level value one can define a quantity namely

$$a_\mu = \frac{g_\mu - 2}{2}. \quad (55)$$

This quantity has been precisely measured by the CERN experiments and later on by the E821 experiment. The current average experimental value is [12]

$$a_\mu^{\text{exp}} = 116592091.0 \pm 54 \pm 33 \times 10^{-11}. \quad (56)$$

On the other hand total theoretical prediction of this quantity considering all kinds of source of contributions in SM is [12]

$$a_\mu^{\text{th}} = 116591823.1 \pm 34 \pm 26 \times 10^{-11}. \quad (57)$$

It is quite evident from the above Eqs. 56 and 57 that both the experimentally measured and theoretically predicted values of a_μ are close to each other, however there still exists some disagreement between these two quantities at the 3.5σ significance which is [12],

$$\Delta a_\mu = a_\mu^{\text{exp}} - a_\mu^{\text{SM}} = 268 \pm 63 \pm 43 \times 10^{-11}. \quad (58)$$

Therefore, this anomaly with respect to the SM expectation requires the interference of BSM theories where one obtains extra contributions from some NP particles. In the present model¹³, apart from the SM contribution, we have two additional one loop diagrams (see Fig. 4) in which the extra neutral gauge boson $Z_{\mu\tau}$ and extra CP-even scalar H_2 are involved.

¹³ See Ref. [134] for a review on $(g - 2)_\mu$ in various BSM extensions.

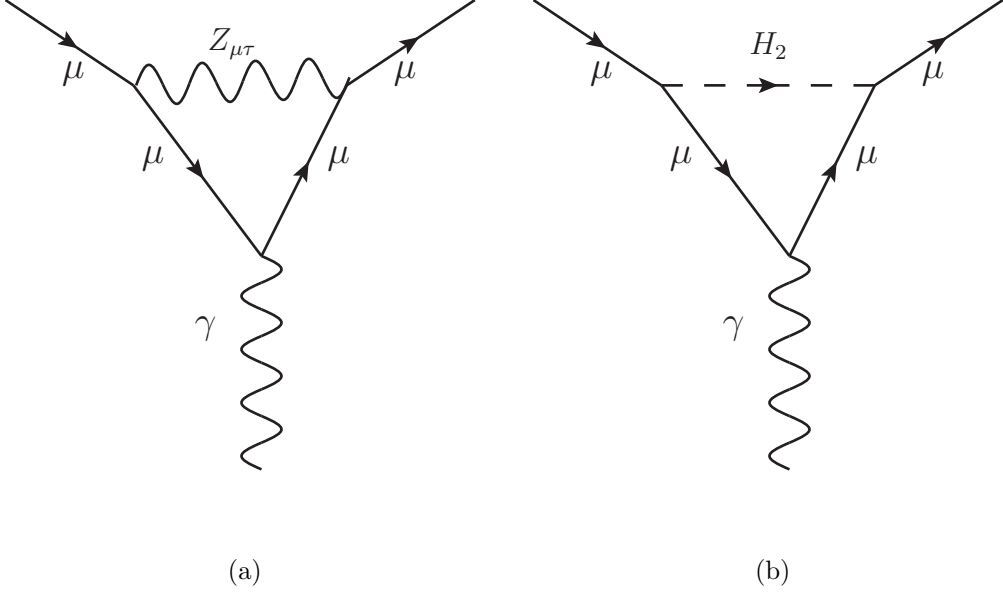


Figure 4: Relevant penguin diagrams that are contributed to the $(g - 2)_\mu$ in addition to the SM.

The additional contribution from Fig. 4a is given by [80, 135],

$$\delta a_{\mu}^{Z_{\mu\tau}} = \frac{1}{8\pi^2} \left(a_{Z_{\mu\tau}}^2 F_{Z_{\mu\tau}}^a(R_{Z_{\mu\tau}}) - b_{Z_{\mu\tau}}^2 F_{Z_{\mu\tau}}^b(R_{Z_{\mu\tau}}) \right) \quad (59)$$

with $R_{Z_{\mu\tau}} \equiv M_{Z_{\mu\tau}}^2/m_\mu^2$ and

$$a_{Z_{\mu\tau}} = \frac{g_2}{4 \cos \theta_W} (1 - 4 \sin^2 \theta_W) \sin \theta_{\mu\tau} - \left(g_{Z_{\mu\tau}} - \frac{3}{4} \frac{g_2 \sin \theta_W \epsilon}{\cos \theta_W} \right) \cos \theta_{\mu\tau} , \quad (60)$$

$$b_{Z_{\mu\tau}} = - \frac{g_2}{4 \cos \theta_W} \left(\sin \theta_{\mu\tau} - \sin \theta_W \epsilon \cos \theta_{\mu\tau} \right) , \quad (61)$$

$$F_{Z_{\mu\tau}}^a(R_{Z_{\mu\tau}}) = \int_0^1 dx \frac{2x(1-x)^2}{(1-x)^2 + R_{Z_{\mu\tau}}x} , \quad (62)$$

$$F_{Z_{\mu\tau}}^b(R_{Z_{\mu\tau}}) = \int_0^1 dx \frac{2(1-x)(3+x)}{(1-x)^2 + R_{Z_{\mu\tau}}x} . \quad (63)$$

Furthermore, the contribution from the extra CP-even scalar H_2 is given by [136, 137]

$$\delta a_{\mu}^{H_2} = \frac{G_F m_\mu^2}{4\pi^2 \sqrt{2}} \sin^2 \theta_s R_{H_2} F_{H_2}(R_{H_2}) , \quad (64)$$

$$(65)$$

with $R_{H_2} \equiv m_\mu^2/M_{H_2}^2$ and

$$F_{H_2}(R_{H_2}) = \int_0^1 dx \frac{x^2(2-x)}{R_{H_2}x^2 - x + 1} . \quad (66)$$

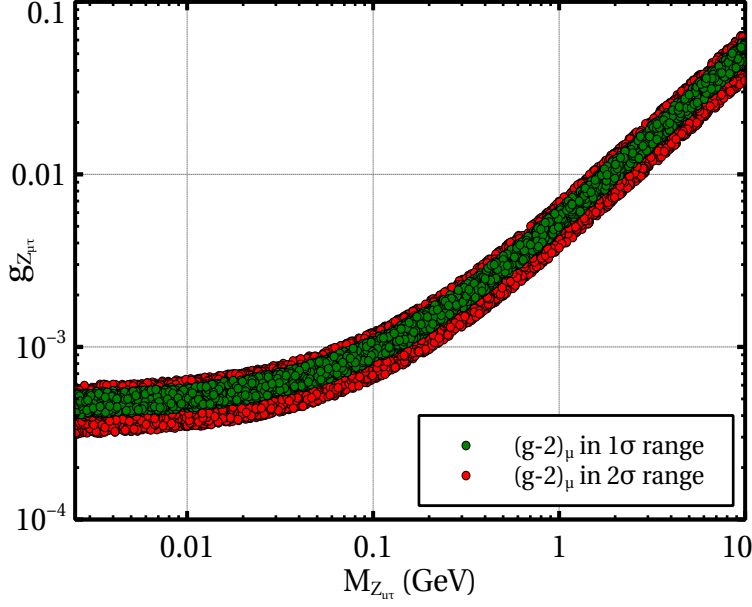


Figure 5: Allowed region in $g_{Z_{\mu\tau}} - M_{Z_{\mu\tau}}$ plane which explains the deviation between theoretical (SM) prediction and experimental result in 1σ (green coloured points) and 2σ (red coloured points) ranges respectively.

However, we have checked that the contribution of CP-even scalar H_2 is insignificant with respect to $Z_{\mu\tau}$ in the allowed parameter space.

In Fig. 5, we have shown the allowed region of $M_{Z_{\mu\tau}}$ and $g_{Z_{\mu\tau}}$ in $g_{Z_{\mu\tau}} - M_{Z_{\mu\tau}}$ plane by red coloured points, which can explain the discrepancy between theoretical prediction (SM) and experimentally measurable value of the anomalous magnetic moment of muon in 2σ range. The corresponding 1σ allowed region is also indicated by green coloured points. We will come back to this parameter space ($g_{Z_{\mu\tau}} - M_{Z_{\mu\tau}}$ plane) with a detailed analysis, which includes constraints like dark matter relic density, direct detection, observables related to rare B -meson decays ($R_{K^{(*)}}$, $\text{Br}(B \rightarrow X_s \gamma)$) and also bounds from ongoing and future experiments like CCFR, LHC, DUNE, Borexino etc. in the next section (see Fig. 12 and related discussions).

V. DARK MATTER

We are in a stage, where we can discuss dark matter phenomenology. The scalar sector of the present scenario contains two \mathbb{Z}_2 -odd scalar representations, one of them is an $\text{SU}(2)_L$ doublet Φ having a nonzero $L_\mu - L_\tau$ charge while the rest is a gauge singlet scalar S . As we have seen earlier in the Section II, the term proportional to λ_8 in the scalar potential (Eq. 10) enforces a mixing between the CP-even component ϕ^0 of the doublet Φ and the singlet S . Therefore, in the odd sector we have three physical neutral scalars namely, ρ_1 , ρ_2 and ρ_3 , out of which ρ_1 and ρ_2 are two mutually orthogonal linear combinations of S and ϕ^0 while ρ_3 coincides with the CP-odd component a^0 as the latter does not have any mixing with others. Being

\mathbb{Z}_2 -odd, the lightest one among the neutral scalars ρ_1 , ρ_2 and ρ_3 is automatically stable and can be an excellent dark matter candidate of the Universe. In this work, we consider ρ_1 as the potential dark matter candidate and depending upon the dark sector mixing angle θ_D , ρ_1 will be either “singlet-like” or “doublet-like” or a mixed state. Later in this Section, we will show that although the combined effects of both dark matter relic density bound and flavour physics anomalies (including $(g-2)_\mu$) considering in this work dictates that the dark matter candidate ρ_1 to be mostly a “single-like” state, its freeze-out process involves extra annihilation channels involving $L_\mu - L_\tau$ gauge boson $Z_{\mu\tau}$, making this scenario significantly different from the case of standard Scalar Singlet dark matter [105–108].

The viability of the proposed dark matter candidate ρ_1 has been investigated first by computing its relic density¹⁴ $\Omega_{\text{DM}} h^2$. This requires comoving number density Y at the present epoch ($T = T_0$, T_0 is the present temperature of the Universe), which is a solution of the Boltzmann equation involving all relevant annihilation and co-annihilation processes in the collision term. The Boltzmann equation in terms of Y is given by [138–140],

$$\frac{dY}{dx} = - \left(\frac{45 G}{\pi} \right)^{-\frac{1}{2}} \frac{M_{\rho_1} \sqrt{g_\star}}{x^2} \langle \sigma v \rangle_{\text{eff}} (Y^2 - (Y^{\text{eq}})^2), \quad (67)$$

where $Y = \sum_i Y_i$ with $Y_i = \frac{n_i}{s}$ being the comoving number density of \mathbb{Z}_2 -odd particle i having number density n_i and s stands for the entropy density of the Universe. Moreover, $x = \frac{M_{\rho_1}}{T}$ is a dimensionless variable and G is the Newton’s gravitational constant. The function g_\star [138] depends on degrees of freedom for entropy and energy densities of the Universe. The quantity $\langle \sigma v \rangle_{\text{eff}}$ has been defined as [139]

$$\langle \sigma v \rangle_{\text{eff}} = \sum_{ij} \langle \sigma_{ij} v_{ij} \rangle \times r_i r_j, \quad (68)$$

where, $\langle \sigma_{ij} v_{ij} \rangle$ is the thermal averaged annihilation cross section between particle i and j having relative velocity v_{ij} . $\langle \sigma_{ij} v_{ij} \rangle$ has the following expression in terms of cross section σ_{ij} ,

$$\begin{aligned} \langle \sigma_{ij} v_{ij} \rangle &= \frac{1}{2 M_i^2 M_j^2 T K_2 \left(\frac{M_i}{T} \right) K_2 \left(\frac{M_j}{T} \right)} \times \int_{(M_i+M_j)^2}^{\infty} \sigma_{ij} p_{ij}^2 \sqrt{s} K_1 \left(\frac{\sqrt{s}}{T} \right) ds, \\ p_{ij} &= \frac{\sqrt{s - (M_i + M_j)^2} \sqrt{s - (M_i - M_j)^2}}{2 \sqrt{s}}, \end{aligned} \quad (69)$$

with

$$r_i = \frac{Y_i^{\text{eq}}}{Y} = \frac{n_i^{\text{eq}}}{n} = \frac{g_i (1 + \Delta_i)^{3/2} \exp[-\Delta_i x]}{\sum_i g_i (1 + \Delta_i)^{3/2} \exp[-\Delta_i x]}, \quad (70)$$

where, K_i is the i^{th} order Modified Bessel function of second kind and s is the Mandelstam variable. Further, Y_i^{eq} and n_i^{eq} are the equilibrium values of Y_i and n_i respectively while $n =$

¹⁴ Here, DM represents the short form of dark matter.

$\sum_i n_i$ is the total number density of all the odd sector particles. This is the most relevant quantity instead of individual n_i s, since all heavier particles, which survive annihilation, will eventually decay into the LOP (ρ_1). This is the actual reason of expressing the Boltzmann equation in terms of total comoving number density Y instead of individual Y_i s. In the above, $\Delta_i = \frac{M_i - M_{\rho_1}}{M_{\rho_1}}$, represents the mass splitting between LOP and other heavier \mathbb{Z}_2 -odd particles. After implementation of the present model in **FeynRules** [141] we have solved Boltzmann equation at $T = T_0$ using **micrOMEGAs** [142]. Finally, we have obtained $Y(T_0)$ which is related to the relic density of LOP through the following relation [140]

$$\Omega_{\text{DM}} h^2 = 2.755 \times 10^8 \left(\frac{M_{\rho_1}}{\text{GeV}} \right) Y(T_0). \quad (71)$$

Relic density $\Omega_{\text{DM}} h^2$ of dark matter has been measured precisely by satellite borne experiments like Planck and WMAP and its present acceptable range is $0.1172 \leq \Omega_{\text{DM}} h^2 \leq 0.1226$ at 67% confidence level (C.L.) [4]. Apart from this, one has to take into account the latest bound on

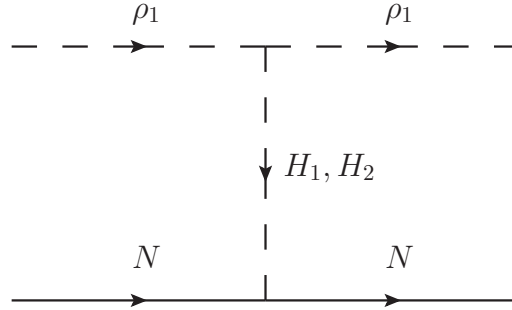


Figure 6: Feynman diagram for the elastic scattering of ρ_1 with nucleon N through the exchange of scalar bosons H_1 and H_2 .

dark matter nucleon scattering cross section from the “ton-scale” direct detection experiment namely XENON1T [109], which till now provides the most stringent upper bound on dark matter nucleon spin independent scattering cross section (σ_{SI}) for dark matter mass ranging from 6 GeV to 1 TeV. Since the dark matter candidate of the present scenario is a scalar, it has only spin independent scattering with nucleon and such scattering is possible only through scalar bosons H_1 and H_2 . Feynman diagrams of such elastic scattering $\rho_1 + N \rightarrow \rho_1 + N$ are shown in Fig. 6. The corresponding expression of σ_{SI} is given by

$$\sigma_{\text{SI}} = \frac{\mu_{\text{red}}^2}{4\pi} \left[\frac{M_N f_N}{M_{\rho_1} v_1} \left(\frac{g_{H_1 \rho_1 \rho_1}}{M_{H_1}^2} + \frac{g_{H_2 \rho_1 \rho_1}}{M_{H_2}^2} \right) \right]^2, \quad (72)$$

where $g_{H_1(H_2) \rho_1 \rho_1}$ is the coupling between $H_1(H_2)$ and a pair of ρ_1 . Expressions of these couplings are listed in Appendix B. Moreover, f_N and M_N are nuclear form factor and nucleon mass respectively. For dark matter scattering mediated by scalars $f_N \sim 0.3$ [108]. We already know that non-observation of any dark matter signal at direct detection experiments impose severe upper bound on σ_{SI} with respect to dark matter mass. From, the above expression of σ_{SI} , it can

be seen clearly that such exclusion limit on σ_{SI} in turn puts an upper bound on the involved couplings like $g_{H_1\rho_1\rho_1}$ and $g_{H_2\rho_1\rho_1}$.

Moreover, SM Higgs to $\rho_1\rho_1$ coupling for $M_{H_1} > 2M_{\rho_1}$ case is also constrained from the maximum allowed limit of Higgs invisible decay width. At present, the upper limit on invisible branching fraction of the SM Higgs boson is 0.24 at 95% C.L. [110]. In the present model, the SM like Higgs boson in addition to its “standard decay modes”, can also decay into $Z_{\mu\tau}Z_{\mu\tau}$, $ZZ_{\mu\tau}$, $\rho_1\rho_1$ and $\rho_1\rho_2$ final states¹⁵. Decay widths of such processes are given below,

$$\Gamma_{H_1 \rightarrow Z_{\mu\tau}Z_{\mu\tau}} = \frac{g_{H_1Z_{\mu\tau}Z_{\mu\tau}}^2 M_{H_1}^3}{128\pi M_{Z_{\mu\tau}}^4} \left(12 \frac{M_{Z_{\mu\tau}}^4}{M_{H_1}^4} - 4 \frac{M_{Z_{\mu\tau}}^2}{M_{H_1}^2} + 1 \right) \sqrt{1 - 4 \frac{M_{Z_{\mu\tau}}^2}{M_{H_1}^2}}, \quad (73)$$

$$\Gamma_{H_1 \rightarrow ZZ_{\mu\tau}} = \frac{g_{H_1ZZ_{\mu\tau}}^2}{64\pi M_{H_1}} \left(8 + \frac{(M_{H_1}^2 - M_{Z_{\mu\tau}}^2 - M_Z^2)^2}{M_Z^2 M_{Z_{\mu\tau}}^2} \right) \sqrt{1 - \left(\frac{M_Z + M_{Z_{\mu\tau}}}{M_{H_1}} \right)^2} \times \sqrt{1 - \left(\frac{M_Z - M_{Z_{\mu\tau}}}{M_{H_1}} \right)^2}, \quad (74)$$

$$\Gamma_{H_1 \rightarrow \rho_1\rho_1} = \frac{g_{H_1\rho_1\rho_1}^2}{32\pi M_{H_1}} \sqrt{1 - 4 \frac{M_{\rho_1}^2}{M_{H_1}^2}}, \quad (75)$$

$$\Gamma_{H_1 \rightarrow \rho_1\rho_2} = \frac{g_{H_1\rho_1\rho_2}^2}{16\pi M_{H_1}} \sqrt{1 - \left(\frac{M_{\rho_1} + M_{\rho_2}}{M_{H_1}} \right)^2} \sqrt{1 - \left(\frac{M_{\rho_2} - M_{\rho_1}}{M_{H_1}} \right)^2}, \quad (76)$$

and

$$\Gamma_{H_1}^{\text{Inv}} = \Gamma_{H_1 \rightarrow Z_{\mu\tau}Z_{\mu\tau}} + \Gamma_{H_1 \rightarrow ZZ_{\mu\tau}} + \Gamma_{H_1 \rightarrow \rho_1\rho_2} + \Gamma_{H_1 \rightarrow \rho_1\rho_1}. \quad (77)$$

Expressions of all the coupling involved in the above decay widths are given in Appendix B. According to the latest results from LHC, $\Gamma_{H_1}^{\text{Inv}} \leq 0.24 \Gamma_{\text{Higgs}}^{\text{SM}}$, where $\Gamma_{\text{Higgs}}^{\text{SM}} = 4.13 \text{ MeV}$, is total decay width of the SM Higgs boson [143].

The dark matter candidate (ρ_1) of the present scenario is a thermal WIMP, which remains in equilibrium with the thermal bath until its freeze-out through annihilations and co-annihilations into various final states allowed by the symmetries of the model. In this work, we have considered M_{ρ_1} between 10 GeV to 1 TeV. For low dark matter masses (i.e. $M_{\rho_1} < 100 \text{ GeV}$), ρ_1 predominantly annihilates into a pair of $Z_{\mu\tau}$. In some cases, depending upon the relevant couplings, $b\bar{b}$, $c\bar{c}$ and $\tau\bar{\tau}$ final states are also possible. Moreover, co-annihilations among the \mathbb{Z}_2 -odd particles in the low mass regime are insignificant as we have considered all heavier \mathbb{Z}_2 -odd particles masses larger than 100 GeV throughout this analysis to evade experimental bounds [104]. Alternatively, for the heavier mass range of ρ_1 , there are various possibilities. First of all depending upon the mass splitting between ρ_1 and other \mathbb{Z}_2 -odd particles (parametrised by a quantity Δ_i , defined earlier) there can either be annihilation or

¹⁵ In this work, we are focusing on low mass $Z_{\mu\tau}$ ($\sim 1 \text{ MeV} - 100 \text{ MeV}$) to address $(g-2)_\mu$ anomaly.

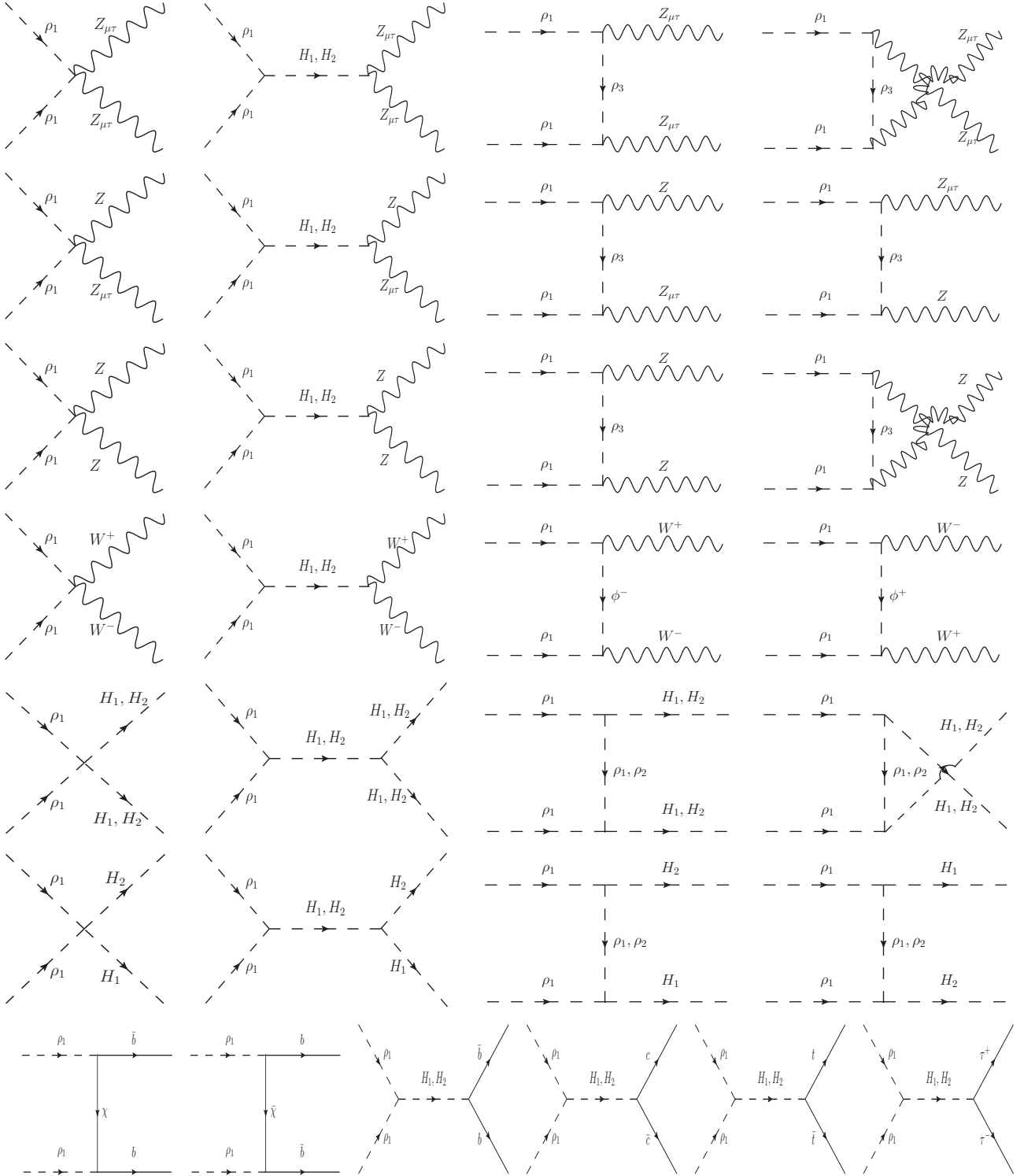


Figure 7: Feynman diagrams of dark matter annihilation channels contributing significantly to the freeze-out process.

co-annihilations. In the former case, depending on the values of the associated couplings $\rho_1 \rho_1 \rightarrow Z_{\mu\tau} Z_{\mu\tau}, ZZ_{\mu\tau}, H_2 H_2, H_1 H_1, H_1 H_2, W^+ W^-, ZZ$ and $t\bar{t}$ final states can be important. On the other hand, co-annihilation plays a pivotal role during the freeze-out of ρ_1 when

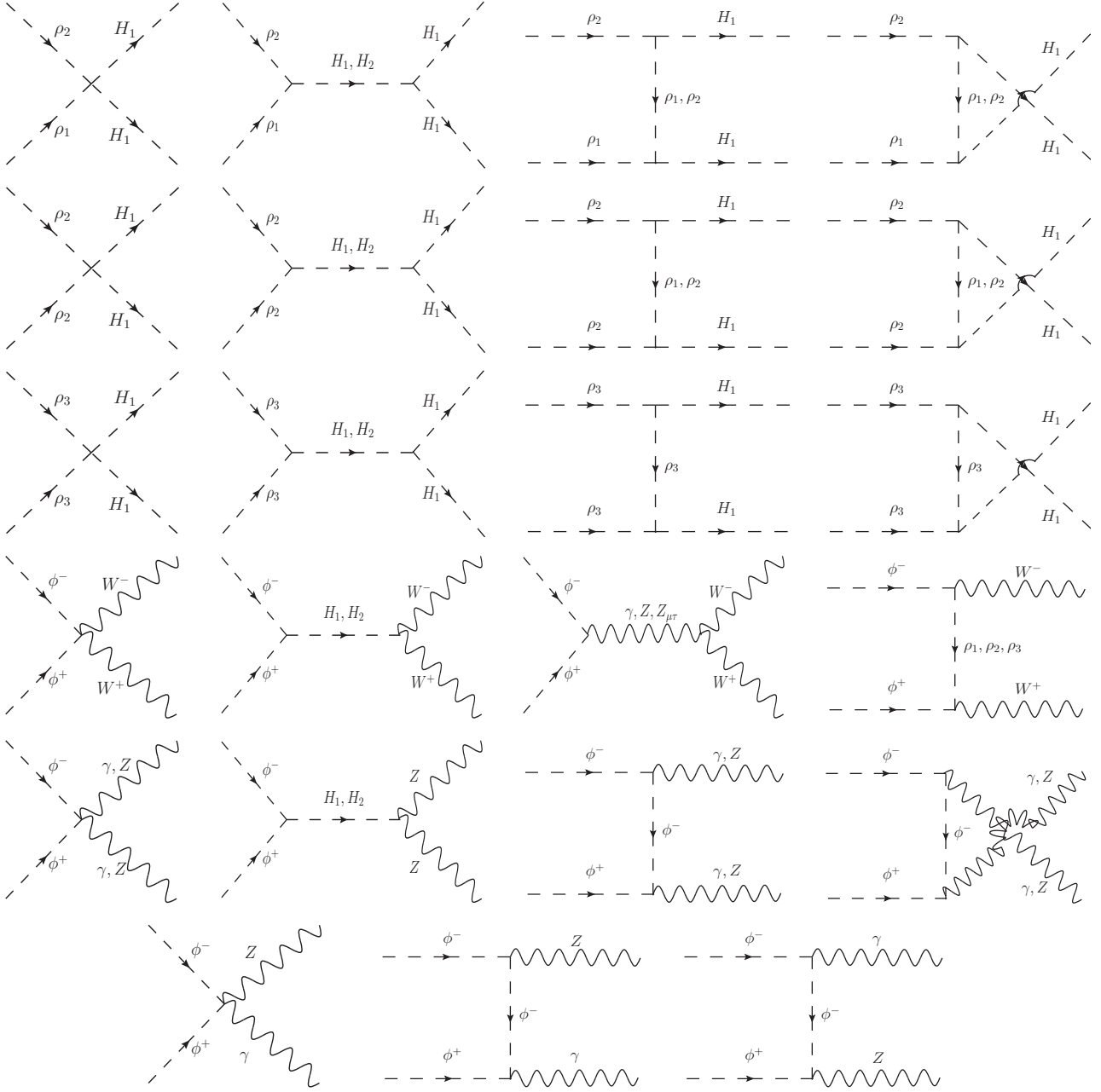


Figure 8: Co-annihilation channels contributing to the relic density of ρ_1 in the high mass region.

$\Delta_i \leq 0.2$ [139] for any \mathbb{Z}_2 -odd particle i ($i = \rho_2, \rho_3, \phi^\pm$). In this circumstances, various co-annihilations among these dark sector particles like $\rho_1\rho_2 \rightarrow H_1H_1$, $\rho_i\rho_i \rightarrow H_1H_1$ ($i = 1-3$), $\phi^+\phi^- \rightarrow W^+W^-$, $\gamma\gamma$, γZ , ZZ etc. become predominant. Feynman diagrams of all significant annihilation and co-annihilation channels are shown in Figs. 7 and 8 respectively.

In Fig.9, we have plotted spin independent scattering cross section σ_{SI} of ρ_1 with its mass M_{ρ_1} , varying between 10 GeV to 1 TeV. In this plot all red coloured points satisfy relic density constraint i.e., $0.1172 \leq \Omega_{\text{DM}}h^2 \leq 0.1226$ and bound related to Higgs invisible decay modes as well. The blue dashed-dot line represents the latest bound on σ_{SI} from XENON1T experiment.

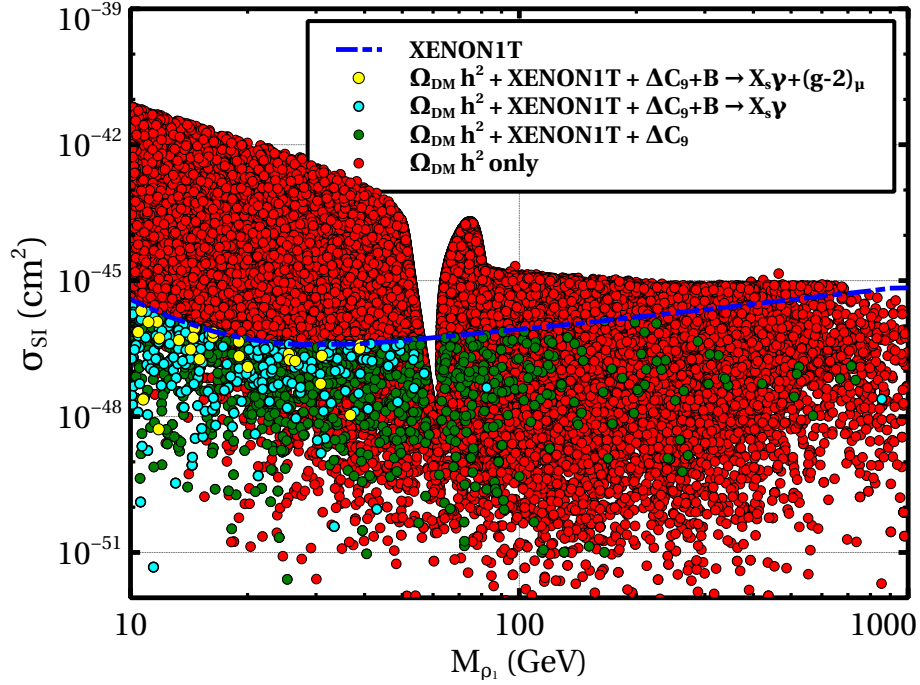


Figure 9: Allowed parameter space in σ_{SI} vs M_{ρ_1} plane subject to various experiments bounds indicated in the legend.

All the parameter space below the blue dashed-dot line are still allowed and can be probed in near future by “multi-ton-scale” direct detection experiments like XENONnT. Therefore, if we consider direct constraints like relic density, direct detection and Higgs invisible decay only, there are still enough parameter space left (although few portions mostly in the low mass dark matter regime have already been ruled-out) for the entire considered mass range of ρ_1 . However, the situation does not remain the same when one tries to explain flavour physics anomalies and $(g - 2)_\mu$ anomaly within this framework. The allowed parameter space in $\sigma_{\text{SI}} - M_{\rho_1}$ plane gets severely restricted when we impose a bound on the NP contribution to the WC C_9 (i.e. $-1.26 \leq \Delta C_9 \leq -0.63$ in 2σ range [27]) to explain $R_{K^{(*)}}$ anomalies. This has been indicated by green coloured points in the above plot where one can notice that the low dark matter mass regime (i.e. $M_{\rho_1} \lesssim 100$ GeV) is the most favourable to address $R_{K^{(*)}}$ anomalies. This can be understood from the behaviour of ΔC_9 (Eq. (36)) with respect to the mass of ρ_1 as illustrated in Fig. 2a, where the magnitude of ΔC_9 sharply decreases with the increase of M_{ρ_1} . Furthermore, in this framework, we have also tried to explain both $\text{Br}(B \rightarrow X_s \gamma)$ and $(g - 2)_\mu$ anomaly, the two long-standing anomalies of the SM from their experimental counterparts. These are indicated by cyan and yellow coloured points respectively in $\sigma_{\text{SI}} - M_{\rho_1}$ plane. For the branching ratio of $B \rightarrow X_s \gamma$, we have used 3σ ($2.84 \leq \text{Br}(B \rightarrow X_s \gamma) \times 10^4 \leq 3.80$ [122]) while the 2σ band i.e. $115.44 \leq \Delta a_\mu \times 10^9 \leq 420.56$ [12] for $(g - 2)_\mu$ has been taken into account¹⁶. We

¹⁶ Here we would like to mention that, another constraint e.g., $B_s^0 - \bar{B}_s^0$ mixing which could be relevant for the present scenario. However, NP contributions to the $B_s^0 - \bar{B}_s^0$ mixing arise from the present scenario via box

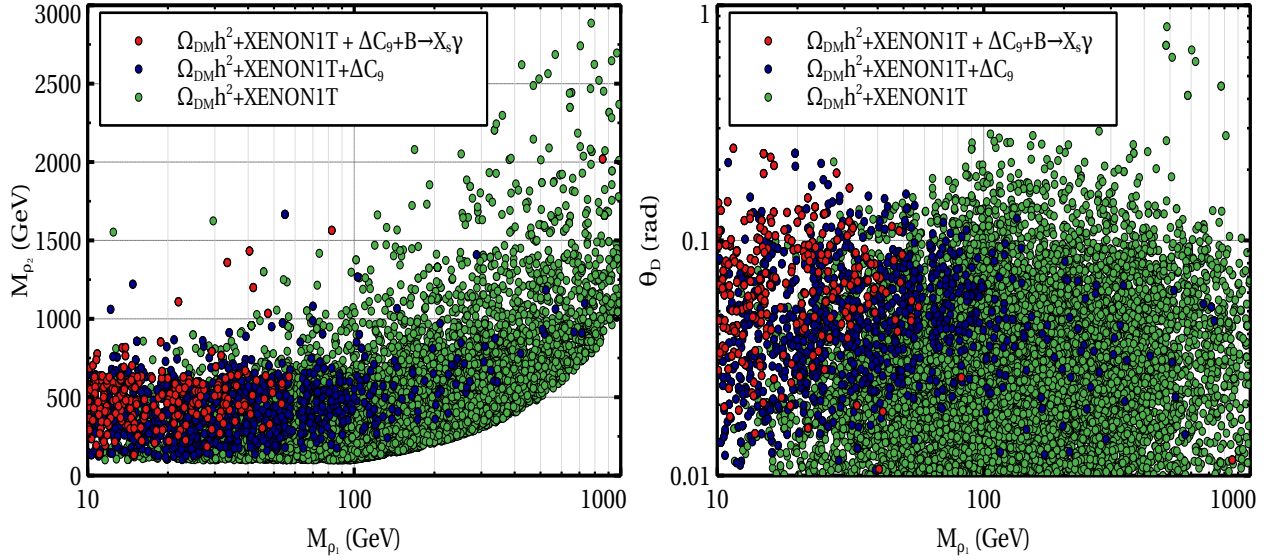


Figure 10: Left(Right) panel: Allowed region in $M_{\rho_2} - M_{\rho_1}(\theta_D - M_{\rho_1})$ plane from various experimental results considered in this work.

have checked that in the low dark matter mass region ($M_{\rho_1} \leq 100$ GeV), ρ_1 predominantly annihilates into the $Z_{\mu\tau}$ pair. This actually makes dark matter physics strongly correlated with the physics of rare B -decays and anomalous magnetic moment of μ , where the role of new gauge boson $Z_{\mu\tau}$ is extremely crucial. Moreover, it also helps us to evade the strong bound coming from the experiments of direct detection [109], indirect detection [145] and also from the collider on Higgs invisible branching [110] for the low mass scalar dark matter [146–148], where $b\bar{b}$ final state is the principal annihilation channel. Therefore, in spite of being a gauge singlet \mathbb{Z}_2 -odd scalar field, the mixing with another \mathbb{Z}_2 -odd field (part of an $SU(2)_L$ doublet) having nonzero $L_\mu - L_\tau$ charge, makes the entire dynamics of our dark matter candidate ρ_1 strikingly different from the standard Scalar Singlet dark matter scenario [105–108]. Finally, for the completeness we would like to mention here that the yellow coloured points in $\sigma_{SI} - M_{\rho_1}$ plane are those which satisfy all the experimental results we have considered in this work.

In the left panel of Fig. 10, we have shown ranges of M_{ρ_1} and M_{ρ_2} allowed by various experimental results. The allowed region in $M_{\rho_2} - M_{\rho_1}$ plane from both relic density as well as direct detection bounds are indicated by the green coloured points. Similar to the previous plot in

diagrams and these are negligibly small. The reason is that, apart from the dark matter particle, all non-standard particles which generate box diagrams are sufficiently massive (especially the non-standard fermion χ , whose mass that we have taken ≥ 1 TeV throughout the analysis). At this point it is relevant to mention that, from the recent 13 TeV LHC data [144], a down-type quark (\mathcal{B}) with charge $(-1/3)$ is excluded for masses below 1.22 TeV for the decay channels $\mathcal{B} \rightarrow Zb/Wt/\text{SM Higgs } b$. However, this bound is not applicable in our case, as in our model the field χ is odd under \mathbb{Z}_2 symmetry, therefore such decays are restricted by the \mathbb{Z}_2 symmetry. Although, for the sake of conservative approach we use $M_\chi \geq 1$ TeV in our analysis. Hence, the loop functions are substantially suppressed. Consequently, the NP contribution to $B_s^0 - \bar{B}_s^0$ mixing would not put any stringent constraint in our scenario.

Fig. 9, here also when we have imposed various flavour physics constraints, the allowed parameter space shrinks to a smaller region concentrated mainly in the low mass regime of ρ_1 . The parameter space which reproduces ΔC_9 in 2σ range for explaining $R_{K^{(*)}}$ anomalies has been shown by the blue coloured points. On the other hand, the red coloured points are indicating those values of M_{ρ_1} and M_{ρ_2} which in addition to above mentioned experimental results also satisfy $\text{Br}(B \rightarrow X_s \gamma)$ in 3σ range. Moreover, as we have already known that the dark matter candidate ρ_1 is an admixture of a real scalar singlet S and a CP-even neutral component (ϕ^0) of a doublet Φ . While both S and Φ are \mathbb{Z}_2 -odd but only Φ has nonzero $L_\mu - L_\tau$ charge. Therefore, the interaction of ρ_1 with $L_\mu - L_\tau$ gauge boson $Z_{\mu\tau}$ (e.g. annihilation of ρ_1 into a pair of $Z_{\mu\tau}$) is governed by the mixing angle θ_D . Larger the mixing angle, larger is the annihilation rate into $Z_{\mu\tau} Z_{\mu\tau}$ final state, making ρ_1 less abundant at the present epoch. Therefore, the relic density bound puts an upper limit on the maximum allowed value of θ_D , which is more stringent in the low dark matter mass region where $Z_{\mu\tau} Z_{\mu\tau}$ is the principal annihilation mode. This feature is clearly visible in the right panel of Fig. 10, where we have shown the allowed range of θ_D with respect to M_{ρ_1} . However, in the high mass regime ($M_{\rho_1} \geq 500$ GeV), large values of $\theta_D \gtrsim 0.3$ rad are still allowed because for such large θ_D , ρ_1 is mostly an $\text{SU}(2)_L$ doublet like state (similar to the Inert Doublet dark matter in high mass range [148–150]) which attains the present abundance of dark matter through co-annihilations with other \mathbb{Z}_2 -odd fields into various bosonic final states (both vector and scalar). Moreover, we have also seen from the Fig. 9 that the magnitude of ΔC_9 (Eq. (36)) decreases with the increasing values of masses of the particles ρ_1 , ρ_2 and ρ_3 involving within $b \rightarrow s$ transition loops. Now, although the masses of ρ_1 and ρ_2 are indeed free parameters of the present model, the mass of the remaining scalar ρ_3 becomes fixed for a particular choice of M_{ρ_1} , M_{ρ_2} and θ_D via Eq. (22). Here, M_{ρ_3} actually oscillates between M_{ρ_2} and M_{ρ_1} as we vary θ_D from 0 to $\pi/2$. As we are working in the limit $M_{\rho_1} < M_{\rho_2}$ (since ρ_1 is our dark matter candidate), large θ_D ensures low mass for ρ_3 (using Eq. (22)) and hence enlarge loop contribution to ΔC_9 . Thus, $R_{K^{(*)}}$ anomalies prefer larger values of θ_D , which is a contrasting situation compared to the low mass regime of ρ_1 , where relic density bound favours relatively smaller values of mixing angle to suppress large annihilation into $Z_{\mu\tau} Z_{\mu\tau}$. As a result, both dark matter relic density bound and $R_{K^{(*)}}$ anomalies are simultaneously addressable for $0.01 < \theta_D$ (rad) < 0.3 , when M_{ρ_1} is mostly concentrated below 100 GeV range. This has been demonstrated by the blue coloured points in $\theta_D - M_{\rho_1}$ plane. Similar to the left panel, here also red colour points represent the portion in the parameter space which has been satisfied by the constraint of $\text{Br}(B \rightarrow X_s \gamma)$ as well.

Since, the allowed values of θ_D which satisfy all the experimental results considered in this work fall in the range $0.01 < \theta_D$ (rad) < 0.3 (red coloured points in the right panel of Fig. 10), this makes M_{ρ_2} and M_{ρ_3} almost degenerate and this has been demonstrated in Fig. 11, where the colour bar is indicating corresponding values of mass of the dark matter candidate ρ_1 .

Finally, in Fig. 12 we have shown our results in $g_{\mu\tau} - M_{Z_{\mu\tau}}$ plane, which is at the present moment extremely constrained by various experimental results. In this figure (Fig. 12), the red coloured points represent those values of $g_{\mu\tau}$ and $M_{Z_{\mu\tau}}$ which explain $(g - 2)_\mu$ in 2σ range. Here, in the

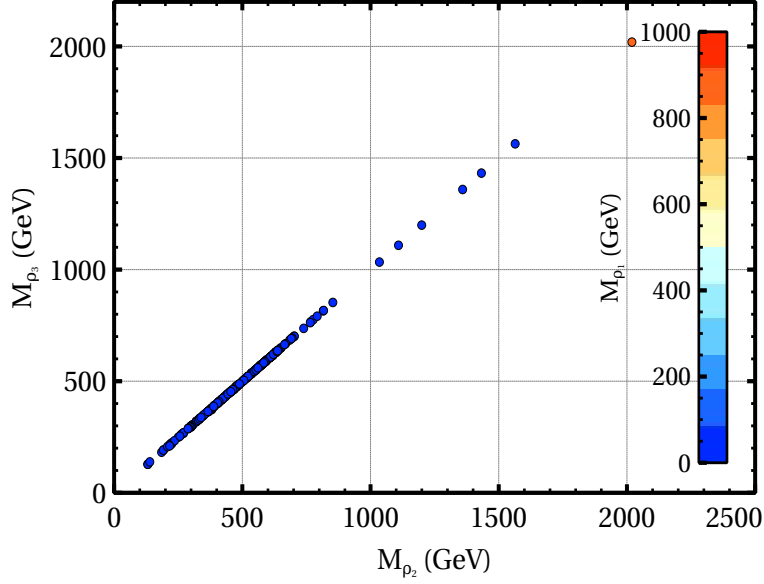


Figure 11: Allowed values of M_{ρ_2} and M_{ρ_3} satisfying all the considered experimental constraints. Degeneracy between M_{ρ_2} and M_{ρ_3} is indicating the fact that low values of θ_D ($0.01 < \theta_D$ (rad) < 0.3) are only allowed while dark matter mass M_{ρ_1} lies below 100 GeV (shown in colour code).

$g_{\mu\tau} - M_{\mu\tau}$ plane, most strongest constraint till now comes from neutrino trident production. Neutrino trident production is a process of producing $\mu^+\mu^-$ pair via neutrino scattering in the Coulomb field of a target nucleus (N), i.e. $\nu_\mu(\bar{\nu}_\mu) + N \rightarrow \nu_\mu(\bar{\nu}_\mu) + \mu^+\mu^- + N$. In the SM, this process is possible via W^\pm and Z bosons only. Moreover, if there exists any new neutral gauge boson (similar to $Z_{\mu\tau}$ in the present work) which couples to both muons and muon-neutrinos then that gauge boson can also contribute significantly to the trident production cross section. However, all the experimental collaborations namely, CCFR [111], CHARM-II [112] and NuTeV [151] have measured neutrino trident events and their measured cross sections are in good agreement with that of the SM prediction i.e. $\frac{\sigma_{\text{CCFR}}}{\sigma_{\text{SM}}} = 0.82 \pm 0.28$, $\frac{\sigma_{\text{CHARM-II}}}{\sigma_{\text{SM}}} = 1.58 \pm 0.57$ and $\frac{\sigma_{\text{NuTeV}}}{\sigma_{\text{SM}}} = 0.72^{+1.73}_{-0.72}$ respectively. These results therefore put strong constraint in the mass-coupling plane of the new gauge boson. In Fig. 12, the crossed region above the black dashed line represents 95% C.L. upper bound [152] on $g_{\mu\tau}$ as a function of $M_{Z_{\mu\tau}}$ using neutrino trident cross section measured by the CCFR collaboration¹⁷. Consequently, all the crossed regions above black dashed line are excluded by neutrino trident production. Besides, there is a further constraint from the measurement of the SM Z boson decay to 4μ final state at the LHC. This

¹⁷ Furthermore, it is clearly evident from the Fig. 12, that, due to the consideration of CCFR experimental data we naturally incorporate the constraint of the branching ratio of $\tau \rightarrow \mu\nu_\tau\bar{\nu}_\mu$. The reason is that the parameter space (in $g_{\mu\tau} - M_{Z_{\mu\tau}}$ plane) which describes all the concerned observables simultaneously does not overlap with the portion that has already been ruled out from the branching ratio of $\tau \rightarrow \mu\nu_\tau\bar{\nu}_\mu$ [96]. Moreover, we have explicitly checked that the NP contribution for the decay $\tau \rightarrow \mu\nu_\tau\bar{\nu}_\mu$ due to $Z_{\mu\tau}$ is practically vanishing in nature in the allowed parameter space of the present scenario.

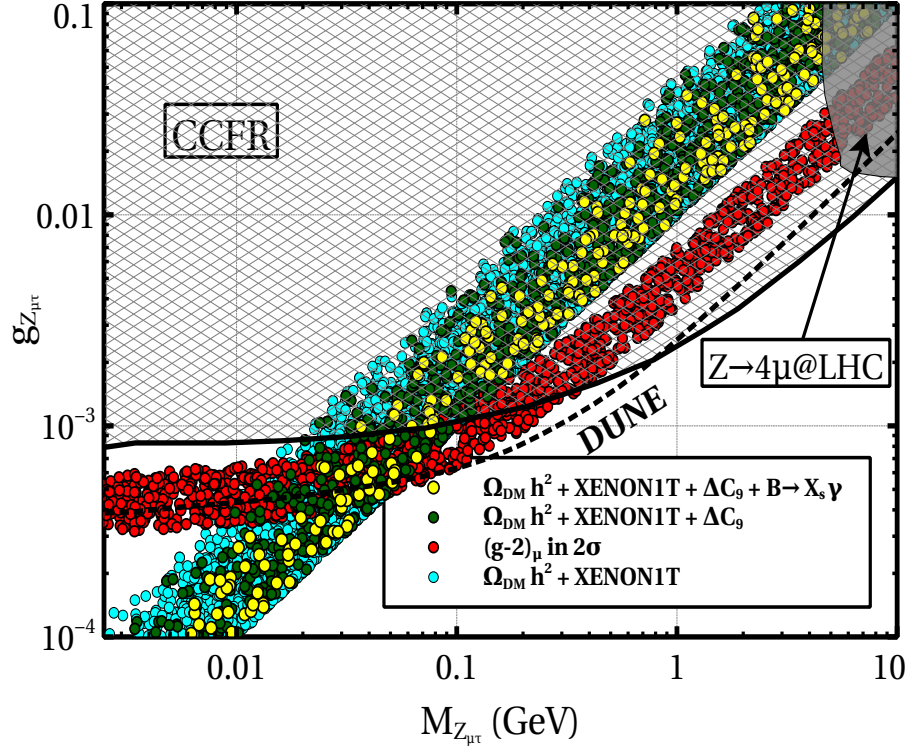


Figure 12: Current status of the $g_{Z_{\mu\tau}} - M_{Z_{\mu\tau}}$ plane in the light of various experimental results. In this plane we have shown the allowed regions satisfying bounds from Planck + XENON1T (cyan coloured points), Planck + XENON1T + $R_{K^{(*)}}$ anomalies (green coloured points) and Planck + XENON1T + $R_{K^{(*)}}$ anomalies + $\text{Br}(B \rightarrow X_s \gamma)$ (yellow coloured points) respectively. Moreover, red coloured points are indicating those values of $M_{Z_{\mu\tau}}$ and $g_{Z_{\mu\tau}}$ which address $(g-2)_\mu$ in 2σ range. In this plot, we have also taken into account the invisible decay branching constraint of the SM-like Higgs boson H_1 .

has also been indicated by the grey region at the topmost corner of right side of this plot. Cyan coloured points represent those values of $g_{Z_{\mu\tau}}$ and $M_{Z_{\mu\tau}}$ which satisfy bounds related to dark matter physics namely, relic density, direct detection and Higgs invisible branching ratio. On top of the existing dark matter constraints, the effects of flavour physics observables like $R_{K^{(*)}}$ anomalies (2σ bound on ΔC_9) and $R_{K^{(*)}} + \text{Br}(B \rightarrow X_s \gamma)$ on the mass as well as the coupling of $Z_{\mu\tau}$ have been shown by green and yellow coloured points respectively. Therefore, from this plot it can be easily seen that although maximum portions of $g_{\mu\tau} - M_{Z_{\mu\tau}}$ plane have already been excluded by the results of CCFR collaboration, there is still a small but interesting region left in this parameter space which is $0.01 \leq M_{Z_{\mu\tau}} \text{ (GeV)} \leq 0.1$ and $3 \times 10^{-4} \leq g_{\mu\tau} \leq 10^{-3}$. This region of the parameter space of the present model can address dark matter, $(g-2)_\mu$ anomaly, $R_{K^{(*)}}$ anomalies and $\text{Br}(B \rightarrow X_s \gamma)$ simultaneously and more exciting thing is that this parameter space can be probed within a few years by the DUNE experiment [153] measuring neutrino trident events (shown by black dashed line) [154]. This will surely be the test of our model, at least the benchmark points (if not the full model) in the low mass dark matter region which are compatible to both dark matter and flavour physics issues. For completeness in Table III, we

present three plausible benchmark points (BP1, BP2 and BP3) and corresponding numerical values of several physical quantities of the present scenario.

Parameters/ Observables	BP1	BP2	BP3
M_{ρ_1} (GeV)	14.499	26.515	36.767
M_{ρ_2} (GeV)	478.254	506.009	450.276
M_{ρ_3} (GeV)	475.201	503.742	449.255
M_{ϕ^\pm} (GeV)	160.591	121.443	101.748
M_{H_2} (GeV)	353.418	401.503	352.41
M_χ (GeV)	1107.840	1300.660	1087.52
$M_{Z_{\mu\tau}}$ (GeV)	5.052×10^{-2}	7.577×10^{-2}	3.167×10^{-2}
v_2 (GeV)	76.328	81.151	71.229
$g_{Z_{\mu\tau}}$	6.619×10^{-4}	9.339×10^{-4}	4.447×10^{-4}
$\tan \theta_{\mu\tau}$	2.752×10^{-6}	1.637×10^{-5}	5.337×10^{-6}
$\tan \theta_D$	0.1135	9.511×10^{-2}	6.769×10^{-2}
$\tan \theta_s$	3.203×10^{-4}	9.893×10^{-4}	4.643×10^{-3}
λ_Φ	0.1	0.1	0.1
λ_S	0.1	0.1	0.1
λ_2	9.520×10^{-3}	7.935×10^{-2}	2.360×10^{-4}
λ_4	2.499×10^{-3}	9.691×10^{-2}	1.128×10^{-3}
λ_5	9.236×10^{-3}	1.994×10^{-4}	1.066×10^{-3}
λ_6	5.364×10^{-4}	1.835×10^{-2}	8.175×10^{-4}
λ_7	4.724×10^{-2}	2.243×10^{-3}	2.599×10^{-4}
$f_2 \times f_3$	1.657	2.533	3.228
$\Omega_{\text{DM}} h^2$	0.1218	0.1206	0.1213
σ_{SI} (cm ²)	5.480×10^{-47}	1.688×10^{-47}	1.076×10^{-48}
$\text{Br}(\Gamma_{H_1}^{\text{Inv}})$	1.639×10^{-4}	1.954×10^{-3}	2.094×10^{-2}
ΔC_9	-0.973	-0.7578	-0.684
$\text{Br}(B \rightarrow X_s \gamma)$	3.196×10^{-4}	3.173×10^{-4}	2.974×10^{-4}
Δa_μ	218.495×10^{-11}	311.557×10^{-11}	129.438×10^{-11}

Table III: Viable benchmark points (BP1, BP2 and BP3) and corresponding numerical values of several physical quantities of the present scenario.

VI. NEUTRINO MASSES AND MIXINGS

In this section, we will discuss briefly about neutrino masses and mixings. It has now been firmly established from the phenomena of neutrino oscillations that there exist two tiny mass square differences between three neutrino mass eigenstates i.e. $\Delta m_{21}^2 = 7.39_{-0.20}^{+0.21} \times 10^{-5} \text{ eV}^2$,¹⁸ and $\Delta m_{31}^2 = 2.525_{-0.032}^{+0.033}(-2.512_{-0.032}^{+0.034}) \times 10^{-3} \text{ eV}^2$ for the normal(inverted) hierarchy [155] in 3σ range. This also indicates that to explain solar, atmospheric and reactor neutrino anomalies through three flavour neutrino oscillation we need at least two neutrino mass eigenstates having nonzero masses corresponding to mass squared differences as mentioned above. Moreover, there are also precise measurements of three intergenerational mixing angles namely the atmospheric mixing angle $(40.3^\circ(40.6^\circ) \leq \theta_{23} \leq 52.4^\circ(52.5^\circ))$ ¹⁹, the solar mixing angle $(31.61^\circ \leq \theta_{12} \leq 36.27^\circ)$ and the reactor mixing angle $(8.22^\circ(8.27^\circ) \leq \theta_{13} \leq 8.99^\circ(9.03^\circ))$ [155]. The latter one is the most recent entry in that list. In the present model, although we do not need any extra fermionic degrees of freedom to cancel $L_\mu - L_\tau$ anomaly which actually cancels between μ and τ generations of charged leptons and corresponding neutrinos, one can still introduce three right handed neutrinos N_{Ri} ($i = e, \mu, \tau$) in an anomaly free manner, in the model, to address neutrino masses and mixings via Type I seesaw mechanism. The Lagrangian for right handed neutrinos are given in Eq. (4). The light neutrino mass matrix m_ν after spontaneous breaking of both $SU(2)_L \times U(1)_Y$ and $U(1)_{L_\mu - L_\tau}$ symmetries has the following structure

$$m_\nu = -M_D \mathcal{M}_R^{-1} M_D^T, \\ = \frac{1}{2p} \begin{pmatrix} y_e^2 M_{\mu\tau} v_1^2 e^{i\xi} & -\frac{y_e y_\mu y_{e\tau} v_1^2 v_2}{\sqrt{2}} & -\frac{y_e y_\tau y_{e\mu} v_1^2 v_2}{\sqrt{2}} \\ -\frac{y_e y_\mu y_{e\tau} v_1^2 v_2}{\sqrt{2}} & \frac{y_\mu^2 y_{e\tau}^2 v_1^2 v_2^2 e^{-i\xi}}{2 M_{\mu\tau}} & \frac{y_\mu y_\tau v_1^2}{2 M_{\mu\tau}} (M_{ee} M_{\mu\tau} - p e^{-i\xi}) \\ -\frac{y_e y_\tau y_{e\mu} v_1^2 v_2}{\sqrt{2}} & \frac{y_\mu y_\tau v_1^2}{2 M_{\mu\tau}} (M_{ee} M_{\mu\tau} - p e^{-i\xi}) & \frac{y_\tau^2 y_{e\mu}^2 v_1^2 v_2^2 e^{-i\xi}}{2 M_{\mu\tau}} \end{pmatrix} \quad (78)$$

while the mass matrix for the heavy neutrinos coincides with \mathcal{M}_R . In the above, $p = y_{e\mu} y_{e\tau} v_2^2 - M_{ee} M_{\mu\tau} e^{i\xi}$. Majorana mass matrix \mathcal{M}_R and Dirac mass matrix M_D are given by,

$$\mathcal{M}_R = \begin{pmatrix} M_{ee} & \frac{v_2}{\sqrt{2}} y_{e\mu} & \frac{v_2}{\sqrt{2}} y_{e\tau} \\ \frac{v_2}{\sqrt{2}} y_{e\mu} & 0 & M_{\mu\tau} e^{i\xi} \\ \frac{v_2}{\sqrt{2}} y_{e\tau} & M_{\mu\tau} e^{i\xi} & 0 \end{pmatrix}, \quad M_D = \frac{v_1}{\sqrt{2}} \begin{pmatrix} y_e & 0 & 0 \\ 0 & y_\mu & 0 \\ 0 & 0 & y_\tau \end{pmatrix}. \quad (79)$$

In the present case, due to $L_\mu - L_\tau$ flavour symmetry, the Dirac mass matrix is exactly diagonal while before $U(1)_{L_\mu - L_\tau}$ symmetry breaking only three elements (only two are independent) are

¹⁸ Δm_{ij}^2 is defined as $m_i^2 - m_j^2$.

¹⁹ Where numbers without(within) brackets are for the normal(inverted) hierarchical scenario.

there in the Majorana mass matrix \mathcal{M}_R . Only after symmetry breaking we get additional elements proportional to v_2 . Therefore, $L_\mu - L_\tau$ symmetry breaking plays a crucial role here to get desired structure of m_ν matrix. Also, looking at both M_D and \mathcal{M}_R matrices, one can easily notice that there can only be one complex element. Phases of other elements can be absorbed by redefining both SM leptons and right handed neutrinos. Now, one can calculate mass eigenvalues and mixing angles of light neutrinos by diagonalising this m_ν matrix, which is a complex symmetric matrix, indicating the Majorana nature of the light neutrinos. If we consider, $v_2 \sim 10^2$ GeV (in the right ballpark to produce desired contribution to $(g - 2)_\mu$), $0.1 \lesssim y_{e\mu}$, $y_{e\tau} \lesssim 1.0$ and $10 \text{ GeV} \lesssim M_{ee}$, $M_{\mu\tau} \lesssim 1 \text{ TeV}$ (100 GeV to TeV scale right handed neutrinos) then we need Dirac couplings $10^{-7} \lesssim y_e, y_\mu, y_\tau \lesssim 10^{-5}$ to reproduce neutrino oscillation parameters. Detail analysis of mass matrix diagonalisation and comparison with latest 3σ range of oscillation parameters have been done in Ref. [84]. Moreover, we would like to mention here that although only two right handed neutrinos (N_R^μ and N_R^τ) are sufficient to make the present model anomaly free, such scenario is unable to reproduce all neutrino oscillation parameters due to special flavour structure of the Dirac mass matrix.

VII. CONSTRAINT FROM DI-LEPTON RESONANCE SEARCH AT 13 TEV LHC

Depending on the mass ranges, the *non-standard* Z boson (which we designate as $Z_{\mu\tau}$ in this article) confronts constraints from collider searches. For example, if the mass of $Z_{\mu\tau}$ is less than SM Z boson then there exists some viable parameter region for the favorable kind among the various NP models that exist in the literature. Furthermore, as the $Z_{\mu\tau}$ has no direct coupling with electron²⁰, hence LEP searches cannot provide direct constraint on the light $Z_{\mu\tau}$. On the other hand, the Tevatron [156, 157] and LHC [115, 158, 159] searches for $Z_{\mu\tau}$ to di-lepton final state only apply, however in this case $M_{Z_{\mu\tau}} > 100 \text{ GeV}$. Moreover, only relevant limit to the light $Z_{\mu\tau}$ case obtained from the LHC searches at $pp \rightarrow Z \rightarrow 4\mu$ [152]. At this point we remark in passing that, in our present article even though in the low mass limit of $Z_{\mu\tau}$ we have obtained certain region of parameter space (depicted in Fig. 12) which has been satisfied by some flavour physics data, dark matter constraints and $(g - 2)_\mu$ anomaly, however, cross section for a process like $pp \rightarrow Z_{\mu\tau} \rightarrow \ell^+\ell^-$ in that region of parameter space is extremely tiny at the 13 TeV LHC.

On the other hand in the high mass region of $Z_{\mu\tau}$, the LHC searches put the tightest bound on its mass ($3 \sim 5 \text{ TeV}$ [115, 158, 159]) in the di-muon final states. Thus, in the present article we use the exclusion data obtained by ATLAS collaboration [115] for a di-lepton resonance search at the LHC experiment to constraint parameter space of the present scenario. In order to embed this limit in the present scenario, we first implement the model using **FeynRules** [141]. Then we generate the cross section for the process $pp \rightarrow Z_{\mu\tau} \rightarrow \ell^+\ell^-$ using **Madgraph5** [160] with the default parton distribution functions **NNPDF3.0** [161] at 13 TeV LHC²¹. Here $\ell (\equiv e, \mu)$,

²⁰ Only possible via Z - $Z_{\mu\tau}$ mixing. Therefore, the interaction strength is insignificant.

²¹ Production of $Z_{\mu\tau}$ at the LHC in the present model is possible due to the couplings of $q_i \bar{q}_i Z_{\mu\tau}$ which are

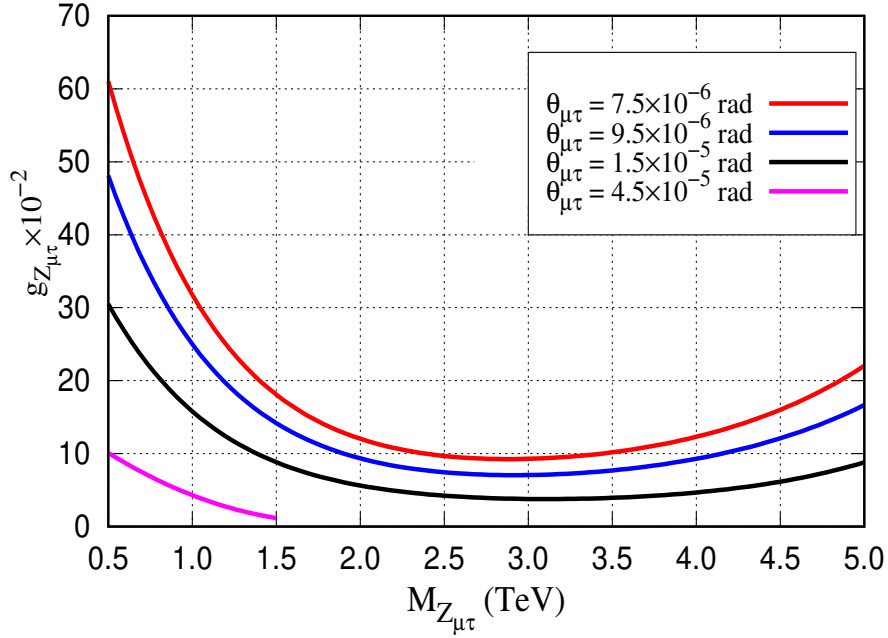


Figure 13: Using the non-observation of a resonant $\ell^+\ell^-$ signal at the LHC running at 13 TeV, we have depicted the exclusion plots at 95% C.L. in the $M_{Z_{\mu\tau}} - g_{Z_{\mu\tau}}$ plane for four different values of Z - $Z_{\mu\tau}$ mixing angle $\theta_{\mu\tau}$. The region above a particular curve has been ruled out from the non-observation of a resonant $\ell^+\ell^-$ signal in the 13 TeV run of LHC by latest ATLAS data [115] considering mass range [0.5, 5] TeV.

however, significant contribution has been generated from $\mu^+\mu^-$ final state. Finally, for a specific combination of coupling $g_{Z_{\mu\tau}}$ and Z - $Z_{\mu\tau}$ mixing angle $\theta_{\mu\tau}$ we compare the theoretical prediction of cross section for any particular value of mass (confined within the range [0.5, 5] TeV) of $Z_{\mu\tau}$ with the corresponding experimental data given by ATLAS collaboration [115].

In Fig. 13 we show the exclusion curves at 95% C.L. in the $M_{Z_{\mu\tau}} - g_{Z_{\mu\tau}}$ plane for four different values of Z - $Z_{\mu\tau}$ mixing angle $\theta_{\mu\tau}$ using the ATLAS data [115] for non-observation of a resonant $\ell^+\ell^-$ signal at the LHC running at 13 TeV with integrated luminosity 139 fb^{-1} . In this case the region above a particular curve has been ruled out at 95% C.L. from the non-observation of a resonant $\ell^+\ell^-$ signal in the 13 TeV run of LHC by ATLAS data [115]. If we focus on a particular curve fixed by a particular value of mixing angle $\theta_{\mu\tau}$ then we observe that for the lower values of mass the coupling $g_{Z_{\mu\tau}}$ rapidly falls with the increasing values of mass $M_{Z_{\mu\tau}}$. This phenomena can be explained in the following way. In the lower mass range if we vary the mass then the cross section does not fall rapidly as desired by the ATLAS data. Hence, to acquire the proper cross section for a particular mass one should decrease the value of the coupling $g_{Z_{\mu\tau}}$. Once the lower mass range is over then with the increasing values of mass the

generated via Z - $Z_{\mu\tau}$ mixing.

curve exactly replicates the exclusion plot as given in [115]. At this point, we would like to mention another notable feature of the exclusion curves (which is true for all over the mass range) that for a fixed value of mass if the mixing angle increases then to satisfy ATLAS data [115] one requires decreasing values of coupling constant $g_{Z_{\mu\tau}}$. Furthermore, it is clearly evident from the Fig. 13 that as the mixing angle $\theta_{\mu\tau}$ increases large amount of area in the $M_{Z_{\mu\tau}} - g_{Z_{\mu\tau}}$ plane has been ruled out by the ATLAS data. Both of the features can be explained, if we analyse the structure of the coupling²² between $Z_{\mu\tau}$ and $\ell^+\ell^-$. If we decompose the coupling then we can find that there is one vectorial part and other is axial vectorial in nature. The latter one has no significant role in the concerned process but totally controlled by the vectorial part. We have also checked that, one can control the coupling (which in turn the vectorial part of the coupling) that satisfy the exclusion data with lower values of mixing angle $\theta_{\mu\tau}$. However, as the mixing increases then one loses the control over the coupling, i.e., there is no variation of coupling with larger mixing angle. Therefore, with larger mixing angle one can not vary the cross section properly, hence one can not have the required cross section for a particular mass. For example, if the mixing is set at 4.5×10^{-4} rad, then one can not go beyond 1500 GeV mass of $M_{Z_{\mu\tau}}$. Since in this situation after 1500 GeV mass we can not have the desired cross section by changing the value of $g_{Z_{\mu\tau}}$. Therefore, in order to translate the exclusion limit obtained by ATLAS data [115] for non-observation of di-lepton resonance search at the LHC experiment in our model we have restricted ourselves within the relatively smaller values of mixings angle $\theta_{\mu\tau}$.

VIII. CONCLUSIONS

In order to simultaneously resolving $R_{K^{(*)}}$ anomalies and dark matter enigma, we have proposed a unified scenario by introducing an extra local $U(1)_{L_\mu-L_\tau}$ gauge symmetry to the Standard Model. This $U(1)_{L_\mu-L_\tau}$ gauge symmetry provides a neutral non-standard gauge boson $Z_{\mu\tau}$ which has versatile effects on different phenomenological aspects that have been considered in this article. For the purpose of breaking of the $U(1)_{L_\mu-L_\tau}$ symmetry spontaneously a complex scalar field η has been invoked to the scalar sector in addition to the usual Standard Model Higgs doublet H . Three singlet right handed neutrinos have also been introduced in order to explain the observed oscillation data by incorporating neutrino masses and mixings via Type-I seesaw mechanism. Furthermore, for the proper establishment of correlation between $R_{K^{(*)}}$ anomalies and dark matter puzzle, a bottom quark like coloured fermion field χ has been included in this scenario. This non-standard fermion field χ is transformed vectorially under the $U(1)_{L_\mu-L_\tau}$ symmetry and further it is odd under the \mathbb{Z}_2 parity. Apart from these, an $SU(2)_L$ scalar doublet Φ with nonzero $U(1)_{L_\mu-L_\tau}$ charge and a real scalar singlet S have also been incorporated in the present scenario. Both of these non-standard scalar fields are odd under \mathbb{Z}_2 symmetry. The mixing (which is parametrised by a mixing angle θ_D) between these two \mathbb{Z}_2 -odd scalar fields gives a potential dark matter candidate ρ_1 and also two heavier \mathbb{Z}_2 -odd physical particles ρ_2

²² The relevant couplings have been given in Appendix B.

and ρ_3 . All of these three scalar fields provide significant contributions not only in dark matter phenomenology but also in rare B -meson decay processes.

Existence of lepton flavour universality violation in neutral current sector has been measured by $R_{K^{(*)}}$ in which $b \rightarrow s\ell^+\ell^-$ ($\ell \equiv e, \mu$) transition is involved. This type of flavour changing neutral current is highly suppressed in the Standard Model and therefore, even for a small deviation between the experimental data and the Standard Model could play significant role for finding of new physics effects. In this work, the introduced new physics particles have played crucial role in the concerned $b \rightarrow s$ transition processes which are in general loop induced²³. Particularly, the dark matter particle ρ_1 with two heavier \mathbb{Z}_2 -odd neutral scalar fields ρ_2, ρ_3 and the non-standard fermion χ generate extra loop contributions. Furthermore, the extra non-standard gauge boson $Z_{\mu\tau}$ behaves as a propagator (in addition to the SM Z boson) for the process $b \rightarrow s\ell^+\ell^-$. Now, due to the very basic structure of our model, the process $b \rightarrow s\mu^+\mu^-$ is more favourable with respect to $b \rightarrow se^+e^-$, consequently one obtains the significant non-standard contribution to the Wilson coefficients C_9^{NP} for “ μ ” but not for “ e ”. Therefore, in our work, we have easily satisfied the current fit result for $C_9^{\text{NP},\mu} \in [-1.26, -0.63]$ in 2σ interval to explain the $R_{K^{(*)}}$ anomalies and thereby we have constrained the parameter space of the proposed scenario. On top of that, we have also calculated another rare decay process $B \rightarrow X_s\gamma$ which has also been a class of processes that characterised by $b \rightarrow s$ transition. We have estimated the branching ratio for $B \rightarrow X_s\gamma$ process, and have used the corresponding experimental data within 3σ interval as one of the constraints in our analysis. Moreover, we have calculated the contribution of non-standard gauge boson $Z_{\mu\tau}$ to the $(g-2)_\mu$ and considering the recent experimental data with some error bars (1σ and 2σ) we have further constrained the parameter space allowed by dark matter and flavour physics observables.

In the present scenario, we have extensively studied the dark matter phenomenology by choosing ρ_1 as a WIMP type dark matter candidate. This ρ_1 is an admixture of a real scalar singlet S and the CP-even neutral component (ϕ^0) of the doublet Φ . In our work, first we have calculated dark matter relic abundance by considering all possible annihilation and co-annihilation channels for a wide range ($10 \text{ GeV} \leq 1 \text{ TeV}$) of the mass of ρ_1 . Thereafter, we have imposed necessary constraints like Planck limit on relic density ($0.1172 \leq \Omega_{\text{DM}}h^2 \leq 0.1226$), latest direct detection bounds on σ_{SI} from XENON1T and also the bound on Higgs invisible branching ratio from LHC to find the allowed parameter space. We have found that in the case of low mass region ($M_{\rho_1} < 100 \text{ GeV}$), our dark matter candidate ρ_1 predominantly annihilates into $Z_{\mu\tau}$ pair while co-annihilations among other \mathbb{Z}_2 -odd particles are insignificant as we have considered all heavier \mathbb{Z}_2 -odd particles masses larger than 100 GeV throughout this analysis to respect the experimental bounds from LEP collider. Due to this primary annihilation channel ($\rho_1\rho_1 \rightarrow Z_{\mu\tau}Z_{\mu\tau}$), in spite of being a gauge singlet \mathbb{Z}_2 -odd scalar field, the mixing with another \mathbb{Z}_2 -odd field (part of an $\text{SU}(2)_L$ doublet) having nonzero $L_\mu - L_\tau$ charge, makes the entire dynamics of our dark matter candidate ρ_1 remarkably different from the standard Scalar Singlet dark

²³ Apart from leptoquark scenarios where $b \rightarrow s$ transition is possible at tree level.

matter scenario where $b\bar{b}$ final state is in general the principal annihilation channel and low mass region has already been ruled out by direct detection, indirect detection and also by the upper limit on Higgs invisible decay branching ratio. On the other hand for the higher values of M_{ρ_1} , depending upon the mass splitting between ρ_1 and other \mathbb{Z}_2 -odd particles several annihilation or co-annihilation channels may appear and have contributed significantly to the relic density. Since, one of our prime motivations of this article is to correlate dark matter puzzle with some specific flavour physics anomalies associated with FCNC processes, therefore, we have used experimental data of some flavour physics observables (e.g., $R_{K^{(*)}}$ anomalies and $\text{Br}(B \rightarrow X_s \gamma)$) as further constraints on the parameter space which is already allowed by experiments related to dark matter physics. As a consequence, both the effects of $R_{K^{(*)}}$ anomalies and dark matter phenomenology allow only a very restrictive values of dark sector mixing angle θ_D which remains confined within a certain range ($0.01 < \theta_D \text{ (rad)} < 0.3$) when $M_{\rho_1} \leq 100 \text{ GeV}$. This is a unique feature of our proposed model.

Additionally, we have used some other constraints which have been relevant to our present scenario. For example, we have imposed constraint from neutrino trident production and for that purpose we have used the CCFR experimental data which is currently the most stringent one for the neutrino trident production process. Furthermore, we have imposed constraint from the measurement of the Standard Model Z boson decay to 4μ final state at the LHC. As a consequence there is a substantial amount of reduction in the parameters space due to the inclusion of such constraints. However, there still exists a few portion of the parameter space of the present model which can address dark matter, $R_{K^{(*)}}$ anomalies, $(g-2)_\mu$ and $\text{Br}(B \rightarrow X_s \gamma)$ simultaneously. Most importantly our predicted parameter space and hence our model can be tested within a few years by neutrino trident processes at DUNE. Therefore, in view of the above discussion we can readily conclude that our proposed scenario can reasonably connect the dark matter puzzle with some of the flavour physics anomalies. Besides, within the scope of our proposed model, we have also briefly discussed the origin of neutrino masses and mixing angles via Type-I seesaw mechanism, which is a common feature of most of the $L_\mu - L_\tau$ models.

Finally, for the purpose of constraining the parameter space of the present scenario from the LHC, we have used the latest ATLAS data of non-observation of a resonant $\ell^+ \ell^-$ signal at the LHC running at 13 TeV with an integrated luminosity 139 fb^{-1} . For this purpose we have estimated the cross section for the process $pp \rightarrow Z_{\mu\tau} \rightarrow \ell^+ \ell^-$ at the 13 TeV LHC for the mass range $M_{Z_{\mu\tau}} \in [0.5, 5] \text{ TeV}$ in the present scenario. By comparing the theoretical predictions of the cross section with corresponding ATLAS data of cross section for non-observation of a resonant $\ell^+ \ell^-$ signal at the 13 TeV LHC one yields some specific combination of coupling $g_{Z_{\mu\tau}}$ and Z - $Z_{\mu\tau}$ mixing angle $\theta_{\mu\tau}$. Consequently, with those combinations we have excluded some portion of the parameter space of the present scenario at 95% C.L. From our analysis it has been observed that, for a larger values of mixing angle one can exclude larger region of parameter space in the $M_{Z_{\mu\tau}} - g_{Z_{\mu\tau}}$ plane. For example if the mixing angle is $4.5 \times 10^{-5} \text{ rad}$ then one can maximally exclude the region of parameter space in the $M_{Z_{\mu\tau}} - g_{Z_{\mu\tau}}$ plane.

Acknowledgments A.S. would like to thank Heerak Banerjee for useful discussions. A.B.

would like to acknowledge the cluster computing facility (<http://www.hri.res.in/cluster/>) of Harish-Chandra Research Institute, Allahabad. He also thanks Alexander Pukhov for a few email conversation regarding the package micrOMEGAs. Moreover, A.B. acknowledges all the members of Particle Group Meeting of IACS, especially Sourov Roy, Satyanarayan Mukhopadhyay, Heerak Banerjee, Sougata Ganguly, Ananya Tapadar and Disha Bhatia for a useful discussion on kinetic mixing between two U(1) gauge groups.

Appendices

A. MULTIPLICATIVE FACTORS AND FUNCTIONS THAT ARE INVOLVED IN FLAVOUR PHYSICS

$$\mathcal{L}_{Z(Z_{\mu\tau})}^9 = \frac{g_2}{4 \cos \theta_W} \left(1 - 4 \sin^2 \theta_W \right) \cos(\sin) \theta_{\mu\tau} \pm \left(g_{Z_{\mu\tau}} - \frac{3}{4} \frac{g_2 \sin \theta_W \epsilon}{\cos \theta_W} \right) \sin(\cos) \theta_{\mu\tau}, \quad (\text{A-1})$$

$$\mathcal{L}_{Z(Z_{\mu\tau})}^{10} = - \frac{g_2}{4 \cos \theta_W} \left(\cos(\sin) \theta_{\mu\tau} \pm \epsilon \sin \theta_W \sin(\cos) \theta_{\mu\tau} \right), \quad (\text{A-2})$$

$$\mathcal{G}_{Z(Z_{\mu\tau})} = \frac{g_2}{3 \cos \theta_W} \sin^2 \theta_W \left(\cos(\sin) \theta_{\mu\tau} \pm \frac{\epsilon}{\sin \theta_W} \sin(\cos) \theta_{\mu\tau} \right) \pm g_{Z_{\mu\tau}} \sin(\cos) \theta_{\mu\tau}, \quad (\text{A-3})$$

$$\mathcal{C}_{Z(Z_{\mu\tau})} = \frac{g_2}{\cos \theta_W} \cos(\sin) \theta_{\mu\tau} \pm \left(2g_{Z_{\mu\tau}} + \frac{g_2 \sin \theta_W \epsilon}{\cos \theta_W} \right) \sin(\cos) \theta_{\mu\tau}, \quad (\text{A-4})$$

$$\mathcal{S}_{Z(Z_{\mu\tau})} = \frac{g_2}{\cos \theta_W} \left(\left(\frac{1}{2} - \frac{\sin^2 \theta_W}{3} \right) \cos(\sin) \theta_{\mu\tau} \pm \epsilon \sin \theta_W \sin(\cos) \theta_{\mu\tau} \right). \quad (\text{A-5})$$

$$h_q(x) = \frac{1}{1-x} + \frac{\ln(x)}{(1-x)^2}, \quad (\text{A-6})$$

$$h_w(x, r) = \frac{3}{2} - \frac{(1+r)^2 \ln(1+r)}{r(1+r-x)} - \frac{x^2 \ln(x)}{(1-x)(1+r-x)}, \quad (\text{A-7})$$

$$h_s(x) = \frac{1}{2} \left(\frac{1-3x}{1-x} - \frac{2x^2 \ln(x)}{(1-x)^2} \right), \quad (\text{A-8})$$

$$h_b(x) = -\frac{x^2 - 5x - 2}{12(1-x)^3} + \frac{z \ln(x)}{6(1-x)^4}. \quad (\text{A-9})$$

B. COUPLINGS REQUIRED FOR DARK MATTER PHENOMENOLOGY, FLVOUR PHYSICS OBSERVABLES AND LHC ANALYSIS

- Trilinear couplings of different SM fermions with $Z(Z_{\mu\tau})$ gauge fields:

$$\begin{aligned} \bar{u}_i u_i Z^\alpha : & i \frac{g_2 \gamma^\alpha}{12 \cos \theta_W} \left[\left(\left(-3 + 8 \sin^2 \theta_W \right) \cos \theta_{\mu\tau} + 5\epsilon \sin \theta_W \sin \theta_{\mu\tau} \right) \right. \\ & \left. + \left(3 \cos \theta_{\mu\tau} + 3\epsilon \sin \theta_W \sin \theta_{\mu\tau} \right) \gamma^5 \right] \end{aligned} \quad (\text{B-10})$$

$$\begin{aligned} \bar{u}_i u_i Z_{\mu\tau}^\alpha : & i \frac{g_2 \gamma^\alpha}{12 \cos \theta_W} \left[\left(\left(-3 + 8 \sin^2 \theta_W \right) \sin \theta_{\mu\tau} - 5\epsilon \sin \theta_W \cos \theta_{\mu\tau} \right) \right. \\ & \left. + \left(3 \sin \theta_{\mu\tau} - 3\epsilon \sin \theta_W \cos \theta_{\mu\tau} \right) \gamma^5 \right] \end{aligned} \quad (\text{B-11})$$

$$\begin{aligned} \bar{d}_i d_i Z^\alpha : & -i \frac{g_2 \gamma^\alpha}{12 \cos \theta_W} \left[\left(\left(-3 + 4 \sin^2 \theta_W \right) \cos \theta_{\mu\tau} + \epsilon \sin \theta_W \sin \theta_{\mu\tau} \right) \right. \\ & \left. + \left(3 \cos \theta_{\mu\tau} + 3\epsilon \sin \theta_W \sin \theta_{\mu\tau} \right) \gamma^5 \right] \end{aligned} \quad (\text{B-12})$$

$$\begin{aligned} \bar{d}_i d_i Z_{\mu\tau}^\alpha : & -i \frac{g_2 \gamma^\alpha}{12 \cos \theta_W} \left[\left(\left(-3 + 4 \sin^2 \theta_W \right) \sin \theta_{\mu\tau} - \epsilon \sin \theta_W \cos \theta_{\mu\tau} \right) \right. \\ & \left. + \left(3 \sin \theta_{\mu\tau} - 3\epsilon \sin \theta_W \cos \theta_{\mu\tau} \right) \gamma^5 \right] \end{aligned} \quad (\text{B-13})$$

In the above, $i = 1, 2, 3$.

$$\begin{aligned} \bar{e} e Z^\alpha : & i \gamma^\alpha \left[\left(\frac{g_2}{4 \cos \theta_W} \left(1 - 4 \sin^2 \theta_W \right) \cos \theta_{\mu\tau} - \frac{3}{4} \frac{g_2 \sin \theta_W \epsilon}{\cos \theta_W} \sin \theta_{\mu\tau} \right) \right. \\ & \left. - \left(\frac{g_2}{4 \cos \theta_W} \left(\cos \theta_{\mu\tau} + \epsilon \sin \theta_W \sin \theta_{\mu\tau} \right) \right) \gamma^5 \right] \end{aligned} \quad (\text{B-14})$$

$$\begin{aligned} \bar{e} e Z_{\mu\tau}^\alpha : & i \gamma^\alpha \left[\left(\frac{g_2}{4 \cos \theta_W} \left(1 - 4 \sin^2 \theta_W \right) \sin \theta_{\mu\tau} + \frac{3}{4} \frac{g_2 \sin \theta_W \epsilon}{\cos \theta_W} \cos \theta_{\mu\tau} \right) \right. \\ & \left. - \left(\frac{g_2}{4 \cos \theta_W} \left(\sin \theta_{\mu\tau} - \epsilon \sin \theta_W \cos \theta_{\mu\tau} \right) \right) \gamma^5 \right] \end{aligned} \quad (\text{B-15})$$

$$\bar{\mu}\mu Z^\alpha : i\gamma^\alpha \left[\left(\frac{g_2}{4 \cos \theta_W} (1 - 4 \sin^2 \theta_W) \cos \theta_{\mu\tau} + \left(g_{Z\mu\tau} - \frac{3}{4} \frac{g_2 \sin \theta_W \epsilon}{\cos \theta_W} \right) \sin \theta_{\mu\tau} \right) \right. \\ \left. - \left(\frac{g_2}{4 \cos \theta_W} (\cos \theta_{\mu\tau} + \epsilon \sin \theta_W \sin \theta_{\mu\tau}) \right) \gamma^5 \right] \quad (\text{B-16})$$

$$\bar{\mu}\mu Z_{\mu\tau}^\alpha : i\gamma^\alpha \left[\left(\frac{g_2}{4 \cos \theta_W} (1 - 4 \sin^2 \theta_W) \sin \theta_{\mu\tau} - \left(g_{Z\mu\tau} - \frac{3}{4} \frac{g_2 \sin \theta_W \epsilon}{\cos \theta_W} \right) \cos \theta_{\mu\tau} \right) \right. \\ \left. - \left(\frac{g_2}{4 \cos \theta_W} (\sin \theta_{\mu\tau} - \epsilon \sin \theta_W \cos \theta_{\mu\tau}) \right) \gamma^5 \right] \quad (\text{B-17})$$

- Trilinear couplings of ρ_i ($i \equiv 1, 2, 3$) with H_1 and H_2 scalar fields:

$$\begin{aligned} \rho_1 \rho_1 H_1 : & i \left(2 \cos^2 \theta_D \left(v_1 \lambda_7 \cos \theta_s - v_2 \lambda_6 \sin \theta_s \right) \right. \\ & + \sqrt{2} \lambda_8 \cos \theta_D \sin \theta_D \left(v_2 \cos \theta_s - v_1 \sin \theta_s \right) \\ & \left. + \sin^2 \theta_D \left(v_1 (\lambda_2 + \lambda_3) \cos \theta_s - v_2 \lambda_4 \sin \theta_s \right) \right) \end{aligned} \quad (\text{B-18})$$

$$\begin{aligned} \rho_1 \rho_1 H_2 : & i \left(2 \cos^2 \theta_D \left(v_1 \lambda_7 \sin \theta_s + v_2 \lambda_6 \cos \theta_s \right) \right. \\ & + \sqrt{2} \lambda_8 \cos \theta_D \sin \theta_D \left(v_2 \sin \theta_s + v_1 \cos \theta_s \right) \\ & \left. + \sin^2 \theta_D \left(v_1 (\lambda_2 + \lambda_3) \sin \theta_s + v_2 \lambda_4 \cos \theta_s \right) \right) \end{aligned} \quad (\text{B-19})$$

$$\begin{aligned} \rho_2 \rho_2 H_1 : & i \left(2 \sin^2 \theta_D \left(v_1 \lambda_7 \cos \theta_s - v_2 \lambda_6 \sin \theta_s \right) \right. \\ & - \sqrt{2} \lambda_8 \cos \theta_D \sin \theta_D \left(v_2 \cos \theta_s - v_1 \sin \theta_s \right) \\ & \left. + \cos^2 \theta_D \left(v_1 (\lambda_2 + \lambda_3) \cos \theta_s - v_2 \lambda_4 \sin \theta_s \right) \right) \end{aligned} \quad (\text{B-20})$$

$$\begin{aligned} \rho_2 \rho_2 H_2 : & i \left(2 \sin^2 \theta_D \left(v_1 \lambda_7 \sin \theta_s + v_2 \lambda_6 \cos \theta_s \right) \right. \\ & - \sqrt{2} \lambda_8 \cos \theta_D \sin \theta_D \left(v_2 \sin \theta_s + v_1 \cos \theta_s \right) \\ & \left. + \cos^2 \theta_D \left(v_1 (\lambda_2 + \lambda_3) \sin \theta_s + v_2 \lambda_4 \cos \theta_s \right) \right) \end{aligned} \quad (\text{B-21})$$

$$\begin{aligned} \rho_1 \rho_2 H_1 : & \frac{i}{2} \left(\sqrt{2} \cos 2\theta_D \lambda_8 \left(v_2 \cos \theta_s - v_1 \sin \theta_s \right) \right. \\ & \left. + \sin 2\theta_D \left(v_1 (\lambda_2 + \lambda_3 - 2\lambda_7) \cos \theta_s - v_2 (\lambda_4 - 2\lambda_6) \sin \theta_s \right) \right) \end{aligned} \quad (\text{B-22})$$

$$\begin{aligned} \rho_1 \rho_2 H_2 : & \frac{i}{2} \left(\sqrt{2} \cos 2\theta_D \lambda_8 \left(v_2 \sin \theta_s + v_1 \cos \theta_s \right) \right. \\ & \left. + \sin 2\theta_D \left(v_1 (\lambda_2 + \lambda_3 - 2\lambda_7) \sin \theta_s + v_2 (\lambda_4 - 2\lambda_6) \cos \theta_s \right) \right) \end{aligned} \quad (\text{B-23})$$

$$\rho_3 \rho_3 H_1 : i \left(v_1 (\lambda_2 + \lambda_3) \cos \theta_s - v_2 \lambda_4 \sin \theta_s \right) \quad (\text{B-24})$$

$$\rho_3 \rho_3 H_2 : i \left(v_1 (\lambda_2 + \lambda_3) \sin \theta_s + v_2 \lambda_4 \cos \theta_s \right) \quad (\text{B-25})$$

- Quartic couplings of ρ_i ($i \equiv 1, 2, 3$) with H_1 scalar fields:

$$\begin{aligned} \rho_1 \rho_1 H_1 H_1 : i \left(-2\sqrt{2} \lambda_8 \cos \theta_s \sin \theta_s \cos \theta_D \sin \theta_D \right. \\ \left. + \cos^2 \theta_s \left(2\lambda_7 \cos^2 \theta_D + (\lambda_2 + \lambda_3) \sin^2 \theta_D \right) \right. \\ \left. + \sin^2 \theta_s \left(2\lambda_6 \cos^2 \theta_D + \lambda_4 \sin^2 \theta_D \right) \right) \end{aligned} \quad (\text{B-26})$$

$$\begin{aligned} \rho_2 \rho_2 H_1 H_1 : i \left(2\sqrt{2} \lambda_8 \cos \theta_s \sin \theta_s \cos \theta_D \sin \theta_D \right. \\ \left. + \cos^2 \theta_s \left(2\lambda_7 \sin^2 \theta_D + (\lambda_2 + \lambda_3) \cos^2 \theta_D \right) \right. \\ \left. + \sin^2 \theta_s \left(2\lambda_6 \sin^2 \theta_D + \lambda_4 \cos^2 \theta_D \right) \right) \end{aligned} \quad (\text{B-27})$$

$$\begin{aligned} \rho_1 \rho_2 H_1 H_1 : i \left(-\sqrt{2} \lambda_8 \cos \theta_s \sin \theta_s \cos 2\theta_D + \cos \theta_D \sin \theta_D \right. \\ \left. \left((\lambda_4 - 2\lambda_6) \sin^2 \theta_s + (\lambda_2 + \lambda_3 - 2\lambda_7) \cos^2 \theta_s \right) \right) \end{aligned} \quad (\text{B-28})$$

$$\rho_3 \rho_3 H_1 H_1 : i \left((\lambda_2 + \lambda_3) \cos^2 \theta_s + \lambda_4 \sin^2 \theta_s \right) \quad (\text{B-29})$$

- Quartic couplings of ρ_i ($i \equiv 1, 2, 3$) with H_2 scalar fields:

$$\begin{aligned} \rho_1 \rho_1 H_2 H_2 : i \left(2\sqrt{2} \lambda_8 \cos \theta_s \sin \theta_s \cos \theta_D \sin \theta_D \right. \\ \left. + \sin^2 \theta_s \left(2\lambda_7 \cos^2 \theta_D + (\lambda_2 + \lambda_3) \sin^2 \theta_D \right) \right. \\ \left. + \cos^2 \theta_s \left(2\lambda_6 \cos^2 \theta_D + \lambda_4 \sin^2 \theta_D \right) \right) \end{aligned} \quad (\text{B-30})$$

$$\begin{aligned} \rho_2 \rho_2 H_2 H_2 : i \Bigg(& -2\sqrt{2}\lambda_8 \cos \theta_s \sin \theta_s \cos \theta_D \sin \theta_D \\ & + \sin^2 \theta_s \left(2\lambda_7 \sin^2 \theta_D + (\lambda_2 + \lambda_3) \cos^2 \theta_D \right) \\ & + \cos^2 \theta_s \left(2\lambda_6 \sin^2 \theta_D + \lambda_4 \cos^2 \theta_D \right) \Bigg) \end{aligned} \quad (\text{B-31})$$

$$\begin{aligned} \rho_1 \rho_2 H_2 H_2 : i \Bigg(& \sqrt{2}\lambda_8 \cos \theta_s \sin \theta_s \cos 2\theta_D + \cos \theta_D \sin \theta_D \\ & \left((\lambda_4 - 2\lambda_6) \cos^2 \theta_s + (\lambda_2 + \lambda_3 - 2\lambda_7) \sin^2 \theta_s \right) \Bigg) \end{aligned} \quad (\text{B-32})$$

$$\rho_3 \rho_3 H_2 H_2 : i \left((\lambda_2 + \lambda_3) \sin^2 \theta_s + \lambda_4 \cos^2 \theta_s \right) \quad (\text{B-33})$$

- Trilinear couplings between \mathbb{Z}_2 odd particles with gauge fields:

$$\rho_1 \phi^\pm W^\mp{}_\alpha : \mp i \frac{e \sin \theta_D}{2 \sin \theta_W} (p_1 - p_2)^\alpha \quad (\text{B-34})$$

$$\rho_2 \phi^\pm W^\mp{}_\alpha : \mp i \frac{e \cos \theta_D}{2 \sin \theta_W} (p_1 - p_2)^\alpha \quad (\text{B-35})$$

$$\rho_3 \phi^\pm W^\mp{}_\alpha : -\frac{e}{2 \sin \theta_W} (p_1 - p_2)^\alpha \quad (\text{B-36})$$

$$\rho_1 \rho_3 Z^\alpha : \frac{\sin \theta_D}{2} \left(\frac{e}{2 \sin \theta_W \cos \theta_W} \cos \theta_{\mu\tau} \left(2g_{Z_{\mu\tau}} + \epsilon \frac{e}{\cos \theta_W} \right) \sin \theta_{\mu\tau} \right) (p_1 - p_2)^\alpha \quad (\text{B-37})$$

$$\rho_1 \rho_3 Z^\alpha_{\mu\tau} : \frac{\sin \theta_D}{2} \left(\frac{e}{\sin \theta_W \cos \theta_W} \sin \theta_{\mu\tau} - \left(2g_{Z_{\mu\tau}} + \epsilon \frac{e}{\cos \theta_W} \right) \cos \theta_{\mu\tau} \right) (p_1 - p_2)^\alpha \quad (\text{B-38})$$

$$\rho_2 \rho_3 Z^\alpha : \frac{\cos \theta_D}{2} \left(\frac{e}{2 \sin \theta_W \cos \theta_W} \cos \theta_{\mu\tau} \left(2g_{Z_{\mu\tau}} + \epsilon \frac{e}{\cos \theta_W} \right) \sin \theta_{\mu\tau} \right) (p_1 - p_2)^\alpha \quad (\text{B-39})$$

$$\rho_2 \rho_3 Z^\alpha_{\mu\tau} : \frac{\cos \theta_D}{2} \left(\frac{e}{\sin \theta_W \cos \theta_W} \sin \theta_{\mu\tau} - \left(2g_{Z_{\mu\tau}} + \epsilon \frac{e}{\cos \theta_W} \right) \cos \theta_{\mu\tau} \right) (p_1 - p_2)^\alpha \quad (\text{B-40})$$

- Quartic couplings of dark matter with gauge fields:

$$\rho_1 \rho_1 W^{+\alpha} W^{-\beta} : i \frac{e^2 \sin^2 \theta_D}{2 \sin^2 \theta_W} g^{\alpha\beta} \quad (\text{B-41})$$

$$\begin{aligned} \rho_1 \rho_1 Z^\alpha Z^\beta : i \frac{\sin^2 \theta_D}{2} \Bigg(& \left(2g_{Z_{\mu\tau}} \sin \theta_{\mu\tau} + \frac{e \cos \theta_{\mu\tau}}{\cos \theta_W \sin \theta_W} \right) \\ & \left(2 \left(g_{Z_{\mu\tau}} + \epsilon \frac{e}{\cos \theta_W} \right) \sin \theta_{\mu\tau} + \frac{e \cos \theta_{\mu\tau}}{\cos \theta_W \sin \theta_W} \right) \Bigg) g^{\alpha\beta} \end{aligned} \quad (\text{B-42})$$

$$\rho_1 \rho_1 Z_{\mu\tau}^\alpha Z_{\mu\tau}^\beta : i \frac{\sin^2 \theta_D}{2} \left(\left(2g_{Z_{\mu\tau}} \cos \theta_{\mu\tau} - \frac{e \sin \theta_{\mu\tau}}{\cos \theta_W \sin \theta_W} \right) \right. \quad (\text{B-43})$$

$$\left. \left(2 \left(g_{Z_{\mu\tau}} + \epsilon \frac{e}{\cos \theta_W} \right) \cos \theta_{\mu\tau} - \frac{e \sin \theta_{\mu\tau}}{\cos \theta_W \sin \theta_W} \right) \right) g^{\alpha\beta}$$

$$\rho_1 \rho_1 Z_{\mu\tau}^\alpha Z^\beta : i \frac{\sin^2 \theta_D}{2} \left(\frac{e^2 \cos \theta_{\mu\tau} \sin \theta_{\mu\tau}}{\cos^2 \theta_W \sin^2 \theta_W} \right. \quad (\text{B-44})$$

$$- \frac{e}{\cos \theta_W \sin \theta_W} \left(2g_{Z_{\mu\tau}} + \epsilon \frac{e}{\cos \theta_W} \right) \cos 2\theta_{\mu\tau} \\ - 2g_{Z_{\mu\tau}} \left(g_{Z_{\mu\tau}} + \epsilon \frac{e}{\cos \theta_W} \right) \sin 2\theta_{\mu\tau} \Big) g^{\alpha\beta}$$

- Trilinear couplings between \mathbb{Z}_2 odd charged particles with H_1 and H_2 scalar fields:

$$\phi^+ \phi^- H_1 : i \left(v_1 \lambda_2 \cos \theta_s - v_2 \lambda_4 \sin \theta_s \right) \quad (\text{B-45})$$

$$\phi^+ \phi^- H_2 : i \left(v_1 \lambda_2 \sin \theta_s + v_2 \lambda_4 \cos \theta_s \right) \quad (\text{B-46})$$

- Trilinear couplings between \mathbb{Z}_2 odd charged particles with gauge fields:

$$\phi^+ \phi^- \gamma^\alpha : -ie(p_1 - p_2)^\alpha \quad (\text{B-47})$$

$$\phi^+ \phi^- Z^\alpha : \frac{i}{2} \left(\frac{e \cos 2\theta_W}{\sin \theta_W \cos \theta_W} \cos \theta_{\mu\tau} - \left(2g_{Z_{\mu\tau}} + \epsilon \frac{e}{\cos \theta_W} \right) \sin \theta_{\mu\tau} \right) (p_1 - p_2)^\alpha \quad (\text{B-48})$$

$$\phi^+ \phi^- Z_{\mu\tau}^\alpha : \frac{i}{2} \left(\frac{e \cos 2\theta_W}{\sin \theta_W \cos \theta_W} \sin \theta_{\mu\tau} + \left(2g_{Z_{\mu\tau}} + \epsilon \frac{e}{\cos \theta_W} \right) \cos \theta_{\mu\tau} \right) (p_1 - p_2)^\alpha \quad (\text{B-49})$$

- Quartic couplings between \mathbb{Z}_2 odd charged particles with gauge fields:

$$\phi^+ \phi^- W^{+\alpha} W^{-\beta} : i \frac{e^2}{2 \sin^2 \theta_W} g^{\alpha\beta} \quad (\text{B-50})$$

$$\phi^+ \phi^- \gamma^\alpha \gamma^\beta : i 2e^2 g^{\alpha\beta} \quad (\text{B-51})$$

$$\phi^+ \phi^- \gamma^\alpha Z^\beta : i \frac{e}{2} \left(\frac{e \cos 2\theta_W}{\sin \theta_W \cos \theta_W} \cos \theta_{\mu\tau} - \left(2g_{Z_{\mu\tau}} + \epsilon \frac{e}{\cos \theta_W} \right) \sin \theta_{\mu\tau} \right) g^{\alpha\beta} \quad (\text{B-52})$$

$$\phi^+ \phi^- Z^\alpha Z^\beta : \frac{i}{2} g^{\alpha\beta} \left(\frac{e \cos 2\theta_W}{\sin \theta_W \cos \theta_W} \cos \theta_{\mu\tau} - 2g_{Z_{\mu\tau}} \sin \theta_{\mu\tau} \right) \\ \left(\frac{e \cos 2\theta_W}{\sin \theta_W \cos \theta_W} \cos \theta_{\mu\tau} - \left(2g_{Z_{\mu\tau}} + \epsilon \frac{e}{\cos \theta_W} \right) \sin \theta_{\mu\tau} \right) \quad (\text{B-53})$$

- Trilinear couplings between CP-even scalar fields:

$$H_1 H_1 H_1 : i \left(6v_1 \lambda_H \cos^3 \theta_s - 3\lambda_1 \left(\cos^2 \theta_s \sin \theta_s - \cos \theta_s \sin^2 \theta_s \right) - 6v_2 \lambda_\eta \sin^3 \theta_s \right) \quad (\text{B-54})$$

$$H_2 H_1 H_1 : i \left(v_2 \lambda_1 \cos^3 \theta_s + 2v_1 (3\lambda_H - \lambda_1) \cos^2 \theta_s \sin \theta_s \right. \\ \left. + 2v_2 (3\lambda_\eta - \lambda_1) \cos \theta_s \sin^2 \theta_s + v_1 \lambda_1 \sin^3 \theta_s \right) \quad (\text{B-55})$$

- Trilinear couplings of CP-even scalar fields with gauge fields:

$$H_1 W^{+\alpha} W^{-\beta} : i \frac{e^2 v_1}{2 \sin^2 \theta_W} \cos \theta_s g^{\alpha\beta} \quad (\text{B-56})$$

$$H_2 W^{+\alpha} W^{-\beta} : i \frac{e^2 v_1}{2 \sin^2 \theta_W} \sin \theta_s g^{\alpha\beta} \quad (\text{B-57})$$

$$H_1 Z^\alpha Z^\beta : i \left(\frac{e v_1}{2 \sin \theta_W \cos \theta_W} \cos \theta_{\mu\tau} \left(\cos \theta_{\mu\tau} \frac{e}{\sin \theta_W \cos \theta_W} \right. \right. \\ \left. \left. + 2 \sin \theta_{\mu\tau} \epsilon \frac{e}{\cos \theta_W} \right) \cos \theta_s - 2g_{Z\mu\tau}^2 v_2 \sin^2 \theta_{\mu\tau} \sin \theta_s \right) g^{\alpha\beta} \quad (\text{B-58})$$

$$H_2 Z^\alpha Z^\beta : i \left(\frac{e v_1}{2 \sin \theta_W \cos \theta_W} \cos \theta_{\mu\tau} \left(\cos \theta_{\mu\tau} \frac{e}{\sin \theta_W \cos \theta_W} \right. \right. \\ \left. \left. + 2 \sin \theta_{\mu\tau} \epsilon \frac{e}{\cos \theta_W} \right) \sin \theta_s + 2g_{Z\mu\tau}^2 v_2 \sin^2 \theta_{\mu\tau} \cos \theta_s \right) g^{\alpha\beta} \quad (\text{B-59})$$

$$H_1 Z_{\mu\tau}^\alpha Z_{\mu\tau}^\beta : i \left(\frac{e v_1}{2 \sin \theta_W \cos \theta_W} \sin \theta_{\mu\tau} \left(\sin \theta_{\mu\tau} \frac{e}{\sin \theta_W \cos \theta_W} \right. \right. \\ \left. \left. - 2 \cos \theta_{\mu\tau} \epsilon \frac{e}{\cos \theta_W} \right) \cos \theta_s - 2g_{Z\mu\tau}^2 v_2 \cos^2 \theta_{\mu\tau} \sin \theta_s \right) g^{\alpha\beta} \quad (\text{B-60})$$

$$H_2 Z_{\mu\tau}^\alpha Z_{\mu\tau}^\beta : i \left(\frac{e v_1}{2 \sin \theta_W \cos \theta_W} \sin \theta_{\mu\tau} \left(\sin \theta_{\mu\tau} \frac{e}{\sin \theta_W \cos \theta_W} \right. \right. \\ \left. \left. - 2 \cos \theta_{\mu\tau} \epsilon \frac{e}{\cos \theta_W} \right) \sin \theta_s + 2g_{Z\mu\tau}^2 v_2 \cos^2 \theta_{\mu\tau} \cos \theta_s \right) g^{\alpha\beta} \quad (\text{B-61})$$

$$H_1 Z^\alpha Z_{\mu\tau}^\beta : i \left(\frac{e v_1}{2 \sin \theta_W \cos \theta_W} \left(\sin 2\theta_{\mu\tau} \frac{e}{2 \sin \theta_W \cos \theta_W} \right. \right. \\ \left. \left. - \cos 2\theta_{\mu\tau} \epsilon \frac{e}{\cos \theta_W} \right) \cos \theta_s + g_{Z\mu\tau}^2 v_2 \sin 2\theta_{\mu\tau} \sin \theta_s \right) g^{\alpha\beta} \quad (\text{B-62})$$

$$H_2 Z^\alpha Z_{\mu\tau}^\beta : i \left(\frac{ev_1}{2 \sin \theta_W \cos \theta_W} \left(\sin 2\theta_{\mu\tau} \frac{e}{2 \sin \theta_W \cos \theta_W} \right. \right. \\ \left. \left. - \cos 2\theta_{\mu\tau} \epsilon \frac{e}{\cos \theta_W} \right) \sin \theta_s - g_{Z_{\mu\tau}}^2 v_2 \sin 2\theta_{\mu\tau} \cos \theta_s \right) g^{\alpha\beta} \quad (\text{B-63})$$

- Trilinear couplings between gauge fields:

$$\gamma^\sigma W^{+\alpha} W^{-\beta} : ie \left(g^{\sigma\alpha} (p_2 - p_1)^\beta + g^{\sigma\beta} (p_1 - p_3)^\alpha + g^{\beta\alpha} (p_3 - p_2)^\sigma \right) \quad (\text{B-64})$$

$$Z^\sigma W^{+\alpha} W^{-\beta} : ie \frac{\cos \theta_W \cos \theta_s}{\sin \theta_W} \left(g^{\sigma\alpha} (p_2 - p_1)^\beta + g^{\sigma\beta} (p_1 - p_3)^\alpha + g^{\beta\alpha} (p_3 - p_2)^\sigma \right) \quad (\text{B-65})$$

$$Z_{\mu\tau}^\sigma W^{+\alpha} W^{-\beta} : ie \frac{\cos \theta_W \sin \theta_s}{\sin \theta_W} \left(g^{\sigma\alpha} (p_2 - p_1)^\beta + g^{\sigma\beta} (p_1 - p_3)^\alpha + g^{\beta\alpha} (p_3 - p_2)^\sigma \right) \quad (\text{B-66})$$

- Trilinear couplings of CP-even fields scalar with different SM fermion fields:

$$H_1 c \bar{c} : -i \frac{e m_c}{\sqrt{2} \sin \theta_W M_W} \cos \theta_s \quad (\text{B-67})$$

$$H_2 c \bar{c} : -i \frac{e m_c}{\sqrt{2} \sin \theta_W M_W} \sin \theta_s \quad (\text{B-68})$$

$$H_1 t \bar{t} : -i \frac{e m_t}{\sqrt{2} \sin \theta_W M_W} \cos \theta_s \quad (\text{B-69})$$

$$H_2 t \bar{t} : -i \frac{e m_t}{\sqrt{2} \sin \theta_W M_W} \sin \theta_s \quad (\text{B-70})$$

$$H_1 b \bar{b} : -i \frac{e m_b}{\sqrt{2} \sin \theta_W M_W} \cos \theta_s \quad (\text{B-71})$$

$$H_2 b \bar{b} : -i \frac{e m_b}{\sqrt{2} \sin \theta_W M_W} \sin \theta_s \quad (\text{B-72})$$

$$H_1 \tau^+ \tau^- : -i \frac{e m_\tau}{\sqrt{2} \sin \theta_W M_W} \cos \theta_s \quad (\text{B-73})$$

$$H_2 \tau^+ \tau^- : -i \frac{e m_\tau}{\sqrt{2} \sin \theta_W M_W} \sin \theta_s \quad (\text{B-74})$$

- Trilinear couplings of χ with SM down-type quarks and ρ_i ($i \equiv 1, 2, 3$) field:

$$\bar{\chi} \rho_1 b_j : -i \frac{f_j}{2\sqrt{2}} (1 - \gamma^5) \sin \theta_D, \quad \bar{b}_j \rho_1 \chi : -i \frac{f_j}{2\sqrt{2}} (1 + \gamma^5) \sin \theta_D \quad (\text{B-75})$$

$$\bar{\chi} \rho_2 b_j : -i \frac{f_j}{2\sqrt{2}} (1 - \gamma^5) \cos \theta_D, \quad \bar{b}_j \rho_2 \chi : -i \frac{f_j}{2\sqrt{2}} (1 + \gamma^5) \cos \theta_D \quad (\text{B-76})$$

$$\bar{\chi} \rho_3 b_j : -\frac{f_j}{2\sqrt{2}} (1 - \gamma^5), \quad \bar{b}_j \rho_3 \chi : -\frac{f_j}{2\sqrt{2}} (1 + \gamma^5) \quad (\text{B-77})$$

- Trilinear couplings of χ with $Z(Z_{\mu\tau})$ gauge field:

$$\bar{\chi} \chi Z^\alpha = -i \gamma^\alpha \left[\frac{g_2}{3 \cos \theta_W} \sin^2 \theta_W \left(\cos \theta_{\mu\tau} + \frac{\epsilon}{\sin \theta_W} \sin \theta_{\mu\tau} \right) + g_{Z_{\mu\tau}} \sin \theta_{\mu\tau} \right] \quad (\text{B-78})$$

$$\bar{\chi} \chi Z_{\mu\tau}^\alpha = -i \gamma^\alpha \left[\frac{g_2}{3 \cos \theta_W} \sin^2 \theta_W \left(\sin \theta_{\mu\tau} - \frac{\epsilon}{\sin \theta_W} \cos \theta_{\mu\tau} \right) - g_{Z_{\mu\tau}} \cos \theta_{\mu\tau} \right] \quad (\text{B-79})$$

-
- [1] CMS collaboration, S. Chatrchyan et al., *Observation of a new boson at a mass of 125 GeV with the CMS experiment at the LHC*, *Phys. Lett.* **B716** (2012) 30–61, [1207.7235].
 - [2] ATLAS collaboration, G. Aad et al., *Observation of a new particle in the search for the Standard Model Higgs boson with the ATLAS detector at the LHC*, *Phys. Lett.* **B716** (2012) 1–29, [1207.7214].
 - [3] WMAP collaboration, G. Hinshaw et al., *Nine-Year Wilkinson Microwave Anisotropy Probe (WMAP) Observations: Cosmological Parameter Results*, *Astrophys. J. Suppl.* **208** (2013) 19, [1212.5226].
 - [4] PLANCK collaboration, P. A. R. Ade et al., *Planck 2015 results. XIII. Cosmological parameters*, *Astron. Astrophys.* **594** (2016) A13, [1502.01589].
 - [5] Y. Sofue and V. Rubin, *Rotation curves of spiral galaxies*, *Ann. Rev. Astron. Astrophys.* **39** (2001) 137–174, [astro-ph/0010594].
 - [6] M. Bartelmann and P. Schneider, *Weak gravitational lensing*, *Phys. Rept.* **340** (2001) 291–472, [astro-ph/9912508].
 - [7] D. Clowe, A. Gonzalez and M. Markevitch, *Weak lensing mass reconstruction of the interacting cluster 1E0657-558: Direct evidence for the existence of dark matter*, *Astrophys. J.* **604** (2004) 596–603, [astro-ph/0312273].
 - [8] SUPER-KAMIOKANDE collaboration, Y. Fukuda et al., *Evidence for oscillation of atmospheric neutrinos*, *Phys. Rev. Lett.* **81** (1998) 1562–1567, [hep-ex/9807003].
 - [9] SNO collaboration, Q. R. Ahmad et al., *Direct evidence for neutrino flavor transformation from neutral current interactions in the Sudbury Neutrino Observatory*, *Phys. Rev. Lett.* **89** (2002) 011301, [nucl-ex/0204008].
 - [10] KAMLAND collaboration, T. Araki et al., *Measurement of neutrino oscillation with KamLAND: Evidence of spectral distortion*, *Phys. Rev. Lett.* **94** (2005) 081801, [hep-ex/0406035].
 - [11] T2K collaboration, K. Abe et al., *Indication of Electron Neutrino Appearance from an Accelerator-produced Off-axis Muon Neutrino Beam*, *Phys. Rev. Lett.* **107** (2011) 041801, [1106.2822].
 - [12] PARTICLE DATA GROUP collaboration, M. Tanabashi et al., *Review of Particle Physics*, *Phys. Rev.* **D98** (2018) 030001.
 - [13] HFAG, “Average of $\mathcal{R}(D)$ and $\mathcal{R}(D^*)$ for FPCP 2017.”
<http://www.slac.stanford.edu/xorg/hflav/semi/fpcp17/RDRDs.html>.
 - [14] LHCb collaboration, R. Aaij et al., *Measurement of the ratio of branching fractions $\mathcal{B}(B_c^+ \rightarrow J/\psi \tau^+ \nu_\tau)/\mathcal{B}(B_c^+ \rightarrow J/\psi \mu^+ \nu_\mu)$* , *Phys. Rev. Lett.* **120** (2018) 121801, [1711.05623].
 - [15] S. Descotes-Genon, L. Hofer, J. Matias and J. Virto, *Global analysis of $b \rightarrow s \ell \ell$ anomalies*,

- JHEP* **06** (2016) 092, [1510.04239].
- [16] M. Bordone, G. Isidori and A. Pattori, *On the Standard Model predictions for R_K and R_{K^*}* , *Eur. Phys. J.* **C76** (2016) 440, [1605.07633].
 - [17] LHCb collaboration, R. Aaij et al., *Search for lepton-universality violation in $B^+ \rightarrow K^+ \ell^+ \ell^-$ decays*, 1903.09252.
 - [18] B. Capdevila, A. Crivellin, S. Descotes-Genon, J. Matias and J. Virto, *Patterns of New Physics in $b \rightarrow s \ell^+ \ell^-$ transitions in the light of recent data*, *JHEP* **01** (2018) 093, [1704.05340].
 - [19] LHCb collaboration, R. Aaij et al., *Test of lepton universality with $B^0 \rightarrow K^{*0} \ell^+ \ell^-$ decays*, *JHEP* **08** (2017) 055, [1705.05802].
 - [20] M. Prim, *Belle collaboration, electroweak interactions and unified theories, 16-23 March, Moriond 2019*.
 - [21] S. Descotes-Genon, J. Matias and J. Virto, *Understanding the $B \rightarrow K^* \mu^+ \mu^-$ Anomaly*, *Phys. Rev.* **D88** (2013) 074002, [1307.5683].
 - [22] G. Hiller and M. Schmaltz, *R_K and future $b \rightarrow s \ell \ell$ physics beyond the standard model opportunities*, *Phys. Rev.* **D90** (2014) 054014, [1408.1627].
 - [23] D. Ghosh, M. Nardecchia and S. A. Renner, *Hint of Lepton Flavour Non-Universality in B Meson Decays*, *JHEP* **12** (2014) 131, [1408.4097].
 - [24] W. Altmannshofer and D. M. Straub, *New physics in $b \rightarrow s$ transitions after LHC run 1*, *Eur. Phys. J.* **C75** (2015) 382, [1411.3161].
 - [25] T. Hurth, F. Mahmoudi and S. Neshatpour, *On the anomalies in the latest LHCb data*, *Nucl. Phys.* **B909** (2016) 737–777, [1603.00865].
 - [26] W. Altmannshofer, P. Stangl and D. M. Straub, *Interpreting Hints for Lepton Flavor Universality Violation*, *Phys. Rev.* **D96** (2017) 055008, [1704.05435].
 - [27] J. Aebischer, W. Altmannshofer, D. Guadagnoli, M. Reboud, P. Stangl and D. M. Straub, *B -decay discrepancies after Moriond 2019*, 1903.10434.
 - [28] R. Gauld, F. Goertz and U. Haisch, *On minimal Z' explanations of the $B \rightarrow K^* \mu^+ \mu^-$ anomaly*, *Phys. Rev.* **D89** (2014) 015005, [1308.1959].
 - [29] S. L. Glashow, D. Guadagnoli and K. Lane, *Lepton Flavor Violation in B Decays?*, *Phys. Rev. Lett.* **114** (2015) 091801, [1411.0565].
 - [30] B. Bhattacharya, A. Datta, D. London and S. Shivashankara, *Simultaneous Explanation of the R_K and $R(D^{(*)})$ Puzzles*, *Phys. Lett.* **B742** (2015) 370–374, [1412.7164].
 - [31] A. Crivellin, G. D’Ambrosio and J. Heeck, *Explaining $h \rightarrow \mu^\pm \tau^\mp$, $B \rightarrow K^* \mu^+ \mu^-$ and $B \rightarrow K \mu^+ \mu^- / B \rightarrow K e^+ e^-$ in a two-Higgs-doublet model with gauged $L_\mu - L_\tau$* , *Phys. Rev. Lett.* **114** (2015) 151801, [1501.00993].
 - [32] A. Crivellin, L. Hofer, J. Matias, U. Nierste, S. Pokorski and J. Rosiek, *Lepton-flavour violating B decays in generic Z' models*, *Phys. Rev.* **D92** (2015) 054013, [1504.07928].
 - [33] A. Celis, J. Fuentes-Martin, M. Jung and H. Serodio, *Family nonuniversal Z models with protected flavor-changing interactions*, *Phys. Rev.* **D92** (2015) 015007, [1505.03079].
 - [34] D. Aristizabal Sierra, F. Staub and A. Vicente, *Shedding light on the $b \rightarrow s$ anomalies with a*

- dark sector, *Phys. Rev.* **D92** (2015) 015001, [1503.06077].
- [35] G. Blanger, C. Delaunay and S. Westhoff, *A Dark Matter Relic From Muon Anomalies*, *Phys. Rev.* **D92** (2015) 055021, [1507.06660].
 - [36] B. Gripaios, M. Nardecchia and S. A. Renner, *Linear flavour violation and anomalies in B physics*, *JHEP* **06** (2016) 083, [1509.05020].
 - [37] B. Allanach, F. S. Queiroz, A. Strumia and S. Sun, *Z models for the LHCb and $g - 2$ muon anomalies*, *Phys. Rev.* **D93** (2016) 055045, [1511.07447].
 - [38] K. Fuyuto, W.-S. Hou and M. Kohda, *Z-induced FCNC decays of top, beauty, and strange quarks*, *Phys. Rev.* **D93** (2016) 054021, [1512.09026].
 - [39] C.-W. Chiang, X.-G. He and G. Valencia, *Z model for bs flavor anomalies*, *Phys. Rev.* **D93** (2016) 074003, [1601.07328].
 - [40] S. M. Boucenna, A. Celis, J. Fuentes-Martin, A. Vicente and J. Virto, *Non-abelian gauge extensions for B-decay anomalies*, *Phys. Lett.* **B760** (2016) 214–219, [1604.03088].
 - [41] S. M. Boucenna, A. Celis, J. Fuentes-Martin, A. Vicente and J. Virto, *Phenomenology of an $SU(2) \times SU(2) \times U(1)$ model with lepton-flavour non-universality*, *JHEP* **12** (2016) 059, [1608.01349].
 - [42] A. Celis, W.-Z. Feng and M. Vollmann, *Dirac dark matter and $b \rightarrow s\ell^+\ell^-$ with $U(1)$ gauge symmetry*, *Phys. Rev.* **D95** (2017) 035018, [1608.03894].
 - [43] W. Altmannshofer, S. Gori, S. Profumo and F. S. Queiroz, *Explaining dark matter and B decay anomalies with an $L_\mu - L_\tau$ model*, *JHEP* **12** (2016) 106, [1609.04026].
 - [44] B. Bhattacharya, A. Datta, J.-P. Guvin, D. London and R. Watanabe, *Simultaneous Explanation of the R_K and $R_{D^{(*)}}$ Puzzles: a Model Analysis*, *JHEP* **01** (2017) 015, [1609.09078].
 - [45] A. Crivellin, J. Fuentes-Martin, A. Greljo and G. Isidori, *Lepton Flavor Non-Universality in B decays from Dynamical Yukawas*, *Phys. Lett.* **B766** (2017) 77–85, [1611.02703].
 - [46] D. Beirevi, O. Sumensari and R. Zukanovich Funchal, *Lepton flavor violation in exclusive $b \rightarrow s$ decays*, *Eur. Phys. J.* **C76** (2016) 134, [1602.00881].
 - [47] I. Garcia Garcia, *LHCb anomalies from a natural perspective*, *JHEP* **03** (2017) 040, [1611.03507].
 - [48] D. Bhatia, S. Chakraborty and A. Dighe, *Neutrino mixing and R_K anomaly in $U(1)_X$ models: a bottom-up approach*, *JHEP* **03** (2017) 117, [1701.05825].
 - [49] P. Ko, T. Nomura and H. Okada, *Explaining $B \rightarrow K^{(*)}\ell^+\ell^-$ anomaly by radiatively induced coupling in $U(1)_{\mu-\tau}$ gauge symmetry*, *Phys. Rev.* **D95** (2017) 111701, [1702.02699].
 - [50] C.-H. Chen and T. Nomura, *Penguin $b \rightarrow s\ell^+\ell'^-$ and B-meson anomalies in a gauged $L_\mu - L_\tau$* , *Phys. Lett.* **B777** (2018) 420–427, [1707.03249].
 - [51] S. Baek, *Dark matter contribution to $b \rightarrow s\mu^+\mu^-$ anomaly in local $U(1)_{L_\mu-L_\tau}$ model*, *Phys. Lett.* **B781** (2018) 376–382, [1707.04573].
 - [52] C. Bonilla, T. Modak, R. Srivastava and J. W. F. Valle, *$U(1)_{B_3-3L_\mu}$ gauge symmetry as a simple description of $b \rightarrow s$ anomalies*, *Phys. Rev.* **D98** (2018) 095002, [1705.00915].

- [53] B. Barman, D. Borah, L. Mukherjee and S. Nandi, *Correlating the anomalous results in $b \rightarrow s$ decays with inert Higgs doublet dark matter and muon $(g - 2)$* , 1808.06639.
- [54] S. Biswas, D. Chowdhury, S. Han and S. J. Lee, *Explaining the lepton non-universality at the LHCb and CMS within a unified framework*, *JHEP* **02** (2015) 142, [1409.0882].
- [55] B. Gripaios, M. Nardecchia and S. A. Renner, *Composite leptoquarks and anomalies in B -meson decays*, *JHEP* **05** (2015) 006, [1412.1791].
- [56] S. Sahoo and R. Mohanta, *Scalar leptoquarks and the rare B meson decays*, *Phys. Rev.* **D91** (2015) 094019, [1501.05193].
- [57] D. Beirevi, S. Fajfer and N. Konik, *Lepton flavor nonuniversality in $b \rightarrow s\ell^+\ell^-$ processes*, *Phys. Rev.* **D92** (2015) 014016, [1503.09024].
- [58] R. Alonso, B. Grinstein and J. Martin Camalich, *Lepton universality violation and lepton flavor conservation in B_s -meson decays*, *JHEP* **10** (2015) 184, [1505.05164].
- [59] L. Calibbi, A. Crivellin and T. Ota, *Effective Field Theory Approach to $b \rightarrow s\ell\ell'$, $B \rightarrow K(*)\nu\bar{\nu}$ and $B \rightarrow D(*)\tau\nu$ with Third Generation Couplings*, *Phys. Rev. Lett.* **115** (2015) 181801, [1506.02661].
- [60] W. Huang and Y.-L. Tang, *Flavor anomalies at the LHC and the R -parity violating supersymmetric model extended with vectorlike particles*, *Phys. Rev.* **D92** (2015) 094015, [1509.08599].
- [61] H. Ps and E. Schumacher, *Common origin of R_K and neutrino masses*, *Phys. Rev.* **D92** (2015) 114025, [1510.08757].
- [62] M. Bauer and M. Neubert, *Minimal Leptoquark Explanation for the $R_{D(*)}$, R_K , and $(g - 2)_g$ Anomalies*, *Phys. Rev. Lett.* **116** (2016) 141802, [1511.01900].
- [63] S. Fajfer and N. Konik, *Vector leptoquark resolution of R_K and $R_{D(*)}$ puzzles*, *Phys. Lett.* **B755** (2016) 270–274, [1511.06024].
- [64] R. Barbieri, G. Isidori, A. Pattori and F. Senia, *Anomalies in B -decays and $U(2)$ flavour symmetry*, *Eur. Phys. J.* **C76** (2016) 67, [1512.01560].
- [65] S. Sahoo and R. Mohanta, *Lepton flavor violating B meson decays via a scalar leptoquark*, *Phys. Rev.* **D93** (2016) 114001, [1512.04657].
- [66] I. Dorner, S. Fajfer, A. Greljo, J. F. Kamenik and N. Konik, *Physics of leptoquarks in precision experiments and at particle colliders*, *Phys. Rept.* **641** (2016) 1–68, [1603.04993].
- [67] S. Sahoo and R. Mohanta, *Effects of scalar leptoquark on semileptonic Λ_b decays*, *New J. Phys.* **18** (2016) 093051, [1607.04449].
- [68] D. Das, C. Hati, G. Kumar and N. Mahajan, *Towards a unified explanation of $R_{D(*)}$, R_K and $(g - 2)_\mu$ anomalies in a left-right model with leptoquarks*, *Phys. Rev.* **D94** (2016) 055034, [1605.06313].
- [69] C.-H. Chen, T. Nomura and H. Okada, *Explanation of $B \rightarrow K^{(*)}\ell^+\ell^-$ and muon $g - 2$, and implications at the LHC*, *Phys. Rev.* **D94** (2016) 115005, [1607.04857].
- [70] D. Beirevi, N. Konik, O. Sumensari and R. Zukanovich Funchal, *Palatable Leptoquark Scenarios for Lepton Flavor Violation in Exclusive $b \rightarrow s\ell_1\ell_2$ modes*, *JHEP* **11** (2016) 035,

- [1608.07583].
- [71] D. Beirevi, S. Fajfer, N. Konik and O. Sumensari, *Leptoquark model to explain the B-physics anomalies, R_K and R_D* , *Phys. Rev.* **D94** (2016) 115021, [1608.08501].
 - [72] S. Sahoo, R. Mohanta and A. K. Giri, *Explaining the R_K and $R_{D^{(*)}}$ anomalies with vector leptoquarks*, *Phys. Rev.* **D95** (2017) 035027, [1609.04367].
 - [73] R. Barbieri, C. W. Murphy and F. Senia, *B-decay Anomalies in a Composite Leptoquark Model*, *Eur. Phys. J.* **C77** (2017) 8, [1611.04930].
 - [74] P. Cox, A. Kusenko, O. Sumensari and T. T. Yanagida, *$SU(5)$ Unification with TeV-scale Leptoquarks*, *JHEP* **03** (2017) 035, [1612.03923].
 - [75] A. K. Alok, B. Bhattacharya, A. Datta, D. Kumar, J. Kumar and D. London, *New Physics in $b \rightarrow s\mu^+\mu^-$ after the Measurement of R_{K^*}* , *Phys. Rev.* **D96** (2017) 095009, [1704.07397].
 - [76] C. Hati, G. Kumar, J. Orloff and A. M. Teixeira, *Reconciling B-meson decay anomalies with neutrino masses, dark matter and constraints from flavour violation*, *JHEP* **11** (2018) 011, [1806.10146].
 - [77] X. G. He, G. C. Joshi, H. Lew and R. R. Volkas, *NEW Z-prime PHENOMENOLOGY*, *Phys. Rev.* **D43** (1991) 22–24.
 - [78] X.-G. He, G. C. Joshi, H. Lew and R. R. Volkas, *Simplest Z-prime model*, *Phys. Rev.* **D44** (1991) 2118–2132.
 - [79] E. Ma, D. P. Roy and S. Roy, *Gauged $L(\mu) - L(\tau)$ with large muon anomalous magnetic moment and the bimaximal mixing of neutrinos*, *Phys. Lett.* **B525** (2002) 101–106, [hep-ph/0110146].
 - [80] S. Baek, N. G. Deshpande, X. G. He and P. Ko, *Muon anomalous $g-2$ and gauged $L(\mu) - L(\tau)$ models*, *Phys. Rev.* **D64** (2001) 055006, [hep-ph/0104141].
 - [81] J. Heeck and W. Rodejohann, *Gauged $L_\mu - L_\tau$ Symmetry at the Electroweak Scale*, *Phys. Rev.* **D84** (2011) 075007, [1107.5238].
 - [82] K. Harigaya, T. Igari, M. M. Nojiri, M. Takeuchi and K. Tobe, *Muon $g-2$ and LHC phenomenology in the $L_\mu - L_\tau$ gauge symmetric model*, *JHEP* **03** (2014) 105, [1311.0870].
 - [83] W. Altmannshofer, C.-Y. Chen, P. S. Bhupal Dev and A. Soni, *Lepton flavor violating Z explanation of the muon anomalous magnetic moment*, *Phys. Lett.* **B762** (2016) 389–398, [1607.06832].
 - [84] A. Biswas, S. Choubey and S. Khan, *Neutrino Mass, Dark Matter and Anomalous Magnetic Moment of Muon in a $U(1)_{L_\mu - L_\tau}$ Model*, *JHEP* **09** (2016) 147, [1608.04194].
 - [85] A. Biswas, S. Choubey and S. Khan, *FIMP and Muon $(g - 2)$ in a $U(1)_{L_\mu - L_\tau}$ Model*, *JHEP* **02** (2017) 123, [1612.03067].
 - [86] H. Banerjee, P. Byakti and S. Roy, *Supersymmetric gauged $U(1)_{L_\mu - L_\tau}$ model for neutrinos and the muon $(g - 2)$ anomaly*, *Phys. Rev.* **D98** (2018) 075022, [1805.04415].
 - [87] S. Baek and P. Ko, *Phenomenology of $U(1)(L(\mu)-L(\tau))$ charged dark matter at PAMELA and colliders*, *JCAP* **0910** (2009) 011, [0811.1646].
 - [88] M. Das and S. Mohanty, *Leptophilic dark matter in gauged $L_\mu - L_\tau$ extension of MSSM*, *Phys.*

- Rev.* **D89** (2014) 025004, [1306.4505].
- [89] S. Patra, S. Rao, N. Sahoo and N. Sahu, *Gauged $U(1)_{L_\mu-L_\tau}$ model in light of muon $g-2$ anomaly, neutrino mass and dark matter phenomenology*, *Nucl. Phys.* **B917** (2017) 317–336, [1607.04046].
 - [90] A. Biswas, S. Choubey, L. Covi and S. Khan, *Explaining the 3.5 keV X-ray Line in a $L_\mu - L_\tau$ Extension of the Inert Doublet Model*, *JCAP* **1802** (2018) 002, [1711.00553].
 - [91] P. Foldenauer, *Light dark matter in a gauged $U(1)_{L_\mu-L_\tau}$ model*, *Phys. Rev.* **D99** (2019) 035007, [1808.03647].
 - [92] S. Choubey and W. Rodejohann, *A Flavor symmetry for quasi-degenerate neutrinos: $L(\mu) - L(\tau)$* , *Eur. Phys. J.* **C40** (2005) 259–268, [hep-ph/0411190].
 - [93] B. Adhikary, *Soft breaking of $L(\mu) - L(\tau)$ symmetry: Light neutrino spectrum and Leptogenesis*, *Phys. Rev.* **D74** (2006) 033002, [hep-ph/0604009].
 - [94] S. Baek, H. Okada and K. Yagyu, *Flavour Dependent Gauged Radiative Neutrino Mass Model*, *JHEP* **04** (2015) 049, [1501.01530].
 - [95] Z.-z. Xing and Z.-h. Zhao, *A review of - flavor symmetry in neutrino physics*, *Rept. Prog. Phys.* **79** (2016) 076201, [1512.04207].
 - [96] W. Altmannshofer, S. Gori, M. Pospelov and I. Yavin, *Quark flavor transitions in $L_\mu - L_\tau$ models*, *Phys. Rev.* **D89** (2014) 095033, [1403.1269].
 - [97] W. Altmannshofer and I. Yavin, *Predictions for lepton flavor universality violation in rare B decays in models with gauged $L_\mu - L_\tau$* , *Phys. Rev.* **D92** (2015) 075022, [1508.07009].
 - [98] P. Arnan, L. Hofer, F. Mescia and A. Crivellin, *Loop effects of heavy new scalars and fermions in $b \rightarrow s\mu^+\mu^-$* , *JHEP* **04** (2017) 043, [1608.07832].
 - [99] S. Singirala, S. Sahoo and R. Mohanta, *Exploring dark matter, neutrino mass and $R_{K^{(*)},\phi}$ anomalies in $L_\mu - L_\tau$ model*, *Phys. Rev.* **D99** (2019) 035042, [1809.03213].
 - [100] P. T. P. Hutaauruk, T. Nomura, H. Okada and Y. Orikasa, *Dark matter and B -meson anomalies in a flavor dependent gauge symmetry*, 1901.03932.
 - [101] S. Baek, *Scalar dark matter behind $b \rightarrow s\mu\mu$ anomaly*, 1901.04761.
 - [102] R. Barbieri, L. J. Hall and V. S. Rychkov, *Improved naturalness with a heavy Higgs: An Alternative road to LHC physics*, *Phys. Rev.* **D74** (2006) 015007, [hep-ph/0603188].
 - [103] L. Lopez Honorez, E. Nezri, J. F. Oliver and M. H. G. Tytgat, *The Inert Doublet Model: An Archetype for Dark Matter*, *JCAP* **0702** (2007) 028, [hep-ph/0612275].
 - [104] E. Lundstrom, M. Gustafsson and J. Edsjo, *The Inert Doublet Model and LEP II Limits*, *Phys. Rev.* **D79** (2009) 035013, [0810.3924].
 - [105] J. McDonald, *Gauge singlet scalars as cold dark matter*, *Phys. Rev.* **D50** (1994) 3637–3649, [hep-ph/0702143].
 - [106] C. P. Burgess, M. Pospelov and T. ter Veldhuis, *The Minimal model of nonbaryonic dark matter: A Singlet scalar*, *Nucl. Phys.* **B619** (2001) 709–728, [hep-ph/0011335].
 - [107] A. Biswas and D. Majumdar, *The Real Gauge Singlet Scalar Extension of Standard Model: A Possible Candidate of Cold Dark Matter*, *Pramana* **80** (2013) 539–557, [1102.3024].

- [108] J. M. Cline, K. Kainulainen, P. Scott and C. Weniger, *Update on scalar singlet dark matter*, *Phys. Rev.* **D88** (2013) 055025, [1306.4710].
- [109] XENON collaboration, E. Aprile et al., *Dark Matter Search Results from a One Ton-Year Exposure of XENON1T*, *Phys. Rev. Lett.* **121** (2018) 111302, [1805.12562].
- [110] CMS collaboration, V. Khachatryan et al., *Searches for invisible decays of the Higgs boson in pp collisions at $\sqrt{s} = 7, 8$, and 13 TeV*, *JHEP* **02** (2017) 135, [1610.09218].
- [111] CCFR collaboration, S. R. Mishra et al., *Neutrino tridents and $W Z$ interference*, *Phys. Rev. Lett.* **66** (1991) 3117–3120.
- [112] CHARM-II collaboration, D. Geiregat et al., *First observation of neutrino trident production*, *Phys. Lett.* **B245** (1990) 271–275.
- [113] A. G. Riess et al., *A 2.4% Determination of the Local Value of the Hubble Constant*, *Astrophys. J.* **826** (2016) 56, [1604.01424].
- [114] M. Escudero, D. Hooper, G. Krnjaic and M. Pierre, *Cosmology With a Very Light $L_\mu - L_\tau$ Gauge Boson*, 1901.02010.
- [115] ATLAS collaboration, T. A. collaboration, *Search for high-mass dilepton resonances using 139 fb^{-1} of pp collision data collected at $\sqrt{s} = 13$ TeV with the ATLAS detector*, *ATLAS-CONF-2019-001* (2019) .
- [116] A. Hook, E. Izaguirre and J. G. Wacker, *Model Independent Bounds on Kinetic Mixing*, *Adv. High Energy Phys.* **2011** (2011) 859762, [1006.0973].
- [117] J. M. Cline, G. Dupuis, Z. Liu and W. Xue, *The windows for kinetically mixed Z' -mediated dark matter and the galactic center gamma ray excess*, *JHEP* **08** (2014) 131, [1405.7691].
- [118] J. Kawamura, S. Okawa and Y. Omura, *Interplay between the $b \rightarrow s \ell \ell$ anomalies and dark matter physics*, *Phys. Rev.* **D96** (2017) 075041, [1706.04344].
- [119] S. Jger, M. Kirk, A. Lenz and K. Leslie, *Charming new physics in rare B -decays and mixing?*, *Phys. Rev.* **D97** (2018) 015021, [1701.09183].
- [120] LHCb collaboration, R. Aaij et al., *Measurement of the $B_s^0 \rightarrow \mu^+ \mu^-$ branching fraction and effective lifetime and search for $B^0 \rightarrow \mu^+ \mu^-$ decays*, *Phys. Rev. Lett.* **118** (2017) 191801, [1703.05747].
- [121] CDF collaboration, T. Aaltonen et al., *Search for the Decays $B_s^0 \rightarrow e^+ \mu^-$ and $B_s^0 \rightarrow e^+ e^-$ in CDF Run II*, *Phys. Rev. Lett.* **102** (2009) 201801, [0901.3803].
- [122] HFLAV collaboration, Y. Amhis et al., *Averages of b -hadron, c -hadron, and τ -lepton properties as of summer 2016*, *Eur. Phys. J.* **C77** (2017) 895, [1612.07233].
- [123] M. Misiak et al., *Updated NNLO QCD predictions for the weak radiative B -meson decays*, *Phys. Rev. Lett.* **114** (2015) 221801, [1503.01789].
- [124] G. Buchalla, A. J. Buras and M. E. Lautenbacher, *Weak decays beyond leading logarithms*, *Rev. Mod. Phys.* **68** (1996) 1125–1144, [hep-ph/9512380].
- [125] A. J. Buras and R. Fleischer, *Quark mixing, CP violation and rare decays after the top quark discovery*, *Adv. Ser. Direct. High Energy Phys.* **15** (1998) 65–238, [hep-ph/9704376].
- [126] A. J. Buras, A. Poschenrieder, M. Spranger and A. Weiler, *The Impact of universal extra*

- dimensions on $B \rightarrow X_s \gamma$, $B \rightarrow X_s \text{gluon}$, $B \rightarrow X_d \mu^+ \mu^-$, $K(L) \rightarrow \pi^0 e^+ e^-$ and ϵ'/ϵ , *Nucl. Phys.* **B678** (2004) 455–490, [[hep-ph/0306158](#)].
- [127] A. J. Buras, *Weak Hamiltonian, CP violation and rare decays*, in *Probing the standard model of particle interactions. Proceedings, Summer School in Theoretical Physics, NATO Advanced Study Institute, 68th session, Les Houches, France, July 28-September 5, 1997. Pt. 1, 2*, pp. 281–539, 1998, [[hep-ph/9806471](#)].
- [128] T. Inami and C. S. Lim, *Effects of Superheavy Quarks and Leptons in Low-Energy Weak Processes* $K_L \rightarrow \mu \bar{\mu}$, $K^+ \pi^+ \nu \bar{\nu}$ and $K^0 \leftrightarrow \bar{K}^0$, *Prog. Theor. Phys.* **65** (1981) 297.
- [129] K. G. Chetyrkin, M. Misiak and M. Munz, *Weak radiative B meson decay beyond leading logarithms*, *Phys. Lett.* **B400** (1997) 206–219, [[hep-ph/9612313](#)].
- [130] A. L. Kagan and M. Neubert, *QCD anatomy of $B \rightarrow X_s \gamma$ decays*, *Eur. Phys. J.* **C7** (1999) 5–27, [[hep-ph/9805303](#)].
- [131] M. Misiak et al., *Estimate of $\mathcal{B}(\bar{B} \rightarrow X_s \gamma)$ at $O(\alpha_s^2)$* , *Phys. Rev. Lett.* **98** (2007) 022002, [[hep-ph/0609232](#)].
- [132] A. Datta and A. Shaw, *Effects of non-minimal Universal Extra Dimension on $B \rightarrow X_s \gamma$* , *Phys. Rev.* **D95** (2017) 015033, [[1610.09924](#)].
- [133] A. Arhrib, R. Benbrik, C. H. Chen, J. K. Parry, L. Rahili, S. Semlali et al., *$R_{K^{(*)}}$ anomaly in type-III 2HDM*, [1710.05898](#).
- [134] M. Lindner, M. Platscher and F. S. Queiroz, *A Call for New Physics : The Muon Anomalous Magnetic Moment and Lepton Flavor Violation*, *Phys. Rept.* **731** (2018) 1–82, [[1610.06587](#)].
- [135] S. N. Gninenko and N. V. Krasnikov, *The Muon anomalous magnetic moment and a new light gauge boson*, *Phys. Lett.* **B513** (2001) 119, [[hep-ph/0102222](#)].
- [136] M. Krawczyk and J. Zochowski, *Constraining 2HDM by present and future muon ($g-2$) data*, *Phys. Rev.* **D55** (1997) 6968–6974, [[hep-ph/9608321](#)].
- [137] A. Dedes and H. E. Haber, *Can the Higgs sector contribute significantly to the muon anomalous magnetic moment?*, *JHEP* **05** (2001) 006, [[hep-ph/0102297](#)].
- [138] P. Gondolo and G. Gelmini, *Cosmic abundances of stable particles: Improved analysis*, *Nucl. Phys.* **B360** (1991) 145–179.
- [139] K. Griest and D. Seckel, *Three exceptions in the calculation of relic abundances*, *Phys. Rev.* **D43** (1991) 3191–3203.
- [140] J. Edsjo and P. Gondolo, *Neutralino relic density including coannihilations*, *Phys. Rev.* **D56** (1997) 1879–1894, [[hep-ph/9704361](#)].
- [141] A. Alloul, N. D. Christensen, C. Degrande, C. Duhr and B. Fuks, *FeynRules 2.0 - A complete toolbox for tree-level phenomenology*, *Comput. Phys. Commun.* **185** (2014) 2250–2300, [[1310.1921](#)].
- [142] G. Belanger, F. Boudjema, A. Pukhov and A. Semenov, *micrOMEGAs3: A program for calculating dark matter observables*, *Comput. Phys. Commun.* **185** (2014) 960–985, [[1305.0237](#)].
- [143] A. Denner, S. Heinemeyer, I. Puljak, D. Rebuszi and M. Spira, *Standard Model Higgs-Boson*

- Branching Ratios with Uncertainties*, *Eur. Phys. J.* **C71** (2011) 1753, [1107.5909].
- [144] ATLAS collaboration, M. Aaboud et al., *Combination of the searches for pair-produced vector-like partners of the third-generation quarks at $\sqrt{s} = 13$ TeV with the ATLAS detector*, *Phys. Rev. Lett.* **121** (2018) 211801, [1808.02343].
 - [145] MAGIC, FERMI-LAT collaboration, M. L. Ahnen et al., *Limits to Dark Matter Annihilation Cross-Section from a Combined Analysis of MAGIC and Fermi-LAT Observations of Dwarf Satellite Galaxies*, *JCAP* **1602** (2016) 039, [1601.06590].
 - [146] GAMBIT collaboration, P. Athron et al., *Status of the scalar singlet dark matter model*, *Eur. Phys. J.* **C77** (2017) 568, [1705.07931].
 - [147] J. A. Casas, D. G. Cerdeo, J. M. Moreno and J. Quilis, *Reopening the Higgs portal for single scalar dark matter*, *JHEP* **05** (2017) 036, [1701.08134].
 - [148] A. Biswas and A. Shaw, *Explaining Dark Matter and Neutrino Mass in the light of TYPE-II Seesaw Model*, *JCAP* **1802** (2018) 029, [1709.01099].
 - [149] T. Hambye, F. S. Ling, L. Lopez Honorez and J. Rocher, *Scalar Multiplet Dark Matter*, *JHEP* **07** (2009) 090, [0903.4010].
 - [150] N. Chakrabarty, D. K. Ghosh, B. Mukhopadhyaya and I. Saha, *Dark matter, neutrino masses and high scale validity of an inert Higgs doublet model*, *Phys. Rev.* **D92** (2015) 015002, [1501.03700].
 - [151] NUTeV collaboration, T. Adams et al., *Evidence for diffractive charm production in muon-neutrino Fe and anti-muon-neutrino Fe scattering at the Tevatron*, *Phys. Rev.* **D61** (2000) 092001, [hep-ex/9909041].
 - [152] W. Altmannshofer, S. Gori, M. Pospelov and I. Yavin, *Neutrino Trident Production: A Powerful Probe of New Physics with Neutrino Beams*, *Phys. Rev. Lett.* **113** (2014) 091801, [1406.2332].
 - [153] DUNE collaboration, R. Acciarri et al., *Long-Baseline Neutrino Facility (LBNF) and Deep Underground Neutrino Experiment (DUNE)*, 1512.06148.
 - [154] W. Altmannshofer, S. Gori, J. Martn-Albo, A. Sousa and M. Wallbank, *Neutrino Tridents at DUNE*, 1902.06765.
 - [155] I. Esteban, M. C. Gonzalez-Garcia, A. Hernandez-Cabezudo, M. Maltoni and T. Schwetz, *Global analysis of three-flavour neutrino oscillations: synergies and tensions in the determination of θ_{23} , δ_{CP} , and the mass ordering*, *JHEP* **01** (2019) 106, [1811.05487].
 - [156] D0 collaboration, V. M. Abazov et al., *Search for a heavy neutral gauge boson in the dielectron channel with 5.4 fb⁻¹ of $p\bar{p}$ collisions at $\sqrt{s} = 1.96$ TeV*, *Phys. Lett.* **B695** (2011) 88–94, [1008.2023].
 - [157] CDF collaboration, T. Aaltonen et al., *Search for High Mass Resonances Decaying to Muon Pairs in $\sqrt{s} = 1.96$ TeV $p\bar{p}$ Collisions*, *Phys. Rev. Lett.* **106** (2011) 121801, [1101.4578].
 - [158] CMS collaboration, V. Khachatryan et al., *Search for narrow resonances in dilepton mass spectra in proton-proton collisions at $\sqrt{s} = 13$ TeV and combination with 8 TeV data*, *Phys. Lett.* **B768** (2017) 57–80, [1609.05391].

- [159] ATLAS collaboration, M. Aaboud et al., *Search for new high-mass phenomena in the dilepton final state using 36 fb¹ of proton-proton collision data at $\sqrt{s} = 13$ TeV with the ATLAS detector*, *JHEP* **10** (2017) 182, [1707.02424].
- [160] J. Alwall, R. Frederix, S. Frixione, V. Hirschi, F. Maltoni, O. Mattelaer et al., *The automated computation of tree-level and next-to-leading order differential cross sections, and their matching to parton shower simulations*, *JHEP* **07** (2014) 079, [1405.0301].
- [161] NNPDF collaboration, R. D. Ball et al., *Parton distributions for the LHC Run II*, *JHEP* **04** (2015) 040, [1410.8849].